Doctoral Dissertations

Graduate School

Winter 2013

Microfluidic devices applied on enriching post –translational modified proteins for proteomics

Hui Xia

MICROFLUIDIC DEVICES APPLIED ON ENRICHING

POST –TRANSLATIONAL MODIFIED PROTEINS

FOR PROTEOMICS

by

Hui Xia, B. S.

A Dissertation Presented in Partial Fulfillment
of the Requirements of the Degree
Doctor of Philosophy

COLLEGE OF ENGINEERING AND SCIENCE
LOUISIANA TECH UNIVERSITY

March 2013

UMI Number: 3570076

UMI

Dissertation Publishing

ProQuest

LOUISIANA TECH UNIVERSITY

THE GRADUATE SCHOOL

<u>**JULY 23, 2012**</u>
Date

We hereby recommend that the dissertation prepared under our supervision by

Hui Xia, B. S.

entitled **Microfluidic Devices Applied on Enriching**

Post-Translational Modified Proteins

For Proteomics

be accepted in partial fulfillment of the requirements for the Degree of

PhD in Biomedical Engineering
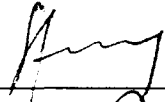
Supervisor of Dissertation Research
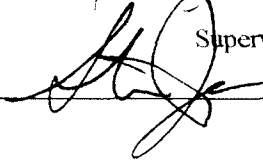
Head of Department

Department

Recommendation concurred in:
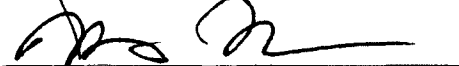
Advisory Committee

Approved:
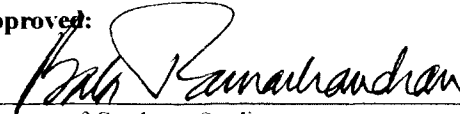
Director of Graduate Studies

Dean of the College

Approved:

Dean of the Graduate School

GS Form 13a
(6/07)

ABSTRACT

In this work, microfluidic devices were developed for enriching post-translational modified proteins. Post-translational modifications (PTM) of proteins play essential roles in cellular physiology and disease. The identification of protein substrates and detection of modification site helps understand PTM-mediated regulation in essential biological pathways and functions in various diseases. However, PTM proteins are typically present only at trace levels, making them difficult to identify in mass spectrometry based proteomics. This work study is about the design, fabrication and testing of the microfluidic device for the enrichment of abundant amount of PTMs. Carbonylated protein is used as a representative PTM to illustrate the wide application of this method for any PTMs converted into a tractable tag after derivatization. The surface topography, surface functional group mapping and elemental composition changes after each modification step of the treatment process were systematically measured qualitatively and quantitatively. Quantitative study of capture efficiency and elution efficiency of the device was also studied. Furthermore, there are also ideas that this proteome enrichment device can be assembled with other lab-on-a-chip components for follow-up protein analysis. For example, coupling with mass spectrometry will allow automatic low-volume fraction deposition on mass spectrometry.

As a part of the microfluidic device designing, this work also aims at optimizing the operating parameters and geometric parameters of microfluidic devices with

microscale posts. The operating parameters studied are Reynolds number, Peclet number, Damköhler number, and equilibrium reaction constant. These parameters encompass the influence of velocity, diffusivity, density, viscosity, hydraulic diameter, inlet concentration of species and forward and backward reaction constants. This work theoretically analyzes the influence of the above mentioned operating parameters using finite element analysis software COMSOL Multiphysics 4.2.a. The results of this study would improve the design of microfluidic devices used for chemical reactions as well as that used for protein enrichment.

APPROVAL FOR SCHOLARLY DISSEMINATION

The author grants to the Prescott Memorial Library of Louisiana Tech University the right to reproduce, by appropriate methods, upon request, any or all portions of this Dissertation. It is understood that "proper request" consists of the agreement, on the part of the requesting party, that said reproduction is for his personal use and that subsequent reproduction will not occur without written approval of the author of this Dissertation. Further, any portions of the Dissertation used in books, papers, and other works must be appropriately referenced to this Dissertation.

Finally, the author of this Dissertation serves the right to publish freely, in the literature, at any time, any or all portions of this Dissertation.

Author _____

Date _____

TABLE OF CONTENTS

LIST OF TABLES

LIST OF FIGURES

ACKNOWLEDGMENTS

Most of all, I would like to thank the sky and earth for everything they grant me -- I will move on to honor them.

CHAPTER 1

INTRODUCTION

1.1   Research Hypothesis

1.1.1   Central Problem

The objective of this work is to design and develop microfluidic devices for the

fast and effective analysis of proteins with specific focus on coupling microfluidic

devices to facilitate and enhance proteomics study in aging related disease (in this work,

Alzheimer's disease (AD) is used as the research model). While in practical, most of the

work done is related with reactive oxygen species (ROS) generated protein post-

translational modifications (PTM). Based on the knowledge the author has acquired, the

hypothesis below is made:

In an organism that possesses a central nervous system, the number of oxidized

(e.g. carbonylated) proteins and their relative modification abundance ratio are correlated

with aging and AD. The increase in carbonylation levels of these particular proteins lead

to the clinical symptoms observed in AD. For individual cases, protein carbonyl

modification results in compromised protein function during the transition from normal

aging to AD.

1.1.2   <u>Dissertation Aims</u>

The hypothesis has marked up a route between known (current knowledge in proteomics and protein PTM) and unknown (the real reason for age-related disease), and methodology in microfluidics and proteomics provide feet to travel on the route. Works made along this route will provide targets for future testing, putting human beings a step closer to understanding the role of protein PTM in aging-related brain function decline. The following three Aims have been established to accomplish these goals:

Aim 1- Develop and use a solid-phase device to enrich carbonylated proteins from clinical samples.

Aim 2- Evaluate different strategies of the microfluidic device for protein carbonylation enrichment.

Aim 3- Use mathematical simulation tools to explore chemical functionalized microfluidic device models that enrich target proteins from flow-through solution and make optimization in geometric and operating features.

1.2   Approach

Proteomics works on age-related disease must work with low concentrations and small quantities of carbonylated proteins. A feasible and efficient carbonylated protein enrichment method is necessary. Conventional methods detecting specific proteins are mainly immunoassays, which provide accurate quantitative proteomic measurements while it is time-consuming and complex in experiments. The development of an effective enrichment method for a protein sample of small concentration in existence is necessary. Furthermore, there are also demands in the protein samples purification process, which could and should also be integrated on the microfluidic enriching device. Chapters 3 and

4 introduce the design and fabrication of two sets of microfluidic devices, of different materials and fabrication methods, that enriches carbonylated proteins from sample solutions with affinity based and antibody-antigen based methods. After the protein enrichment device described in Aim 1 is developed, it is necessary to quantitatively test the amount of carbonylated proteins enriched from the sample. In Chapters 3 and 4, fluorescence spectrometry is used to quantitatively study the capture and elute efficiency of the devices developed.

The work of Aims 1 and 2 provide microfluidic enhanced proteomics study, the operate parameters, such as the density of affinity receptor and antibody chemical modification of the device, and geometric parameters, such as the shape of the microposts used, greatly affect the efficiency and reaction speed of the device. Chapter 5 works on providing possible relationships among different parameters and the performance of the device, and further summarizes and makes optimization suggestions.

1.3   Overview

Chapter 2 introduces the background knowledge and current research work on microchip proteomics, microfabrication and microfluidic simulation. Chapter 3 describes the first set of micropost structured microfluidic device operated by a pressure-driven flow for protein carbonylation enrichment. The second set of microfluidic device, described in Chapter 5, uses a material that supports resealing or hot-plugging and is more specific in target protein enriching. The simulation optimization of a common model of the microfluidic device that enriches proteins, which stand for the two sets of experiments above, is described in Chapter 5.

CHAPTER 2

BACKGROUND

2.1 Relationship Between Protein and Aging Related Diseases

2.1.1 Proteins in Cell Functioning

Proteins are biological macromolecules biopolymers that built by amino acids, whose sequence is encoded by genes. The amino acids are connected with peptide bonds to form polypeptides, while a protein molecule could be composed from more than one polypeptide chain. Proteins have various functions and play essential roles in every cell functioning process, including enzymes that catalyze in biochemical reactions, structural supporting, mechanical functions, cell signaling, immune responses, cell adhesion—just to mention a few.

The variety of protein functions come from their different amino acid sequence and post-translation modification, which are based on the process of protein synthesis. The process of synthesizing a protein begins with the deoxyribonucleic acid (DNA) being transcribed into a messenger ribonucleic acid (mRNA) in the nucleus. After mRNA transport out of the nucleus, it bonds with ribosome at the start codon (AUG), which is recognized by the initiator transfer RNA (tRNA). tRNAs transfer amino acids corresponding to the codon on mRNA, and ribosome will "do the patchwork" that builds the amino acids into polypeptides. This progress is called "translation." After translation,

the amino acid residues in the poly-peptide chain are often chemically modified by posttranslational modification, which will change mechanical and chemical properties, folding structure and functional groups on the proteins.

2.1.2 Free Radical Theory of Aging

2.1.2.1 Overview

Free radical theory of aging, proposed by Denham Harman in 1956, states that it is possible that "one factor in aging may be related to deleterious side attacks of free radicals (which are normally produced in the course of cellular metabolism) on cell constituents" (D. Harman 1956). Originally, "free radical" refers to OH and HO_2 radicals that are present in living cells. By tracing of metals such as iron, cobalt, and manganese, Harman states that "free radicals probably arise largely through reactions involving molecular oxygen catalyzed in the cell by oxidative enzymes and in the connective tissues" (D. Harman 1956). "Free radical" is produced when a "free molecule" (or saying, small molecules that can freely move in cytoplasm) gains or loses an electron and thus becomes charged. "Free radical" tends to obtain another electron from other molecules it encounter, in order to have its free electron paired. This "electron robbing" process may result in molecule damage: The free radical often pulls an electron off a neighboring molecule, causing the affected molecule to become a free radical itself. The new free radical can then pull an electron off the next molecule, and a chemical chain reaction of radical production occurs (Cui, Kong and Zhang 2011).

2.1.2.2 The Effect of Reactive Oxygen Species

In the 1970s, Harman further developed the free radical theory of aging and specialization implying that reactive oxygen species (ROS), such as superoxide anion

(O_2^-), hydroxyl radical ($^.OH$), and hydrogen peroxide (H_2O_2) are produced in the mitochondria (D. Harman 1972). In this theory, ROS in the cell is mainly produced by the mitochondria in the process of oxidative phosphorylation, a process that consumes most of the oxygen, and reproduces most of the ATP molecule in the cell. The production of ROS happens on the mitochondrial membrane as a part of the electron transport chain, as shown in Figure 2-1. On the membrane of mitochondria, complex III is classically considered as the main source of ROS, and release ROS into the mitochondrial matrix (Boveris and Cadenas 2000). Recent study shows that complex I also plays the role as a main ROS generator in the mitochondria in the heart and brain cells (Genova, et al. 2001) (Drouge 2002). As a result, mitochondrial proteins have a much higher chance being affected by the generated ROS.

Oxidative damage initiated by ROS is considered as a major contributor to the process of cellular aging (Dalle-Donne, et al. 1999). The cell itself generates a defense on ROS, for example, superoxide dismutase (SOD, which converts O_2^- to H_2O_2), to ease the chance of being damaged by ROS. Proof shows that transgenic flies with extra copies of SOD caused "a decrease in protein oxidative damage along with a one-third increase of mean and maximum life span" (Orr and Sohal 1994). It is noticeable that deletion of the mitochondrial SOD2 can EXTEND the lifespan in *Caenorhabditis elegans* (Van Raamsdonk and Hekim 2009). Considering that deleting the mitochondrial SOD gene in transgenic mice model leads to the central nervous system neurons severely affected and a shortened lifespan (Wallace and Melov 1998), it is possible that SOD is only important in specific cells, for example, in neuron cells.
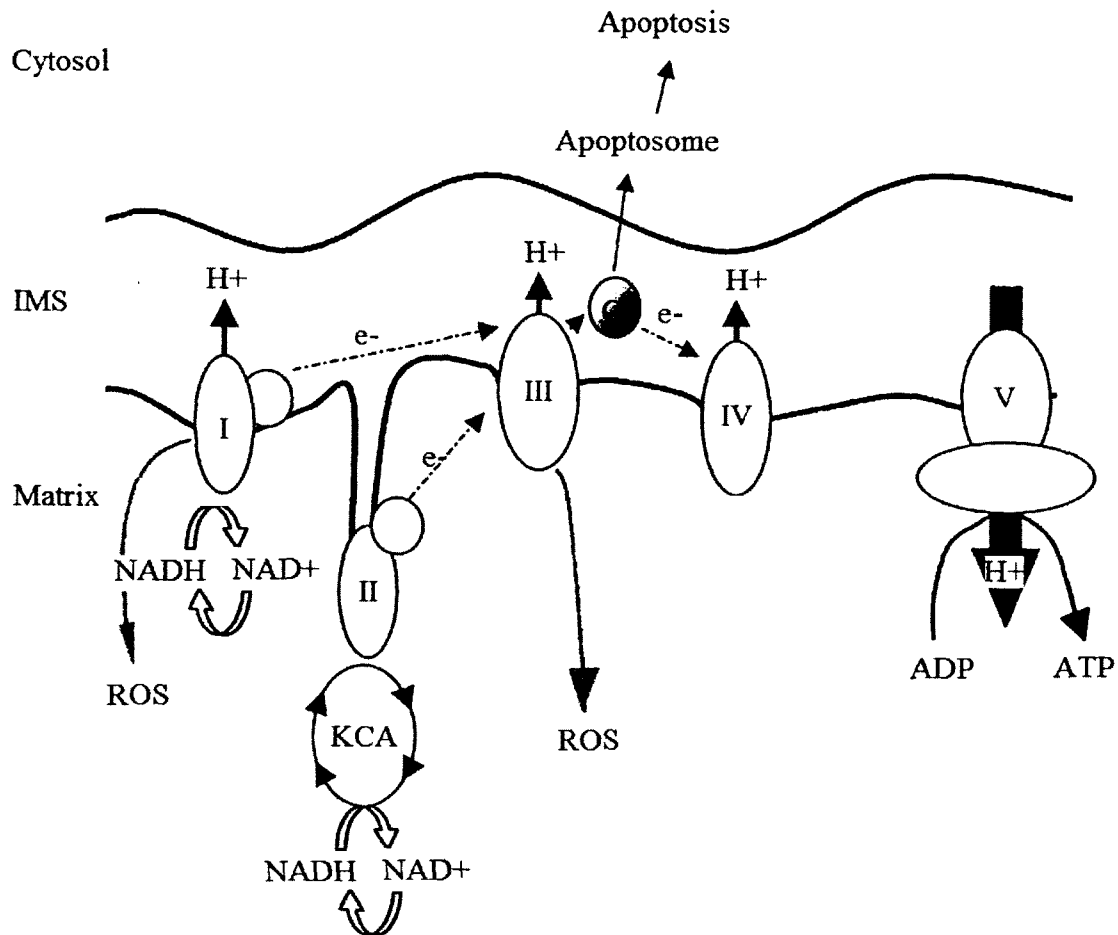
Figure 2-1: Electron transport chain, ATP generation, and ROS production. Different complexes (I–V) of the electron transport chain are represented in the inner membrane (IM) of the mitochondria (Ricci, Waterhouse and Green 2003).

2.1.2.3   ROS in Neural Systems and Degenerative Disease

Degenerative disease indicates that the disease will result in the function and/or structure of the affected tissues or organs progressively deteriorating over time. Current study focuses on the role ROS plays in the process of aging-related disease development (Stadtman, Protein oxidation and aging 2006). Especially, various studies indicate that ROS is relevant with neural cell diseases and neurodegenerative diseases. The degeneration of dopaminergic cell, which is a hallmark Parkinson's disease, is considered relevant to the effect of ROS (Jenner 2003). Also, numerous studies indicate oxidative

stress is also one of the effects that happen at the very start of the development of Alzheimer's disease (Honda, et al. 2004).

2.1.2.4   Protein Post-translational Modification

Post-translational modification (PTM) of protein is a chemical process, in which a ribosomally coded amino acid residue is modified into a non-standard amino acid residue by an enzymatic reaction. Currently, more than 300 various types of protein PTMs have been discovered. Majority of them are considered to play key roles in cellular physiology and disease (Zhao and Jensen 2009). The identification of protein substrates and detection of modification site helps understand PTM-mediated regulation in essential biological pathways and functions in aging or age related disease.

PTM are not typically homogeneous, and a single gene can lead to various numbers of products due to alternative splicing and the combination of different modifications. Hence, the total amount of protein in a single modification states in a very small fraction of the total amount of products (Mann and Jensen 2003). The scale of protein concentrations one can look for can range from milimolar (10^{-3}) to yoctomolar (10^{-24}) (which is less than one molecule per liter). Thus, the determination of post-translational modifications presents formidable challenges in mass spectrometry-based proteomic research due to a lack of suitable methods. High sensitivity is desired in PTM proteomics to detect a low abundant protein in the biological samples. So far, only a small fraction of PTM has been extensively exploited at the proteome level. Currently, the global systematic proteomic study for the post-translationally modified proteins in proteomic comprises affinity-based enrichment and extraction methods, multidimensional separation technologies followed with mass spectrometry (Jensen 2004) (Zhao and

Jensen 2009). Therefore, a selective enrichment of modified proteins is critical for identification of PTMs in complex protein mixture.

One of the widely used tube-based purification of PTM derives from the affinity tagging. For example, carbonylated protein can be labeled by a Schiff reaction between carbonyl and biotin hydrazide, and consecutively enriched by avidin using biotin-avidin strong binding affinity (Ortega-Castro et al., 2010). Also, other PTMs such as nitrated proteins, nitrosylated proteins, glutathionylated proteins have been enriched for proteomics study using this affinity tagging approach (Casoni et al., 2005; Lind et al., 2002; Lindermayr et al., 2005). Alternatively, immunoprecipitation (IP) has been widely used in biological and clinical research to specifically pull down a protein or proteins sharing the same functional groups from complex samples using the immuno-based capture followed by washing and eluting. For example, anti-dinitrophenyl (DNP) beads were modified to target carbonylated proteins (Kristensen et al., 2004).

2.1.2.5   Protein Carbonylation

Protein carbonylation is a well-used biomarker of severe oxidative protein damage, which plays a fundamental role in human diseases (Rossi, et al. 2008). Carbonyl (CO) groups (aldehydes and ketones) are produced on oxidization of protein side chains of lysine, arginine, proline and threonine residues, as shown in Figure 2-2.

2-pyrrolidone   glutamic semialdehyde   aminoadipic semialdehyde   2-amino-3-ketobutyric acid
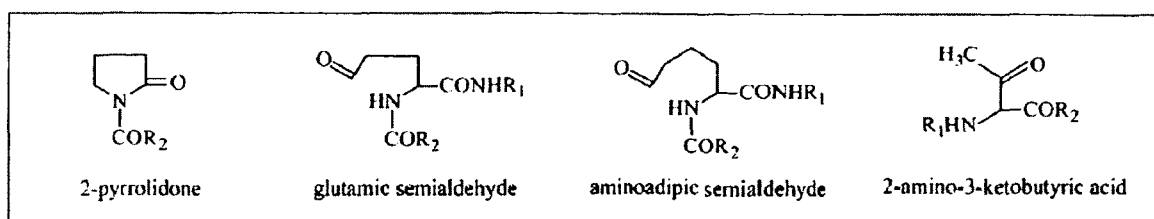
Figure 2-2: The structure of carbonyl derivatives produced by direct oxidation of amino acid side chains: 2-pyrrolidone from prolyl residue, glutamic semialdehyde from arginyl and prolyl residue, a-aminoadipic semialdehyde from lysyl residue, and 2-amino-3-ketobutyric acid from threonyl residue (Dalle-Donne, et al. 1999).

The accurate quantitative proteomics analysis of protein carbonylation will provide important information to characterize and help establish effective therapy to relate carbonyl to oxidative stress induced disease, such as AD (Boyd-Kimball, et al. 2005). To obtain how oxidative pressure modifies protein by carbonylation, effective proteomic study on protein modification is needed. However, the traditional time and sample consuming experimental methods are restricting the further development of proteomics (Nägele, Vollmer and Hörth 2003). Progress in the identification of carbonylated proteins could provide a new diagnostic biomarker identification method of increased accuracy, efficient sample analysis and less sample requirements for oxidative damage, and yield the basic information to aid the establishment of an efficacious antioxidant therapy. In this dissertation work, purification, separation and digestion of carbonylated proteins in the microfluidic device is used as a proof of principle: the microfluidic device described here will provide an accurate dynamic analysis of low abundant protein modifications in a wide range of PTMs, other than carbonylation studied here.

A widely accepted method to study *in vivo* carbonyl groups was developed by the Levine group based on the reaction between carbonyl groups and dinitrophenylhydrazine (DNPH), which form a stable hydrazone product. The DNP derivatized proteins can be further separated by SDS-PAGE and then analyzed for carbonyl content by Western-blot immunoassay with anti-DNP antibodies (Shacter, Williame and Levine 1994). Also, the DNP group itself absorbs ultraviolet light at 370 nm as a spectrophotometric assay which could be used to find the total carbonyl content in the protein sample (Levine, et al. 1994). Enzyme-linked immunosorbent assay (ELISA) which applies biotinylated anti-DNP and streptavidin-biotinylated affinity assay to quantitatively study the amount of protein carbonyls (Winterbourn and Buss 1999). Currently, 2D-PAGE and subsequent Western blot immunoassay the most commonly used method for the identification of oxidized proteins in AD, and a more ideal result could be expected when the Western blot analyses are followed by mass spectrometry (Choi, et al. 2002) for the identification of carbonylated proteins (Dalle-Donne, et al. 1999).

2.2   Proteomics

The word "proteomics" come from the analogy of the word "genomics" (James 1997), which describes the process of the processes that analyze the structures and functions of proteins in a macro perspective -- analysis of a proteome -- the entire complement of proteins including post-translational modification (Steen and Mann 2004). Unlike genomics, in which the problem is somehow constant due to the chemical's stable property of DNA, the existence of protein post-translational modification add variety in the set of proteins. Two approaches named top-down and bottom-up proteomics are used in the proteomics study. In the top-down proteomics process, proteins are separated

(mainly by 2D SDS-PAGE gel electrophoresis) and enzymatically digested into peptides. Peptides from each separate protein will be fed into tandem mass spectrometry analysis. A variation of the top-down approach is called "shotgun proteomics," in which proteins are first digested, then separated as peptides, prior to being fed into mass spectrometer (usually, separation and MS are combined together, such as LC-MS/MS) for protein identification (Washburn, Wolters and Yates 2001). In the bottom-up proteomics process, the protein mixture is digested and then directly sent to MS analysis -- without separation of proteins or peptides (Kelleher, et al. 1999).

2.3   Microfluidic Device for On-chip Proteomics

As mentioned in Section 2.1.2, protein PTMs serve as the biomarker of severe oxidative protein damage, which plays a fundamental role in human diseases (Rossi, et al. 2008). The accurate quantitative proteomics analysis of PTM will provide important information to characterize and help establish effective therapy to relate PTM to an oxidative stress induced disease such as AD. To obtain how oxidative pressure modifies protein by carbonylation, effective proteomic study on protein modification is needed.

The conventional proteomics process typically extracts protein from the biological sample: cells or tissues, followed by separation and detection by gel electrophoresis. Protein bands of interest will then be cut-out and the protein will be obtained via in-gel digestion, followed by MS analysis of the resulting peptide mixture. The conventional target proteomics process leads to protein/peptide loss and decreased purity. Because large samples with high purity are advantageous, gel-free proteomics can complement the existing methods well. In non-gel proteomic approaches, a large volume of solution is always used for separation. The required volume will also adversely affect

the efficiency of protein analysis. Other than low efficiency, traditional processes are also slow and labor intensive.

Although the conventional proteomics study methods have a wide application for protein purifications, those time and sample consuming experimental methods are restricting the further development of proteomics (Nägele, Vollmer and Hörth 2003). Compared with the conventional proteomic study methods, application of microfluidic device in proteomics study would provide in less time-consuming, less chemical consuming and possibly automatic protein sample cleaning, reduction, and digestion steps. Furthermore, the chemical/enzymatic reactions are performed and made more efficient by the enhanced concentration micro-scale environment. Another advantage of the microfluidic device is its low cost: current microfluidic device are made of polymers, and a small volume also grants smaller chemical consumption. The incorporation of microfluidic methods in PTM treatment experiments opens the door to a faster processing of low abundant samples such as biopsy tissues or single cells.

2.3.1   Fabrication of Microfluidic Device

The microfluidic devices used for biochemistry experiments or biosensors are originally fabricated in the silicon or oxidized silicon materials (i.e., glass). The fast development of silicon-based microfluidic devices are tightly related with the technology already extensively developed in the microelectronics industry such as photolithography, thin-film deposition, and anisotropic etching prior and around the 1990s. For the first time, under the possibility of precisely microfabrication methods, research interest in the territory of microfluidic sensor system has been vastly developed. For example, DNA electrophoresis arrays made of SiO_2 with photolithographic methods (Volkmuth and

Austion 1992), enzyme-immobilized column detecting glucose make of silicon and glass with anisotropic etching (Murakami, et al. 1993), gas chromatographic air analyzer fabricated on a silicon wafer with photolithography and chemical etching techniques (Terry, Jerman and Angell 1979), and microfluidic system for patterning neuron cells on silicon micromachined and chemical etched substrates (Martinoia, et al. 1999). Some of them are prototypes of current research interest in the microfluidic sensor, just with different materials.

However, silicon based materials' origin in microelectronics industry have limitations in the area of microfluidic sensors, such a slow and high requirements in the fabrication process (as of in in microelectronics industry, a clean room is usually required), time consuming bonding process (e.g. anodic bonding), and brittle, fragile and expensive material. After the 2000s, various substrates have been developed for the fabrication of the microfluidic based on different requirements (Freire and Wheeler 2006) (Shadpour, et al. 2006). For example, silicon oxide has been preferably used in areas such as capillary electrophoresis and electrochromatographyraphy (Jacobson, Koutny, et al. 1994) (Jacobson, Moore and Ramsey, Fused Quartz Substrates for Microchip Electrophoresis 1995), due to its high requirement of cleaning and limited surface modification potential (Silberzan, Leger, et al. 1991) (Silberzan, Perutz, et al. 1994). Compared with brittle glass or silicon substrates, polymer substrates are more versatile and can be shaped into the required structures by various techniques such as micromachining or hot embossing (Becker and Locascio 2002) (Stachowiak, et al. 2003). Furthermore, the cost to make polymeric microfluidic devices is substantially lower than the glass or silicon counterparts.

Polymeric microfluidic chip systems have been developed extensively in recent microfluidic studies (Duffy, et al. 1998) (Becker and Locascio 2002) (Sun, et al. 2007). In this study, poly(methyl methacrylate) (PMMA) was used as the substrate of the microfluidic device due to its potential for chemical and the various modification possibilities of methyl ester function group on the surface of PMMA substrate (McCarley, et al. 2005) (Adams, et al. 2008). This feature could lead to surface modification pathways of variety, for example, carboxylic acid modification (Wei, et al. 2005) or amine modification (Henry, et al. 2000), which potentially lead to flexible and various usages.

2.3.2   Proteomics in Microfluidic Devices

2.3.2.1   Sample Purification

Two successive major targets need to be accomplished for the "wanted" protein sample: (1) to extract the proteins of interest from the biological sample and (2) to remove salts and other impurities from the protein sample. The microfluidic device usually provides solid-phase extraction, in which analytes are "captured" on stationary phase. Various surface modification methods are developed based on related based substrate, target proteins and other specific requirements via the hydrophobic, the electrostatic and/or the affinity interactions methods. Aldehyde is widely used as a crosslinker to covalently bind protein onto glass (Zhu, et al. 2001) or PDMS surfaces (Sandison, et al. 2010). Affinity molecules could also be used on the microfluidic devices to provide strong, highly specific and low background protein collection. In detail, specifically purify biotinylated proteins by the avidin functionalized microfluidic device (Orth, Clark and Craighead 2003), or purify Hisx6 tagged proteins by the Ni-NTA

functionalized microfluidic device (Zhu, et al. 2001). Other substrates used to enrich

protein or peptides include gold-coated silicon surface (Houseman, et al. 2002), thin

layered agarose film on glass substrate (Afanassiev, Hanemann and Wölfla 2000) and

polymers via layer-by-layer techniques (Rao, Anderson and Bachas 1999) (Katsuhiko,

Takashi and Tsuyoshi 2006). Other than solid-phase extraction of proteins, the solid-

phase is also used to remove impurities from analytes. For example, polymeric

membranes such as polyvinylidene difluoride (PVDF) are used to produce high surface-

area solid-phase extraction phases, which could be used for protein desalting prior to ESI-

MS (Lion, et al. 2003).

Chapters 3 and 4 focus on the methodology of purification of specific protein

target (PTM proteins, especially carbonylated proteins) via the method of solid-phase

extraction. In the microfluidic device with monolithic microposts, antibodies or affinity

molecules were immobilized to selectively purify tagged proteins from a mixture.

2.3.2.2   Protein Separation

Compared with the widely used one- or two-dimensional gel electrophoresis as

conventional proteomics method, which is considered time-consuming and labor

intensive (Chen, Wu and Mao 2002), the microfluidic devices provide the possibility for

fast, high throughput and automatic protein analysis system. Moreover, in a microfluidic

device, the problem of protein purification is basically avoided compared with the

conventional method.

A typical research topic on microfluidic protein separation is microscale

electrophoresis. Isoelectric focusing (IEF) on the chip has been described (Figeys and

Pinto 2001). Moreover, as a work under the spotlight, various microchip 2D

electrophoresis systems under a different methodology for protein separations have been recently developed. Osiri et al. developed a 2D SDS μ-CGE and micellar electrokinetic chromatography (MEKC) electrophoresis system on PMMA substrate (Osiri, et al. 2008), while Yang et al. reported a 2D electrophoresis system using IEF and PAGE as first and second dimension, respectively (Yang, et al. 2009). Ross and coworkers have also developed a system of 2D separations on a 1D chip, which combines gradient elution moving boundary electrophoresis (GEMBE) and chiral capillary zone electrophoresis (CZE) (Ross, et al. 2010). Although electrophoresis experiments are all of somewhat quantitative, those 2D microfluidic electrophoresis methods that emphases on quantitative study have been developed. Xu et al. have developed an on chip system that separates samples by MEKC in the first dimension and by CZE in the second, which could separate 20 kinds of standard amino acids under 20 minutes, as shown Figure 2-3 (Xu, et al. 2009).
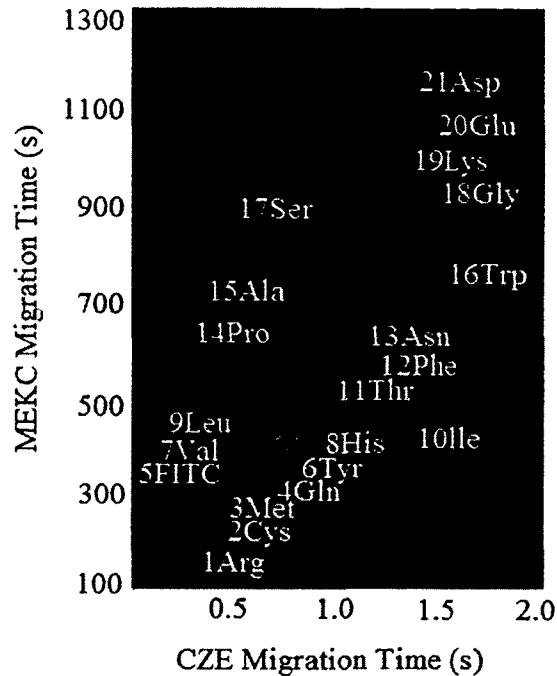
Figure 2-3: Standard amino acid samples being separated with MEKC and CZE 2D electrophoresis system developed by Xu et al. (Xu, et al. 2009).

Another method that is widely applied to protein separation experiments other than electrophoresis is chromatography, which is one of the most powerful separation techniques in protein analysis work (Faure 2010).

A simplest microfluidic chromatography is to integrate a stationary phase by coating the channel walls of the microfluidic device with interacting solid phase. Research frontier based on this very simple chromatography has two major directions. The most direct idea is increasing the available wall surface. For example, fabricate pillar-type structures in the microchannel of the microfluidic device. This target could become a reality on some of the materials. Some of the examples of this idea are mentioned in Section 2.3.1, pillar structures could be fabricated on PMMA materials by hot-embossing (Becker and Locascio 2002) (Stachowiak, et al. 2003), on PDMS materials by soft lithography (Whitesides, et al. 2001), on a silicon wafer by the well-

developed wet or dry etching methods, and on a glass or metal substrate by

micromachining (Martinoia, et al. 1999).

A more conventional idea to prepare stationary phase for the microfluidic

chromatography is to fill the microchannels with externally prepared material. Figeys's

group has developed a "proteomic reactor" by filling the strong cation exchange (SCX)

beads into the capillary tubing, in which proteins will bound to the beads at low pH and

digested at high pH where trypsin enzyme was activated (Ethier, et al. 2006), as shown in

Figure 2-4. The commercially available Agilent HPLC-Chip, which is made of polyimide

and packed with slurries of conventional silica particles, is able to provide a smooth

connection between on chip liquid chromatography and MS (LC/MS) (Yin and Killeen

2007).
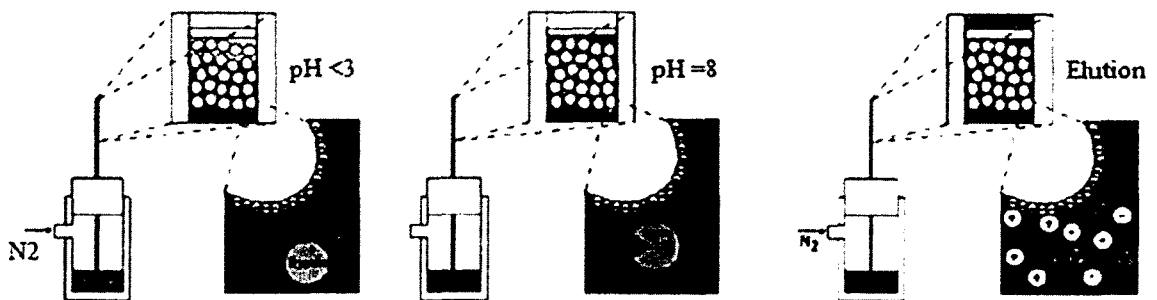
Figure 2-4: Left: Schematic representation of the proteomic reactor. The protein and trypsin are bound to the SCX material. Middle: Trypsin is activated by adjusting the pH to eight. The flow was stopped to let the digestion proceed without losing peptides. Right: Peptides were eluted by using an ammonium bicarbonate solution. (Ethier, et al. 2006).

2.3.2.3   Enzyme Digestion

Microfluidic devices are also developed to avoid the labor intensive and time

consuming process of conventional in-gel digestion process. Following the idea

mentioned in the last section, the microfluidic device with a trypsin functionalized

surface in the microchannel that has a built-in pillar (Lee, Soper and Murray 2009) or

monoliths developed on the glass (Peterson, et al. 2002) have been described. Also,

trypsin-coated microparticles are being packed into the microchannels for digestion

(Wang, et al. 2000). A more well-integrated system is the above mentioned "proteomic

reactor" from Figeys group, by which separation and digestion are accomplished in one

system (Ethier, et al. 2006).

2.4   Simulation

2.4.1   Overview

As mentioned in Section 2.3.2, application of a microfluidic device to proteomics

study would provide a less time-consuming, less chemical consuming, low cost, more

efficient, and possibly automatic protein sample cleaning, reduction, and digestion

method. Microfluidic devices are widely used to identify disease susceptibility prior to

the appearance of physiological symptoms. Protein targeting microfluidic systems have

been developed for immunoassays of rapid saliva-based clinical diagnostics (Herr, et al.

2007), chip-based oral cancer screening (Ziober, et al. 2008), and embryo metabolism

measurement (Griffiths 2008). The microfluidic devices based on affinity interactions

selectively capture target molecules with the affinity-based functionalized surface, and

provide quantitatively and/or qualitatively analysis of specific protein molecules and

nucleotide sequences (Rogers 2000) (Mark, et al. 2010).

2.4.2   Modeling

In a microfluidic device, a protein of interest in the solution will be absorbed onto

the inner surface of the microchannel. This process can generally be separated into two

steps (Lionello, et al. 2005): (1) the protein in the solution diffuses toward the protein-

absorbing surface, and (2) the protein is absorbed onto the surface, and simultaneously some proteins on the surface are desorbed. When the adsorption step is much faster than the diffusion, the process is diffusion controlled. When the diffusion step is faster, the process is surface reaction controlled (depending on absorption/desorption constant) (Dulm and Norde 1983).

A variety of factors such as protein shape, protein orientation on the surface, and properties of the surrounding environment, and protein and surface (Norde 1986) (Haynes and Norde 1994) affect the protein absorption. Those factors dictate the strength of different interactions between the protein and the surface, which include hydrophobic interactions, repulsive and attractive ionic or electrostatic interactions, and weaker interactions such as hydrogen bonding and van der Waals interactions (Norde 1986). The rates of protein adsorption and desorption depend on the absorption and desorption reaction constants, respectively, which in turn depend on both the protein and the surface. To simplify the problem, the Langmuir isotherm model is used, which is widely used to describe the surface-protein absorption/desorption process (Lundström 1985) (Andrade and Hlady 1986) (Skidmore, Hortsmann and Chase 1990). The Langmuir isotherm model states the relationship between the proteins and the surface by the "active sites" coverage and absorption/desorption reaction constants, which avoided the specific properties of the protein and the substrate, and refocus the analysis with a more common point of view on the design of the microfluidic device itself.

Another important process that affects the microfluidic device is protein diffusion. Diffusion time is a major consideration in the design of the micro-scale microfluidic device. Under a wide variety of conditions, the diffusion velocity of proteins in the

solution is relatively constant. For example, the widely used antibody protein IgG

requires about three and a half hours to diffuse for 1 mm (Dodge, et al. 2001). Most

analytes of interest are smaller than IgG, and hence diffuse somewhat faster.

2.4.3   Effect of Geometric Parameters

Geometric parameters have been widely studied for their effect on heat transfer.

Heat fins, for example, are a major consideration in heat flow optimization (Cobble

1971). Heat exchangers (Tsai, Sheu and Lee 1999) and heat sinks (Grannisa and

Sparrowb 1991) for optimization and enhancement of heat flow have also been widely

studied. Although geometric optimization for an improved transport has not been

extensively used in protein enrichment related microfluidic device, practical work that

increases the available wall surface has been published, as indicated in Section 2.3.2. For

example, pillar-type structures in the microchannel of the microfluidic device (Lee, Soper

and Murray 2009), and pack silica particles in the microfluidic device (Figeys and Pinto

2001) can directly increase the surface area. Given that the amount of protein captured in

a microfluidic device depends on absorption and diffusion and that both of these

processes depend on geometric features, geometric optimization in protein enriching

microfluidic devices is likely to enhance performance greatly. Therefore, simulations will

be performed to examine these geometric effects.

CHAPTER 3

AVIDIN-FUNCTIONALIZED CHROMATOGRAPHY ON PMMA MICROFLUIDIC DEVICE FOR LOW ABUNDANT POST-TRANSLATIONAL MODIFIED PROTEIN ENRICHMENT

3.1   Introduction

This chapter focuses on the design, surface modification, and both qualitative and

quantitative characterizations of a microfluidic microposts-structured PMMA chip.

Specifically, a brass mold master was prepared using micromilling and subsequently used

to replicate polymer microposts via hot embossing. The avidin-affinity microchip is

accomplished by surface modifications involving carboxylic acid modification by UV,

followed with EDC/NHS-mediated carboxyl-to-amine crosslinking between PMMA and

avidin. This avidin terminated PMMA chip allows the enrichment of carbonylated

proteins from biological samples injected by a pressure-driven flow and further provide

samples for proteomic study on aging and Alzheimer's Disease. Micropost arrays were

used to increase the encounter rate between functionalized avidin substrate and

biotinylated carbonylated proteins in the streamline, and further improve the enrichment

process. Various techniques including atomic force microscopy, X-ray photoelectron

spectroscopy and fluorescence microscopy were incorporated to characterize the PMMA

surface topography, surface functional group mapping, and elemental composition

changes after each modification step of the treatment process. In addition, a quantitative

study of biotinylated carbonylated protein capture recovery and elution efficiency of the device was investigated. To validate the performance of the chip, we used *in vitro* carbonylated standard proteins bovine serum albumin (BSA). This device requires a significantly less sample -- approximately 106 fold less than the current commercial avidin column, making it useful for any biological experiments or analysis requiring avidin affinity enrichment. Also, this microdevice can be readily translated for fractionation of other PTMs proteins, as long as they can be biotinylated tagged. Therefore, this microfluidic affinity enrichment analysis device will provide an accurate tool for dynamic analysis of low abundant protein modifications in a wide range of PTMs, other than the carbonylation described here.

3.2   Method and Materials

3.2.1   <u>Reagent and Materials</u>

PMMA used as the coverslip and microfluidic device substrate were purchased from GoodFellow (Berwyn, PA). Chemicals used for PMMA surface modification assays including 1-ethyl-3-[3-dimethylaminopropyl] carbodiimide hydrochloride (EDC), N-hydroxysuccinimide (NHS), avidin were purchased from Fluka (Steinheim, Germany) and Thermo (Rockford, IL), respectively. MES monohydrate was purchased from Alfa Aesar (Ward Hill, MA). Albumin bovine serum was purchased from Sigma-Aldrich (St. Louis, MO). Biotin Hydrazide and Sodium cyanoborohydride that were used for biotin-derivatization of protein carbonylation were purchased from Sigma-Aldrich (St. Louis, MO). Standard RC dialysis tubing of 3.5 K MWCO was purchased from Spectrum Labs, INC (Greensboro, NC). Fluorescent dye 3-(2-furoyl)-quinoline-2-carboxaldehyde (FQ) was purchased from Invitrogen (Madison, WI). Fluorescein Biotin was purchased from

Biotium, Inc. (Hayward, CA). Fluorescein Biotin was prepared in 0.4 M stock solution in phosphate buffered saline (PBS) buffer and was stored in the dark at -20° C in vials which contain 150 μl stock solutions each. BCA protein kit was purchased from Pierce to measure protein concentration.

Syringe pump were purchased from Next advance (Averill Park, NY, USA). Adapters and capillary tubes which were used to connect the syringe and microfluidic device were purchased from IDEX Health & Science LLC (Oak Harbor, WA) and Polymicro Technologies (Phoenix, AZ), respectively. Epoxy glue used to glue the capillary tube with the microfluidic device was purchased from Henkel Corporation (Rocky Hill, CT).

3.2.2   Fabrication of Microfluidic Device

A PMMA microfluidic channel containing microposts inside was used to enrich biotinylated carbonylated proteins. The pattern of the microchip is depicted in Figure 3-1. The micropost-filled channels are 24 mm long, 1.4 mm wide and 100 μm tall. The microchannel contained a circular array of microposts 100 μm tall and 50 μm in diameter with an average 100 μm between the microposts. A total of 3600 microposts was incorporated within a surface area of 114 mm² for capturing the biotinylated carbonylated BSA. The pillars are arranged to maximize the possibility of proteins coming into contact with these functionalized microposts. If they were arranged in an array parallel to the flow direction, it was predicted that the protein would follow the streamline between the microposts and have little chance of contacting the microposts. However, this staggered pattern forces proteins to change their trajectory and hence enhance the encounter rate with the microposts and further improve protein capture recovery.
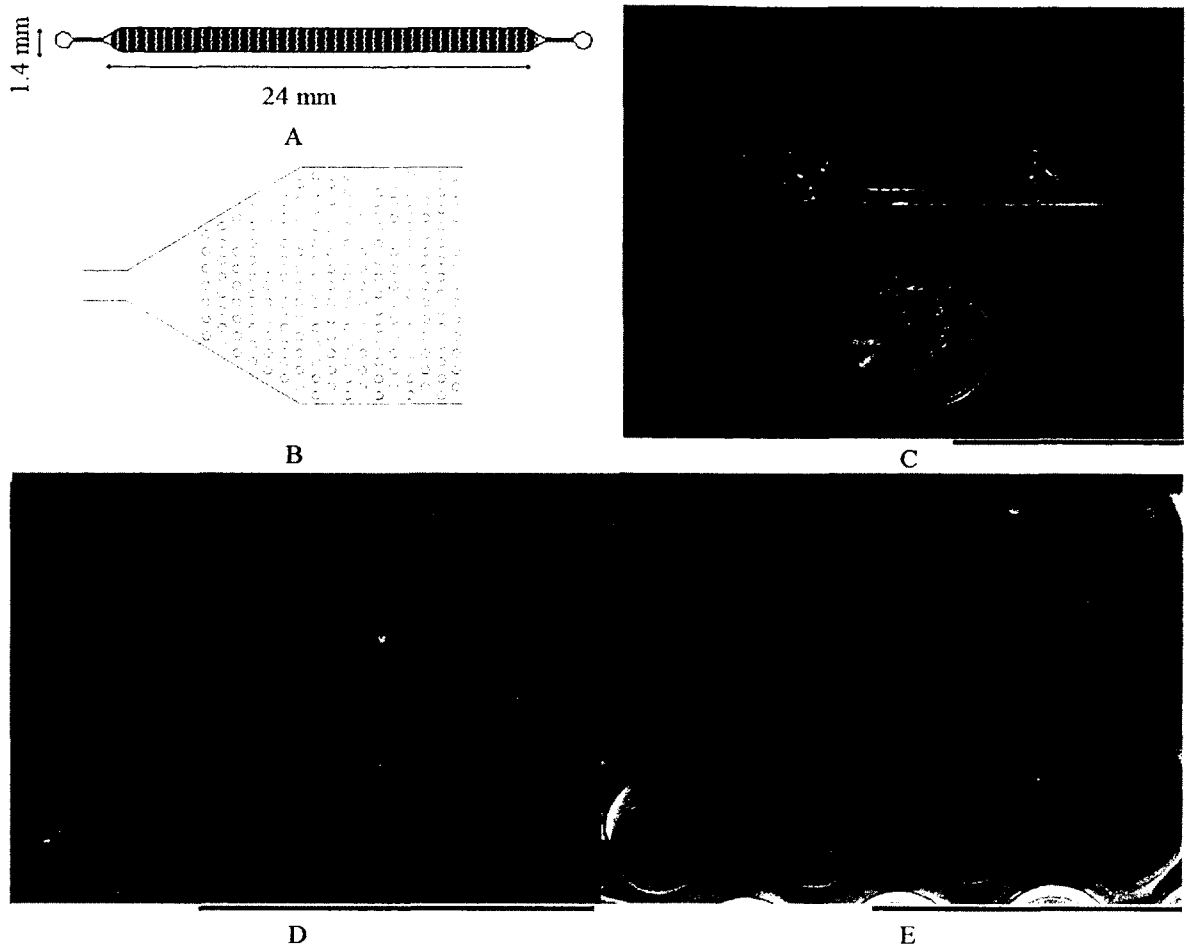
Figure 3-1: Solid-Phase microfluidic device: geometry and configurations. A. Details of the microchannel, 1.4 mm in width, 0.1 mm in depth and 24 mm in length; B. 3600 microposts of 50 μm diameter is arrayed inside of channel; C. Actual microfluidic device (scale bar is 4 cm); D-E. Scanning electron microscope (SEM) images showing the microposts (scale bar for Figure 3-1D is 1 mm and for Figure 3-1E is 200 μm).

3.2.2.1   Mechanical Process

The process flow of the mechanical fabrication steps of the microfluidic device is shown in Figure 3-2. In detail, a mold master was prepared using micromilling and subsequently used to replicate polymer microparts via hot embossing (Soper, et al. 2000) The microfluidic post array was designed using computer-aided design software. The brass plate was first cut into a 5 mm thick and 12 cm diameter circle and the

aforementioned patterns were then milled with a micro-milling machine (MNP 2522,

KERN Micro-& Feinwerktechnik GmbH & Co. KG, Germany) to generate the mold

master.
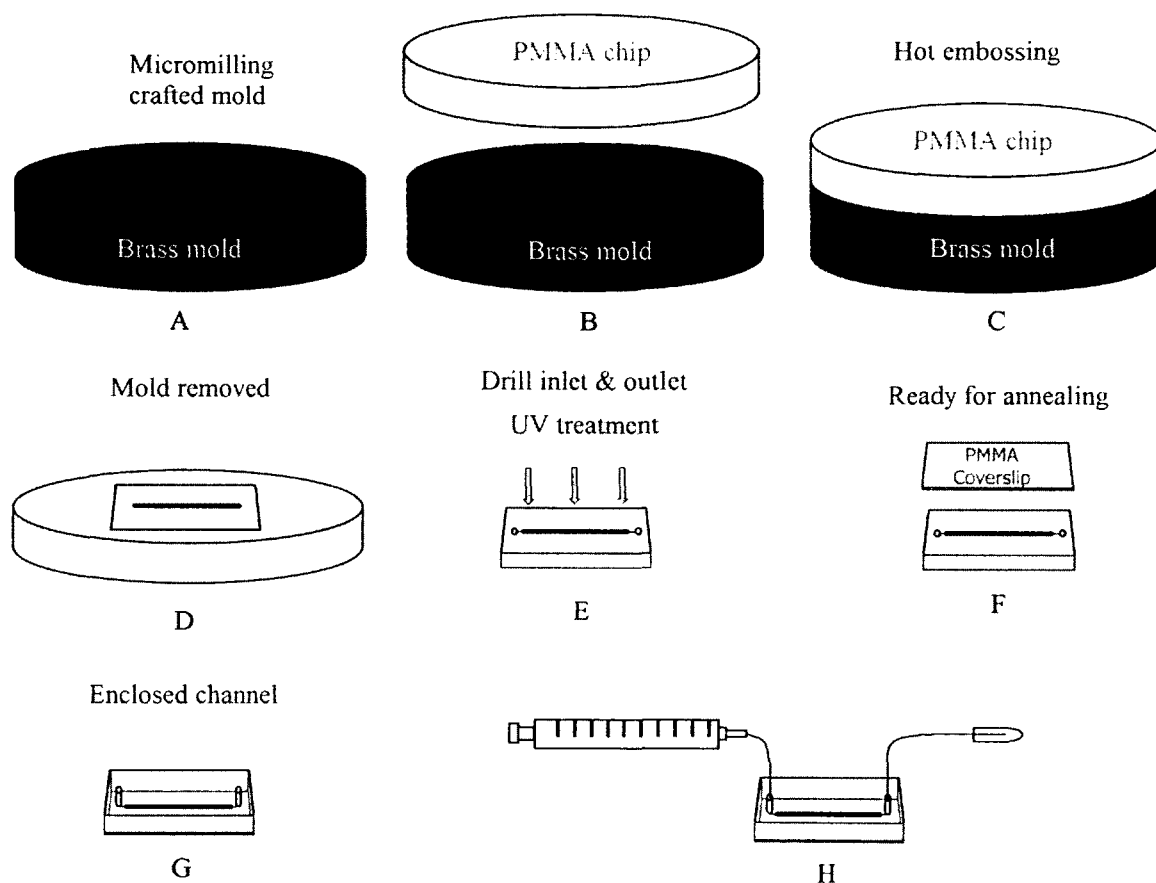
Figure 3-2: A. The mold master is crafted by micromilling a contrary structure of the microchannel with microposts on brass; B-C. The mold master is used to replicate PMMA polymer microparts via hot embossing; D. After the mold is removed, the micropost pattern is left on PMMA chip; E. After hot-embossing, the microchip is cut from PMMA substrate, with inlet and outlet drilled. It is then cleaned and treated with UV before consecutive surface modification; F-G. A PMMA coverslip is annealed on the top of the microchannel to form an enclosed structure; H. After annealing, silica capillary tubes were glued to the annealed microchip by Epoxy glue on both inlet and outlet ports, and the micro-device is ready for further chemical treatments.

The micromilling process was accomplished at 40,000 rpm and a feed rate of 10-

20 mm/minute using a 50 μm carbide bit (McMaster-Carr or Quality Tools, Hammond,

LA). This process was monitored by an optical microscope (Zoom 6000, Navitar, Rochester, NY) and a laser measuring system (Laser Control NT, Blum-Novotest GmbH, Germany) was employed to determine the tool length and radius. After milling, the mold master was polished using a 3 μm grain size polishing paper (Fibrmet Discs-PSA, Buehler, Lake Fluff, IL). Additionally, burrs at the surface of the microstructures were removed by a polypropylene cloth (Engis, Wheeling, IL) with a 1 μm diamond suspension (Metadi Diamond Suspension, Buehler).

The microfluidic channels on the PMMA chip were fabricated using hot embossing methods previously reported (McCarley, et al. 2005) (Lee, Soper and Murray 2009). Briefly, the structure of the microchannel is replicated by HEX 02 hot embossing system (Jenoptik Mikrotechnik, Germany) with the brass mold master hot-embossed on the PMMA substrate. During embossing, the molding die was heated to 155° C and pressed into the PMMA substrate a force of 950 PSI for 150 seconds. The master was rapidly cooled to just below 155° C prior to removal from the mold.

3.2.2.2   Chemical Surface Modification

After hot-embossing, the microchip was cut from PMMA substrate and washed by 10% surfactant and IPA solution and DI water by sequence and then gently dried under nitrogen. The avidin immobilization method is based on PMMA carboxylic acid modification via UV treatment and carboxyl-to-amine crosslinking chemistry (McCarley, et al. 2005) (Lee, Soper and Murray 2009). Figure 3-3 demonstrated individual modification steps taken for avidin-biotin mediated coupling of carbonylated proteins to PMMA attachment sites of the microchips.
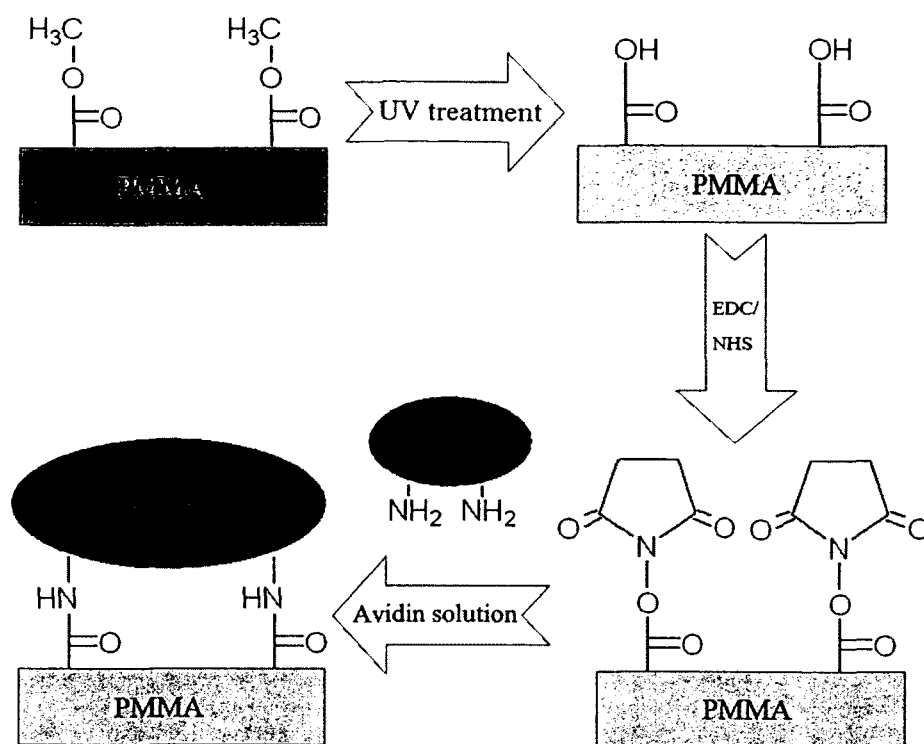
Figure 3-3: PMMA surface modification to generate avidin-terminated microchip for affinity chromatography.

In order to generate the carboxyl group on the surface of the PMMA substrate, the microfluidic chip and same sized 0.25 mm PMMA cover slip were exposed to a 254 nm UV lamp at 16 mW·cm^{-2} for 30 minutes (Wei, et al. 2005). The UV modified substrate and cover slip were clamped together between two glass plates and heated in the oven (101° C 30 min) to anneal the substrate with the coverslip to form an enclosed microfluidic channel. After annealing, 200 μm inner diameter silica capillary tubes were connected to a syringe that will be glued to the annealed microchip by Epoxy glue on both inflow and outflow ports.

To generate avidin functional groups on PMMA, the UV modified channels were chemically treated with a mixture of 5 mM 1-ethyl-3-[3-dimethylaminopropyl]

carbodiimide hydrochloride (EDC) and 5 mM N-hydroxysuccinimide (NHS) solution for

15 minutes. Avidin was then immobilized on the surface of the UV modified

microchannels by flowing 1.36 mg/mL avidin solution prepared in PBS buffer (pH 7.4)

through the microfluidic channel for two hours with a flow rate of 2 μl/minute.

3.2.3 Protein Sample Labeling and Purification

3.2.3.1 *In vitro* Carbonylation of BSA

BSA was oxidized with a hydroxyl radical-generating system consisting of

ascorbate/Fe(III)/O_2 (Requena, et al. 2001). Briefly, BSA was dissolved in 1 mL of

oxidation buffer (50 mM HEPES, 100 mM KCl, 10 mM $MgCl_2$, pH 7.4) to make a 10

mg/mL solution. Oxidation was carried out by adding ascorbate and $FeCl_3$ to a final

concentration of 25 mM and 0.1 mM, respectively, and incubating overnight at 37° C,

while constantly shaking. After incubation, the oxidation was stopped by the addition of

EDTA to a final concentration of 1 mM. The reaction mixture was dialyzed overnight

against oxidation buffer containing 1 mM EDTA at pH 7.4 (Requena, et al. 2001) (Feng

and Arriaga 2008).

3.2.3.2 Determination Carbonyls with DNPH Assay

The carbonyl content of MCO-BSA was determined using the well-established

DNPH spectrometry method, according to the procedure described by Levine (R. L.

Levine 2002). Briefly, 500 mL of 10 mM, DNPH in 2 M HCl was added to 100 mL of

oxidized BSA solution. The mixture was allowed to stand at room temperature for one

hour. After the reaction, TCA was added to obtain a concentration of 10%. Then, the

mixture was incubated on ice for 30 minutes after which the solution was centrifuged at

11000 g for three minutes; the supernatant was discarded. The pellet was washed three

times with ethanol–ethyl acetate (1:1), and the precipitated protein was redissolved in 6

M guanidine. The carbonyl content was calculated from the absorbance of the DNPH

derivative at 375 nm (molar absorption coefficient, 22000 $M^{-1}cm^{-1}$).

3.2.3.3 Biotinylation of Protein Carbonyls

In vitro oxidized BSA proteins were chemically labeled with biotin hydrazide

using modified procedure by Yoo (Yoo and Reginer 2004). The biotinylation of

carbonyls in oxidized BSA allowed subsequent biotin-avidin enrichment via affinity

based microchip. Biotin hydrazide binds to carbonyl groups through the hydrazide group

(–NH-NH$_2$), forming a hydrazone linkage. A volume of 1 mL of oxidized BSA (2.5

mg/mL) was incubated with 1 mL of 10 mM biotin hydrazide in DMSO at 37° C for two

hours with shaking. To stabilize the Schiff reaction product, 2 mL of 30 mM sodium

cyanoborohydride in PBS buffer was added and the mixture was cooled down to 0° C on

ice for 40 minutes. To remove the unreacted and excess biotin hydrazide and SDS, the

prepared sample underwent dialysis three times (four hours/each time) against PBS

buffer. After removal of the excess biotin hydrazide, the biotin derivatized carbonylated

BSA stock solution is ready for the avidin-affinity based enrichment in the microchip and

the final concentration of biotinylated carbonylated BSA was further identified using

protein assay.

3.3 Testing the Microfluidic Device

Surface properties of PMMA for each modification step of the treatment process

(as shown in Figure 3-3) were systematically investigated qualitatively and quantitatively

by water contact angle measurement, atomic force microscopy (AFM), X-ray

photoelectron spectroscopy (XPS), and specific functional group labeling using fluorescence microscopy.

3.3.1 Surface Modifications Examination

Water contact angle of PMMA substrate that have been treated by UV modification and control have been measured with optical contact angle system OCA 15 goniometer from Future Digital Scientific Corp (Garden City, NY, USA). In the water contact angle experiment, 1 μL 18 MΩ RO water droplet is dropped and water contact angle is measured by a digital video camera and the controlling software, which is provided by the manufacturer, for three times on pristine and UV treated PMMA substrates. The UV treatment is done by exposing the pristine PMMA substrate under 16 mW/cm^2 UV for 20 minutes.

3.3.2 Surface Topology Characterization

AFM studies were performed with a commercial instrument (Nanosurf easyScan 2 equipped with a TFT-LCD display) operating in contact mode, using Silicon SPM-Sensor (NanoWorld, Neuchâtel, Switzerland) with 0.2 N/m spring constant and 13 kHz response frequency. The detector is of 2 μm thick, 450 μm long, and 50 μm wide. The detector side is ammonium-coated. All images were recorded in air at room temperature, at a scan speed of 1.4 Hz. The background slope was resolved using the program provided by the manufacturer. No further filtering was performed. The surface topographies over a 20 μm × 20 μm of area of the pristine, UV modified, EDC/NHS treated, avidin immobilized and biotinylated carbonylated protein captured PMMA materials were analyzed individually. Surface roughness (root-mean-square over area) was calculated by the software provided by the manufacture. The three-dimensional

images were obtained by SPIP software version 5.1.5 from Nanoscience Instruments, Inc. (Phoenix, AZ, USA).

3.3.3   Surface Elemental Composition Profiling

PMMA sheets of 250 μm thickness from Goodfellow were used in the surface function characterization using both Atomic Force Microscopy (AFM) and X-ray photoelectron spectrometer (XPS). To evaluate the changes in compositions and functional groups in PMMA after each four modification steps including (1) UV radiation, (2) EDC/NHS treatment, (3) avidin attachment, and (4) capture of biotinylated carbonylated BSA, the polymer surfaces were analyzed with an Axis 165 X-ray photoelectron spectrometer (Kratos Analytical) with monochromatized Al Kα (1486.6 eV) X-ray source at 150 W power.

3.3.4   Fluorescence Validation of Surface Modification

To test the chemical treatment effect, avidin immobilization and biotinylated protein captured on the surface onto PMMA substrate surfaces, a series of fluorescence experiments was used to evaluate different surface modification reactions. PMMA sheets were viewed with an Olympus IX51 inverted microscope (Olympus Corporation, Tokyo, Japan), using Plan N 10X objective (NA: 0.25) and a WHN 10X eye piece. EXFO X-Cite 120 mercury vapor arc lamp from Lumen Dynamics (Mississauga, Canada) was used as the fluorescence source, band-pass filters of 488 nm-535 nm (green) and 535 nm-615 nm (red) were used to choose s supposed fluorescence wavelength. A CCD camera was used for image recording. This camera provides a 1360 × 1024 pixel (1.4 million) image. Images were analyzed using software DPController version 3.2.1.276 from Olympus Corporation.

3.3.4.1   Fluorescence Mapping of Immobilized Avidin

To confirm the biochemical functionality and uniformity of carboxylic acid layers

on PMMA, surfaces prepared on bare PMMA substrates from UV radiation at 254 nm

and EDC/NHS pretreatment were labeled with 1.36 mg/mL of 3-(2-furoyl)-quinoline-2-

carboxaldehyde (FQ) labeled-avidin for two hours at room temperature. For the long term

use, FQ was initially dried and stored in the dark at -20° C in vials which contain 200

nmol FQ each. For FQ labeling of avidin, 200 nmol FQ were dissolved in 10 μl of 10

mM potassium cyanide (KCN) solution. After chemical treatment of EDC/NHS solution,

the PMMA substrate was covered with FQ-labeled avidin solution (20 μM) for two hours

at room temperature, and then rinsed carefully with DI water three times. After drying,

the prepared sample was studied with an excitation wavelength of 480 nm and 2.5

seconds of exposure time. Fluorogenic reagent FQ in the presence of a nucleophile (CN-

), which fluoresces only upon covalent binding to the protein primary amide group (-

NH_2) (Michels, et al. 2007). When binding on protein, FQ absorbs blue light at 490 nm

and emits red fluorescence at 525 nm.

3.3.4.2   Validation of Biotinylated Proteins Capture

The avidin terminated microposts were used to capture biotin hydrazide-labeled

carbonylated protein. To evaluate the binding reaction between biotin with captured

avidin on the PMMA chip, PMMA with immobilized avidin were immersed with 0.4 M

fluorescence-labeled biotin (Biotin-4-Fluorescein, B4F). After 30 minutes incubation at

room temperature, the samples were then washed with DI water three times and air-dried.

The samples were studied under fluorescence microscopy using a wavelength of 516 nm

with the exposure time of one second. B4F absorbs blue (Ex: 488) light and emits green

fluorescence (Em: 516). The control experiment was performed by omitting the avidin

treatment step prior to B4F incubation. Also, to investigate the nonspecific binding

between biotin with PMMA surface, we performed a control experiment by replacing

avidin with native BSA before the incubation with B4F.

Additionally, FQ-labeled biotinylated carbonylated BSA were used to investigate

the capture event with avidin-based affinity enrichment inside the microchip. After

chemical treatment of the EDC/NHS solution, avidin-modified PMMA surfaces were

immersed in (20 µM) biotin derivatized BSA solution in PBS for two hours at room

temperature, and then the samples were rinsed extensively with DI water and air-dried.

The fluorescence image was taken with an excitation wavelength of 525 nm and of 2.5

seconds of the exposure time.

3.4 Quantitative Examination of the Microfluidic Device

3.4.1   Quantization of Capture Recovery

The purification efficiency of the biotinylated carbonylated BSA by affinity

chromatography on the avidin-functionalized microchip was investigated. Specifically,

the capture efficiency is to find out how much carbonylated protein was captured by the

avidin-modified microfluidic channel. The capture efficiency is defined as Eq. 3-1:

$$Capture\ Recovery = 1 - \frac{amount\ of\ eluted\ protein\ inflow\ through}{injected\ protein\ amount}.$$

Eq. 3-1

A syringe pump of 5 µl/minute flow rate was used to inject FQ labeled

biotinylated carbonylated BSA solution (6.25 µg/ml) flow through the avidin-

immobilized microfluidic channel. The total injection time is 24 minutes. In a previous

study by Edel's group, 1.5 µl/minute flow was used as the optimal flow rate to study

biotin-streptavidin binding kinetics in the microfluidics with comparable dimensions for

this thesis (Srisa-Art, et al. 2008). For the case of biotin-avidin binding is stronger than

that of biotin and streptavidin (Wilchek and Bayer 1990), 5 µl/minute is used as the

volume flow rate to test capture and elution efficiency. A volume of 5 µl of flow through

for every minute was collected for consecutive spectrophotometric assay of FQ using

Nanodrop 3000 at the emission wavelength of 570 nm. Figure 3-4 depicted the

experimental scheme on the quantification measurements of both capture recovery and

elution efficiency. A total of 24 points with FQ fluorescence intensity value at 570 nm

was used to evaluate the capture efficiency.
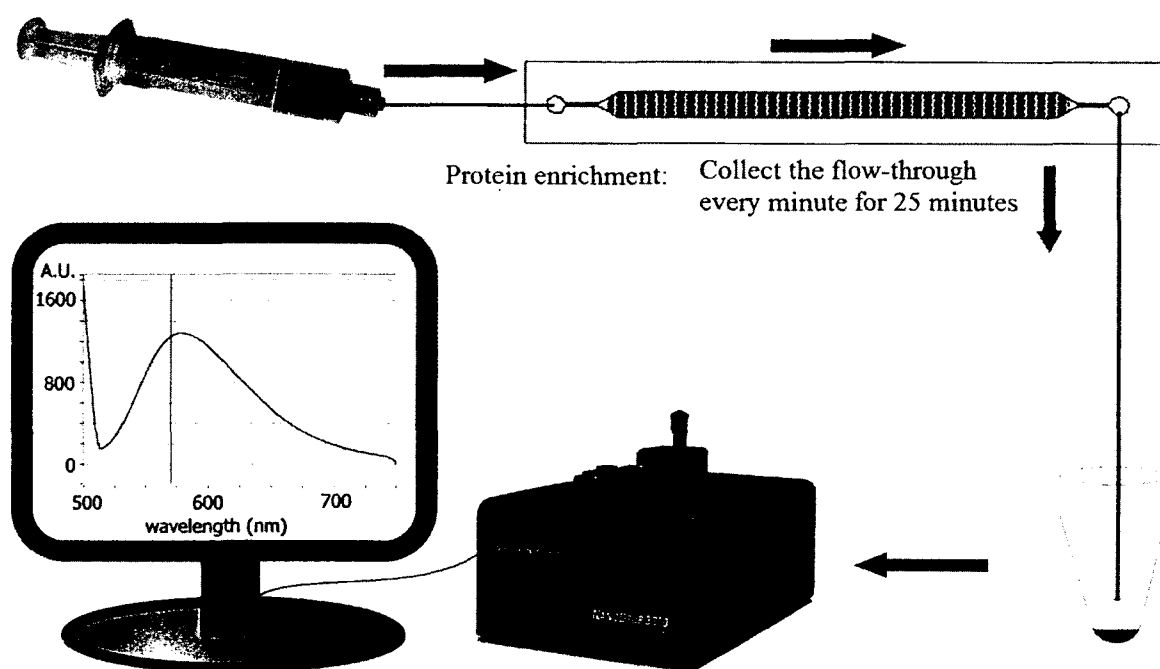
Figure 3-4: Experimental set up sketch of quantitative measurement of capture recovery and elution efficiency.

3.4.2   Quantization of Elution Efficiency

When the microfluidic channel was saturated by biotinylated carbonylated

proteins, elution efficiency was measured by injecting eluting buffer with flow rate of 5

µl/minute and the fluorescence intensities of eluted samples were measured using the

same procedure mentioned above every minute. The eluting buffer (0.4% SDS, 0.8%

methanol, 0.4% NaCl in water solution) was used to break avidin-biotin interaction by

denaturing proteins. After elution, proteins are stabilized and renatured by removing the

denaturing agent, SDS, through an Amicon Ultra-4 centrifugal filter unit (3500 Da MW

cut-off). Specifically, the sample was centrifuged a total of three times at 7500g for 20

minutes. The washing solvent was PBS buffer.

The eluting efficiency was further measured and defined as shown in Eq. 3-2:

$$elute\ efficiency = \frac{eluted\ protein\ amount}{captured\ protein\ amount}. \qquad \text{Eq. 3-2}$$

3.5   Results and Discussion

3.5.1   Surface Modifications Examination

As shown in Figure 3-3, the pristine PMMA substrate is covered with a $-CH_3$

group, which is hydrophobic, and the UV treated PMMA substrate is covered with –

COOH group, which is hydrophilic. As per the research from McCarley et al. the surface

concentration of carboxylic acid groups on PMMA increases strongly with exposure time

in UV treatment (McCarley, et al. 2005). To test the affection of UV modification on

PMMA coverslip/substrate, the water contact angle will be measured. The water contact

angle shows a decrease in water contact angle (or an increase in surface hydrophobicity)

on both PMMA chip and the substrate. The results obtained from this experiment are

shown in Figure 3-5 and Table 3-1. Water contact angle of pristine PMMA substrate is

approximately 70°, while more hydrophilic UV treated PMMA substrate has a water

contact angle of approximately 30°, which agrees with the referred study result well, in

which the water contact angle of PMMA substrate treated by 15 mWcm^{-2} UV for 20

minutes and the referred sample an control are 78° and 28°, respectively (Wei, et al.

2005).
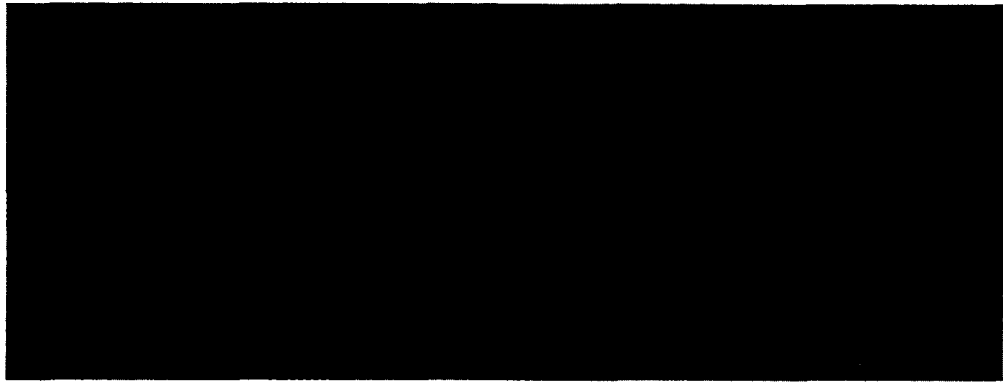
Figure 3-5: water contact angle compartment of a 1 μL 18 MΩ RO water droplet on pristine (left, ~70° of water contact angle) and 20 minutes UV treated PMMA coverslip (right, ~40° of water contact angle).

Table 3-1: Average water contact angle of pristine and 20 minutes of 16 mW/cm2 UV treated PMMA coverslip and substrate.

Substrate	UV modified coverslip	UV modified substrate	Pristine coverslip	Pristine substrate
Water Contact Angle (°)	30.87	38.83	75.66	76.52

3.5.2   Surface Topographic Analysis of Modified PMMA Substrate

Atomic force microscopy is most often used to characterize surface morphology

on the nanoscale. To investigate the change of each individual surface modification steps

on microfluidic channel surfaces, AFM was used to analyze the following five modified

PMMA surfaces: pristine, UV modified, EDC/NHS treated, avidin immobilized and

carbonylated protein enriched with their individual AFM images displayed in Figure 3-

6A-E. As indicated from the root mean square (rms) roughness summarized Figure 3-6F,

PMMA surfaces were slightly rougher after each step of surface modification, except the

UV treatment step.

Pristine PMMA sheet has a relatively uniform and smooth surface with a root-

mean-square (rms) surface roughness of 16.8 nm, which is consistent with previous

reports (Wei, et al. 2005). The roughness after UV modification was reduced to 6.8 nm.

It was previously stated that the roughness after UV radiation increases 50%. We highly

speculate that the discrepancy of the reported values is due to the extra IPA rinse step

prior to the AFM study in the previous report. The ester reaction occurs between alcohol

groups on IPA and carboxylic groups on the PMMA. Hence, after IPA wash, the surface

roughness increases compared without the wash.
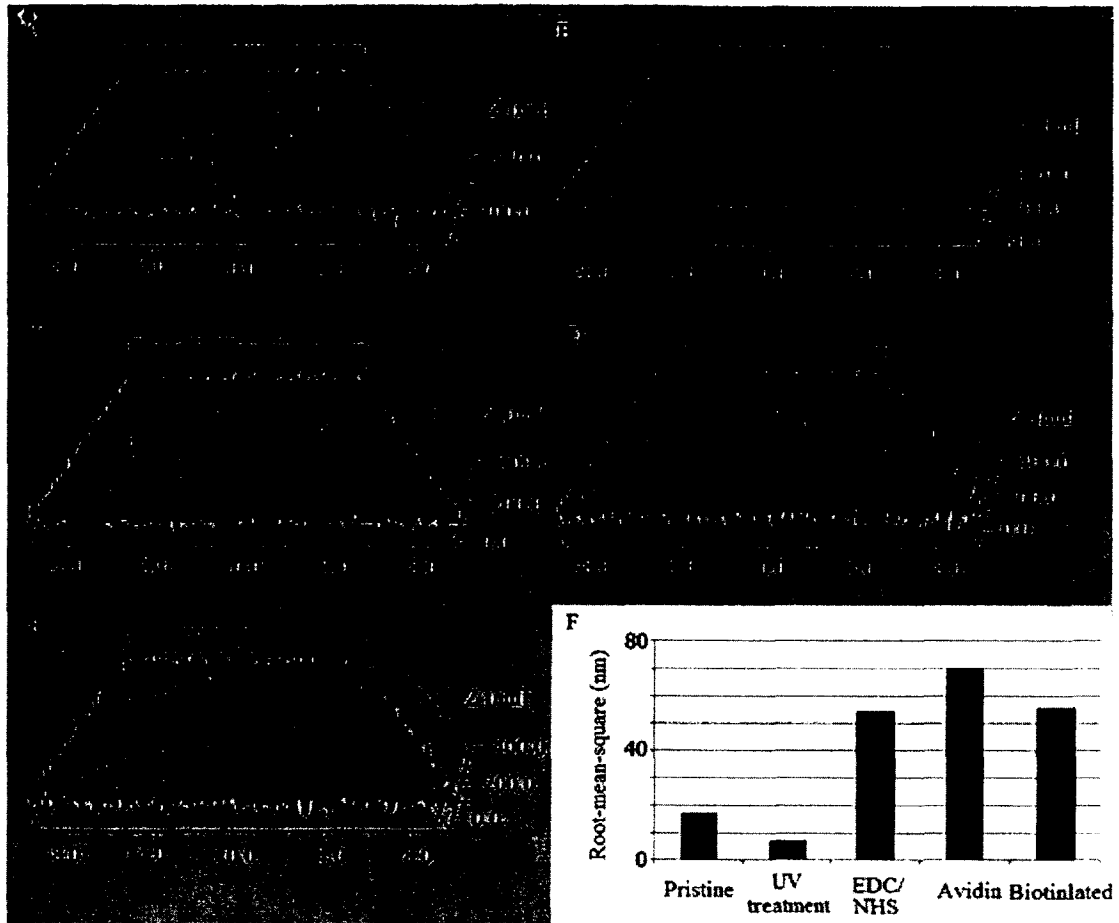
Figure 3-6: Surface topology of PMMA substrate under different chemical modification steps. The scan range for both images is 20 μm × 20 μm, and the Z-range is 200 nm. A-E. 3-dimontional map of pristine, UV treated, chemically treated, avidin coated and biotin carbonylated protein captured PMMA.

The average rpm surface roughness for the EDC/NHS treated PMMA sheet and the avidin coated PMMA sheet are 54.3 nm and 70.1 nm, respectively, which are 3.2 and 4.2 folds higher than that of pristine PMMA. Multiple studies about the surface roughness of PMMA substrate as a function of UV radiation time have been exploited in the last decade (Srinivasan and Lazare 1985) (McCarley, et al. 2005). An optimal condition to achieve the photochemical surface modification route (carboxylic acid

formation) was set for duration of 30 minutes UV under ambient laboratory atmosphere (McCarley, et al. 2005).

The noticeable increase of the surface roughness for the EDC/NHS treatment and avidin coating steps reflects the different chemical functional groups alternating on the PMMA substrate surface: carboxyl group after UV modification, succinimide group after EDC/NHS treatment, and peptides after avidin immobilization. For biotinylated carbonylated protein captured surface, we found a rms roughness of 55.5 nm. The observed roughness change indicates partially surface modification reactions at each step. We currently do not understand the direct relationship between various properties of function groups coated on the surface and the surface roughness. However, for the microfluidic device, an increase in substrate surface roughness upon each chemical modification treatment is desired due to the size of the device feature (50 μm for the smallest scale). Furthermore, the roughness magnifies the wetting and adhesion properties of a solid (Bico, Tordeux and Quéré 2001), so the totally increased surface roughness is slightly helpful among the interactions between solutions and PMMA substrates. The increased roughness of the surface further increases the contact surface area, providing more avidin tethered to PMMA and further increasing the capture efficiency of biotinylated modified proteins. On the other hand, the surface roughness could introduce the steric hindrance of the surface accessibility; and the steric hindrance will restrict the achievement of high bonding density (Kazakevich and LoBrutto 2007). Therefore, surface roughness can be a very critical parameter for the surface accessibility.

Previously, Edwards developed mathematical models and interpreted the binding rate constant obtained from the surface plasmon resonance biosensors to study the

occlusion event due to steric hindrance, In his study, the expression S, steric hindrance, represents the number of receptor sites occluded by the bound state at a particular point. It was shown that S is related to the association process, and it rises with increasing association rate, ka. If ka is very large, S reaches its finite asymptote with a value of 0.0028 s^{-1}. This is due to the fact that the reaction rate becomes infinitely fast, so the system becomes transport limited. On the other hand, if ka is too small, there has not been enough binding for occlusion effects to play a role (Edwards 2007). Based on Edwards' study, for our application of biotin-avidin binding with a relatively high association rate of 7×10^7 M^{-1}s^{-1} (Piran, Riordan and Silbert 1990), the steric hindrance is referred to as 0.0005 s^{-1}. Also, for the extremely low dissociation rate, like 7.5×10^{-8} s^{-1} for avidin-biotin (Piran, Riordan and Silbert 1990), steric hindrance plays a larger role in the reaction.

Additionally, Edward's work demonstrated that steric hindrance, S, varies with P, the volume ratio of ligand to receptor molecule. It indicates that increasing P enhances the steric hindrance accordingly. It was previously observed that the binding rate for the second biotin molecule was decreased due to steric hindrance (Buranda, et al. 1999). Hence, it is highly possible that when the biotin ligand molecules are larger than the spacing of the avidin receptor molecules in the zone, a single binding event will occlude multiple binding sites. Particularly in our application because biotin molecules were attached to carbonylated proteins, so it is possible that steric hindrance from the first biotin binding causes the lower binding kinetics in the second process. Due to the steric hindrance effect, molecules of various sizes could have different accessible surface area. When accounting for the steric hindrance, we speculate that larger biotinylated proteins

would experience higher steric hindrance, and therefore the protein binding and enrichment process might be compromised. With this speculation in mind, microdevices with longer and wider dimensions might be needed to counteract this steric hindrance effect to maintain the high capture efficiency for large molecules. Alternately, digestion of proteins into smaller peptides prior to the affinity chromatography on avidin-functionalized PMMA microchip might be advantageous to overcome the steric hindrance effect in future experiments.

3.5.3   Surface Elemental Mapping of Modified PMMA Substrate

Although the AFM results presented above reflected the potential surface modification reactions, more conclusive results are needed to prove the PMMA substrate surface have been successfully functionalized by steps. To prove the widespread existence of the supposed functional groups, XPS analysis was used to identify the elemental percentage on the surfaces of surface-modified PMMA substrate by steps. As shown in Table 3-2, the X-ray photoelectron spectrum of pristine and UV modified PMMA displayed two element's existence: carbon and oxygen. Furthermore, it is also noticeable that the Carbon/Oxygen ratio of UV treated sample has decreased by approximately 32% compared with that of the pristine PMMA sheets. This observation is in agreement with the prior reported data (McCarley, et al. 2005), which indicates that the alteration of the functional groups on the surface of PMMA substrate from the $-COOCH_3$ group to $-COOH$ group. This semi-quantitative result indicates the introduction of oxygen and carboxylic acid pathways during UV radiation. The survey spectrum for EDC/NHS treated and avidin immobilized PMMA substrate displayed two more elements: nitrogen and sulfur were additions to the peaks. Considering the succinimide

group has a much higher sulfur percentage than proteins, the XPS results reflected the increase of sulfur element decrease from 0.73% to 0.13% between the two steps. These results represented the success of the surface modification of EDC/NHS treatment and avidin coating.

Table 3-2: Surface elemental percentage analysis of surface-modified PMMA substrate by XPS.

Sample	C (at. %)	O (at. %)	N (at. %)	S (at. %)	C/O
pristine	81.33	18.67	0	0	4.36
UV treated	74.8	25.2	0	0	2.97
EDC/NHS	72.37	24.03	2.86	0.73	3.01
avidin	74	22.83	3.04	0.13	3.24
biotinylated	71.61	20.31	7.73	0.35	3.53

3.5.4 Fluorescence Determination of Surface Modification

To evaluate the functional modification on the microfluidic channel, fluorescence characterization and optimization have also been investigated. Immobilization of FQ-labeled avidin in the microchips was imaged using a fluorescence microscope and depicted in Figure 3-7A-B. Figure 3-7A showed FQ red fluorescence signals when both UV and EDC/NHS were performed prior to attaching FQ conjugated avidin onto PMMA chip. By omitting the UV step, the control experiment showed no observation of fluorescence signal Figure 3-7B. Without UV radiation, no carboxylic acid was available for consecutive EDC mediated coupling to avidin. These images verified that the chemical attachment of avidin on micro-PMMA substrates were localized to UV treated, EDC/NHS catalyzed areas, and no attachment of avidin to UV untreated PMMA

substrates were observed. EDC and NHS ester groups facilitate carboxylic group to react with the amine group to form a stable amide bonds. This chemical reaction further helped to anchor avidin on the surface of the COOH-modified PMMA microchip. Altogether, the results indicate that (1) carboxylic acid groups were formed on UV modified PMMA surface and (2) avidin was successfully immobilized on PMMA substrate through EDC/NHS mediated reaction between carboxylic acid and amines.
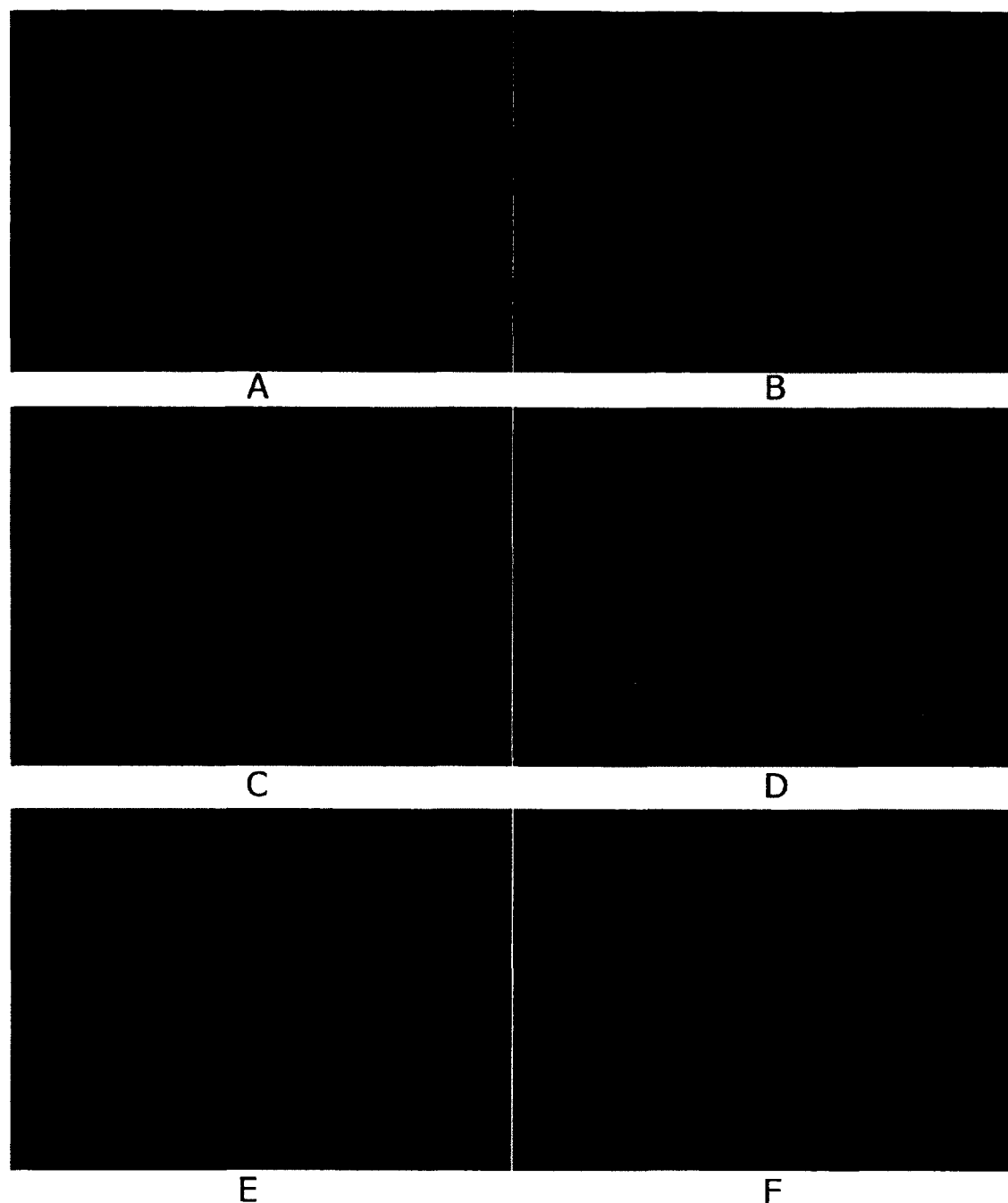
Figure 3-7: Fluorescence determination of surface modification. A. Immobilizing FQ-labeled avidin on UV+EDC/NHS treated PMMA chip; B. Incubation of FQ-labeled avidin after only EDC/NHS treatment and without UV radiation; C. Biotin fluorescein incubation with immobilized avidin PMMA microchip; D. Biotin fluorescein incubation on PMMA surface without avidin-tethered; E. Biotin fluorescein incubation with native BSA coated on PMMA; F. Capture of FQ-labeled biotinylated carbonylated BSA with avidin-terminated microchip.

We also examined whether the immobilized avidin will specifically interact with biotin and further serve as affinity beds for the enrichment of biotin derivatized PTMs. In order to chemically map the functionality of avidin, Biotin-4-Fluorescein (B4F) were used and results were illustrated in Figure 3-7C-E. The image of Figure 3-7C indicated that avidin immobilized PMMA sheet emitted much stronger green fluorescent than its counterpart without the addition of the avidin step (depicted in Figure 3-7D). Also, by replacing avidin treatments with native BSA coating, very little fluorescence signals were observed in Figure 3-7E. Even though native BSA was anchored on the PMMA chip, it could not provide affinity enrichment of biotinylated molecules. This further indicated that little non-specific binding was observed. The images together indicated (1) the strong binding affinity between immobilized avidin and biotin and (2) the effective binding capability of avidin-tethered PMMA to biotin with little non-specific binding.

To further validate that biotinylated carbonylated proteins could be captured by avidin immobilized on the PMMA chip, we also used avidin immobilized surface to capture FQ-labeled biotinylated carbonylated BSA sample. As shown in Figure 3-7F, bright red fluoresce indicated the capture events of biotinylated oxidized BSA with avidin-terminated PMMA. Thus, the avidin tethered to the PMMA microchip provided biotin binding sites and allowed purification of biotinylated carbonylated proteins.

These fluorescence images, which are qualitatively consistent with those obtained by XPS and AFM with regard to the distribution of desired functional groups on the PMMA surface, confirm the functionality of the carboxylic acid, avidin-terminated after surface immobilizations and further validate the enrichment of biotinylated carbonylated BSA.

3.5.5   Quantification of Capture Efficiency

AFM, XPS and fluorescence imaging are limited to provide qualitative and semi-quantitative measurements of the modification and capture procedure. To quantitatively determine the recovery of biotinylated carbonylated protein captured in this functionalized micro device and elution efficiency, we used quantitative fluorescence measurements of effluents collected outside the chip.

In *in vitro* BSA metal catalyzed oxidation, 20 nmol carbonyls per mg of BSA was generated in the oxidation environment outlined in the experimental Section 3.2.3.1. This value was measured by DNPH spectrophotomeric assay. After biotin hydrazide derivatization of *in vitro* oxidized BSA and FQ labeling, the fluorescence intensity indirectly indicating the amount of carbonylated BSA was determined as 41.5 A.U. at an emission of 570 nm. This value served as the basal level for the first injected 5 μL of biotinylated BSA.

As depicted in the experimental sketch in Figure 3-4, a syringe pump was used to push 6.25 μg/ml FQ-labeled biotinylated carbonylated BSA at a flow rate of 5 μL/minute. Hence, 5 μl of biotin derivatized BSA was injected into the avidin-affinity microchip and the flow through was collected every minute. A total of 24 minutes of injection was performed with only 15 pmol (picomole) of carbonyl in 750 ng (nanogram) derivatized BSA injected. Then the collected volume was transferred to Nanodrop for fluorescence measurement. For each segment of 5 μL collection, the trapped and captured biotinylated BSA was calculated as the difference in fluorescence intensity between the initial basal level of 41.5 A.U. and the eluted.

The biotinylated BSA capture recovery, which indicates the amounts of biotinylated BSA captured by the functional PMMA chip with time, was determined by accumulating the captured ones from each of the previous time duration. With the increase of injecting samples to the microchip, the captured protein increases dramatically in the first nine minutes and then it reached a fluorescence plateau around 330 A.U. in the remaining injection, indicating the saturation of the chip, with all avidin groups bound to biotinylated proteins. Accounting the chip was saturated at approximately nine minutes, only 280 ng of biotinylated carbonylated BSA were enriched through the microdevice, which provides attractable feature of enrichment of minuscule samples. If all 750 ng derivatized BSA in the affinity microchip were to be proceeded, an increased geometry with higher surface area would be needed. Also, the captured efficiency of biotinylated carbonylated BSA capture as a function of time was estimated. Capture efficiency is defined as the amount of protein captured in each collecting period (one minute equating to 5 μL of collected flow through) with respect to the amount of the protein injected initially. As indicated in Figure 3-8A, the capture efficiency started at a high level of 75%, and then decreased dramatically with time during the first nine minutes and then dropped to nearly zero for the remaining injection. The initial high capture efficiency was attributed to the geometry design of the microchip. The fluid dynamics imposed by the geometric arrangement of the posts leads the protein mixture down specific streamlines that are interjected frequently by the posts, thereby maximizing interaction of the targeted proteins with the functionalized surfaces, and resulting in a high-efficiency capture of the proteins directly onto the sides of the posts. It is also intuitive that the captured proteins in the affinity based enrichment microchip is

time-dependent, since more accessible biotin-binding cites are at the initial stage of

capture, while with more and more avidin molecules occupied, less captured proteins will

happen.
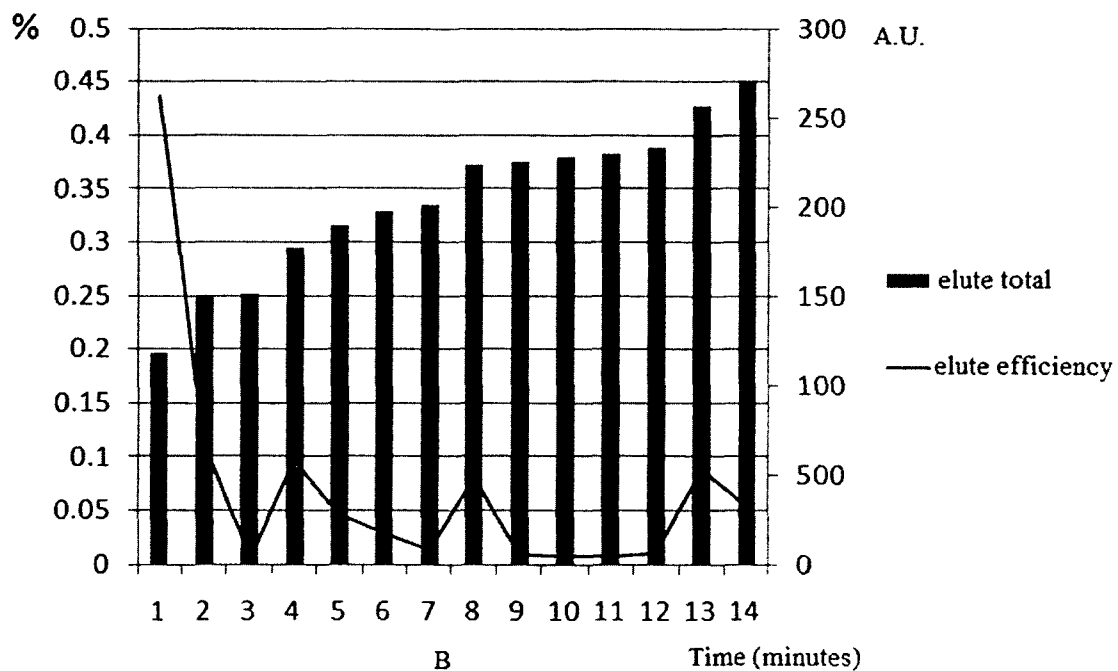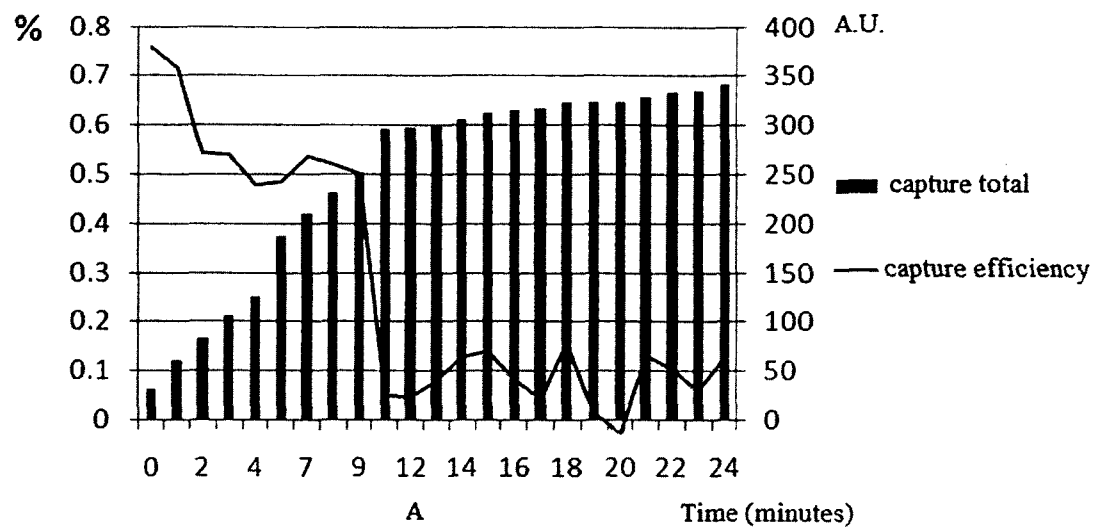
Figure 3-8: A. Capture recovery curve of FQ-labeled biotinylated carbonylated BSA on avidin immobilized microfluidic channel; B. Elution efficiency curve of FQ-labeled biotinylated carbonylated BSA from avidin immobilized microfluidic channel.

The results indicated the effective enrichment regime was provided by this attractive avidin-based affinity microchip. To increase the capture recovery, a longer, wider and taller geometry of micropost-filled microchannels could be utilized in the future designs. In addition, a different arrangement of posts can be configured, such as square array, equilateral triangular array, diagonal square array, etc. Toner's group (Nagrath, et al. 2007) studied the hydrodynamic efficiency for each distribution on the basis of the analytical solution derived by Drummond and Tahir (Drummond and Tahit 1984). It was found that hydrodynamic efficiency of capture as a function of the spacing between the microposts was greatest with the equilateral triangular micropost arrangement. Therefore, we adopted the equilateral triangular array in our application of the enrichment of proteins. To further improve protein captures, shorter center-to-center spacing between the microposts will be beneficial. It is foreseeable that excessive reduction in micropost spacing should not lead to physical trapping of proteins between the microposts because the protein is in the nm range. Additionally, if spacing between the microposts is constant, an increase in the micropost radius will increase the micropost density, resulting in a higher capture area.

3.5.6   Assessment of Elution Efficiency

After the microfluidic channel was saturated by biotinylated carbonylated proteins, elution efficiency was measured by injecting denature/elution solution (0.4% SDS, 0.8% methanol, 0.4% NaCl in water solution) at a flow rate of 5 μL/minute. The accumulated elution with time and elution efficiency as a function of time were both determined. The fluorescence intensity of a collected fraction of 5 μL during each minute elution was determined spectrofluorometrically using Nanodrop. The total elution with

time was assessed by accumulating all the measured fluorescence values in previous elution collection periods. As Figure 3-8B suggested, half of the captured protein was eluted in the first minute, followed by the remaining elution in the next ten minutes. This result indicates that biotinylated carbonylated proteins could be denatured and eluted in a relatively short time-span. The elution efficiency decreased with time. The minor peaks in elution curve elution may indicate that dead volumes exist in the microfluidic channel. The captured biotinylated carbonylated BSA released from avidin functionalized PMMA surfaces could be utilized for further mass spectrometry based proteomics analysis. After elution, proteins were renatured by removing denaturing regent with a MW 3500 Da filtration unit. It is possible that a small fraction of denatured protein still existed or loss of proteins during filtration process, which lead to the loss of proteins that could account for the difference in protein amount observed between captured (330 A.U.) and eluted amounts (280 A.U.).

Currently, a fresh prepared device was used for a new measurement with our current settings. The avidin-tethered substrate cannot be reused, because the avidin-biotin bond is one of the strongest biological bonds known; and the harsh conditions necessary to break this bond to elute and recover bound proteins also destroy the avidin. But the desirable features of PMMA microdevice making via hot embossing allow for low cost and high production, and make the reusability less of a concern. Nevertheless, there are a few approaches to explore in the future to make the microdevices reusable.

Previously, Holmberg et al, showed a short incubation in nonionic aqueous solutions at temperatures above 70° C can efficiently break the interaction without denaturing the streptavidin tetramer, and therefore the molecules can be regenerated and

reused (Holmberg, et al. 2005). (2) Also, replacing tetramer avidin with monomeric avidin, the gentle elution and recovery using 2 mM biotin to compete for the biotin binding site can be used without sacrificing the avidin solid support (Mirzaei and Regnier 2005).

3.6   Summary

Here we reported a novel and sensitive affinity chromatography of the biotin derivatized carbonylated BSA on the avidin-functionalized microchip. An avidin-immobilized microposts-filled microchannel was designed with UV photochemical carboxylic acid pathway and EDC mediated amide coupling with PMMA. It is to facilitate the enrichment of any PTM protein after biotin derivatization. Various characterization techniques, both qualitative and quantitative, were utilized to prove and evaluate the surface modification scheme and enrichment process of biotin derivatized carbonylated BSA. This biomedical microdevice, can proceed μg amount of proteins for enrichment of a trace level of modified protein, 106 fold less than the current commercial avidin column, making it highly desired for any limited amount of biological samples requiring avidin affinity enrichment.

CHAPTER 4

ANTIBODY FUNCTIONALIZED IMMUNOSENSOR ON PDMS MICROFLUIDIC DEVICE FOR LOW ABUNDANT POST-TRANSLATIONAL MODIFIED PROTEIN DETECTION AND PURIFICATION

4.1   Introduction

This chapter reports the fabrication, characterization and assessment of antibody

based μ-chip immunosensor to screen for PTM using a Polydimethylsiloxane (PDMS) μ-

chip. In the work described in Chapter 3, PMMA μ-chip for PTM proteins enrichment

and extraction with avidin/biotin based approach is established. The disadvantage of

PMMA microfluidic device is that PMMA material suffers from its brittle characteristics,

and the PMMA device is fragile under intermediate force. Furthermore, the capillaries to

connect the inlet and outlet of μ-chip with external parts are normally sealed and secured

by glue, which causes the connection defect of easy-breakage, entry blockage and

inability of resealing or hot-plugging. Comparing with PMMA, polydimethylsiloxane

(PDMS) is of extreme elastic and hence, the PDMS device could always be resealed.

The μ-chip embedded with high density post arrays was utilized to specifically

enrich carbonylated proteins. Techniques including atomic force microscopy and

fluorescence microscopy were applied to characterize PDMS surface topography and

surface functional group mapping changes after each modification step of the treatment

process. In addition, a quantitative study of DNP-labeled carbonylated protein capture

and elution efficiencies of the device was investigated. A test protein, *in vitro*

carbonylated cytochrome C was enriched successfully by the chip even with its low

abundant presence among large excess of interfering protein, bovine serum albumin

(BSA). This device requires less than 700 ng protein sample for targeting carbonylated

proteins, which is not achievable using the tube-based immunoprecipitation technique.

This μIP device could be further adapted to purify a wide range of other PTMs to

facilitate proteomics based biomarker discovery.

4.2   Method and Materials

4.2.1   Reagent and Materials

Aminopropyltriethoxysilane (APTES) and glutaraldehyde used for PDMS surface

modification assays were purchased from Alfa Aesar (Ward Hill, MA). For proteins used,

anti-DNP and albumin bovine serum was purchased from Sigma-Aldrich (St. Louis,

MO), and cytochrome C was purchased from EMD Chemicals (San Diego, CA). Tween-

20 and Sodium cyanoborohydride used in the Schiff bond stabilization assay were

purchased from VWR (West Chester, PA) and Sigma-Aldrich (St. Louis, MO),

respectively. As for fluorescent dye, 3-(2-furoyl)-quinoline-2-carboxaldehyde (FQ),

naphthalene-2,3-dicarboxaldehyde (NDA) and Alexa488 labeled anti-DNP were

purchased from Invitrogen (Madison, WI). TRITC-BSA was purchased from Sigma-

Aldrich (St. Louis, MO).

The mold master for the process of soft lithography was fabricated by positive

photoresist S1813 and developer Microposit MT-319, which were both purchased from

Rohm and Haas Electronic Materials LLC (Marlborough, MA). SYLGARD 184 Silocone

elastomer kit (PDMS) and a 3" × 2" glass board used to form the microfluidic devices

were purchased from Dow Corning Corporation (Midland, MI) and GoodFellow

(Oakdale, PA), respectively. UV glue LOCTITE 352 used to bind the silicon mold master

and PMMA pocket with glass board was purchased from Henkel Loctite Corp (Rocky

Hill, CT). The 1/16" × 0.030" Teflon tubing used on the inlet and outlet of the

microfluidic device was obtained from IDEX Health & Science (Oak Harbor, WA).

4.2.2 Fabrication of Microfluidic Device

4.2.2.1 Microfluidic Device Design

Figure 4-1 demonstrates the channel embedded with micro-truncated square

pyramid arrays. The 25.4 mm long, 1.5 mm wide and 150 μm tall channel is filled with

truncated square micropyramids, which are 150 μm in height, 340 μm on the base sides

and 130 μm on the top sides with an average spacing of 100 μm between micro-

pyramids. The pyramid shape with slanted sides rather than straight posts were formed

from silicon wet-etching. Compared with the straight-pillar design, pyramids increase the

surface areas subjected to incoming surface chemical treatment.

A

B
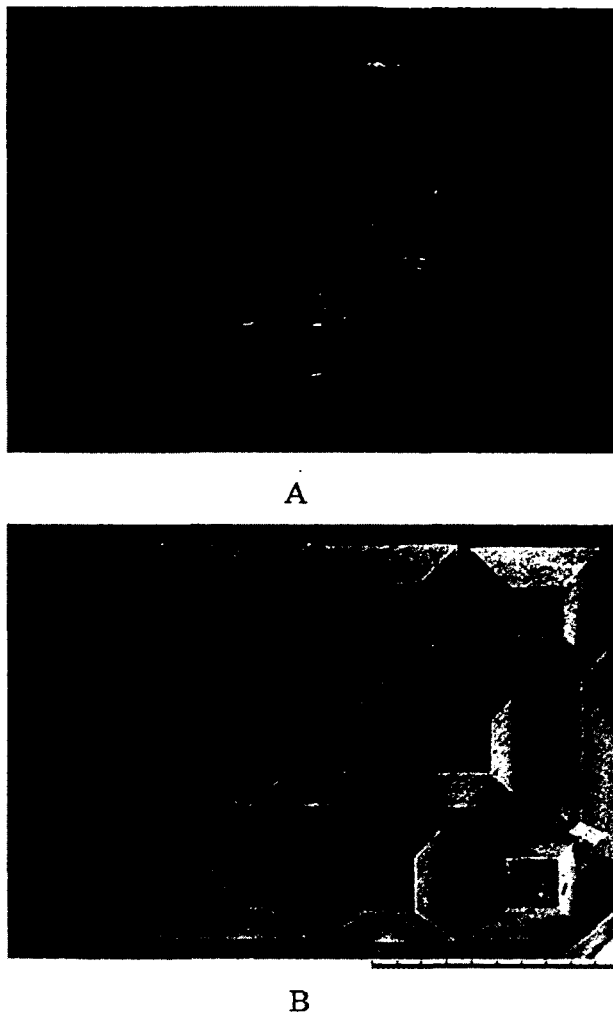
Figure 4-1: A. Overview of the structure of microfluidic device; B. PDMS micropyramid structure in the device. Scale bar is 1 mm in length.

In the µIP device, reactive molecules were chemically immobilized on the surfaces of the pyramid and channel walls to "capture" target protein. The "process of capturing" is based on the interaction between molecules, and it could be considered as an instant reaction. The Reynolds number of the system is roughly around 0.45, the flow pass through the device is therefore strictly laminar and the capture process is primarily affected by three factors, density of antibody-tethered groups, molecular encounter rate and reaction time between the incoming protein and the activated sites on the

functionalized surface. Hence, the micro-pyramid array was arranged in a staggered pattern to increase the chance of the protein interacting with the functionalized surface for improving protein capture efficiency.

4.2.2.2   Fabrication of the Silicon Mold Master

The microfluidic device was fabricated with PDMS, by a previously developed soft lithography method (Whitesides, et al. 2001) (Zhao, Xia and Whitesides 1997) using a silicon master patterned by wet etching. Specifically, an emulsion mask was printed on photographic films using a Linotronic 330 Linotype printer of 25 μm resolution after the desired pyramid arrayed geometries in the micro-channel were designed by CAD (Computer aided design). Positive photoresist S1813 was spin-coated to generate a uniform thickness of ~2 μm on the silicon wafer to serve as a sacrificial layer. After spin-coating, the mask was aligned onto the silicon wafer for a pattern transfer under UV light for about 65 seconds. After UV treatment, the wafer was developed by developer Microposit MT-319. Buffered oxide etching (BOE) was used to etch silicon oxide and further achieve the pattern transfer onto the silicon oxide layer of the silicon wafer. A silicon mold master was prepared by KOH wet-etching method. By the characteristics of wet etching on <100> four-inch silicon wafer, arrays of truncated square pyramids were formed on the silicon wafer, which will further form the micro-pyramid structures on the PDMS replicate during PDMS molding process. To reduce the fragile silicon mold master from breaking, silicon mold master was glued onto a 2" × 3" glass plate by UV induced glue. A frame was also glued around the silicon mold, forming a pocket structure to hold the PDMS mixture in the subsequent soft lithography assay.

4.2.2.3   Soft Lithography

A 10:1 ratio of PDMS base with curing agent from commercially available SYLGARD 184 Silocone elastomer kit was used to form the PDMS mixture, which was poured into the pocket structure of the mold master. Vacuum pump was applied to remove bubbles generated in the mixing step. PDMS mixture, along with the mold master, was cured at 150° C for at least one hour to have the PDMS solidified. After soft lithography fabrication, the PDMS device embedded with micro-pyramids was peeled off from silicon mold master, then cut, punched with 1/16" ID puncher to create inlet/outlet, cleaned with DI water and air dried. Prior to chemical modification steps, the PDMS device was incubated in methanol for one hour and dried on the hot plate at 120° C for 30 minutes to have the PDMS surface become more hydrophilic. The PDMS device and a 2" × 3" glass plate was then treated by oxygen plasma for seven minutes (0.2 mbar), then bound together under pressure to form the microfluidic channel. A 0.30" inner diameter Teflon tubing was used directly to connect the inlet reservoir with a syringe for chemical injections without any glue treatment.

Due to the elastic property of PDMS, inlet reservoir is directly connected with the syringe by Teflon tubing for chemical injections without any glue treatment. The tubing could be swapped freely between samples to prevent contamination. This PDMS property provided user convenience and the reduced failure which often happens in glue-based connections. In this chip, all injection, reaction, washing and elution procedures were achieved by pumping solutions through the attached tubing to inlet reservoir using the syringe pumps.

4.2.3   Protein Sample Labeling and Purification

4.2.3.1   *In vitro* Carbonylation of Protein Samples

Protein solution of cytochrome C and BSA were oxidized with a hydroxyl radical-generating system consisting of ascorbate/Fe(III)/O2 (Requena, et al. 2001). First, the protein was dissolved in 1 mL of oxidation buffer (50 mM HEPES, 100 mM KCl, 10 mM $MgCl_2$, pH 7.4) to reach a final concentration of 10 mg/mL. Ascorbate and $FeCl_3$ was added to the mixture for final concentration of 25 mM and 0.1 mM, respectively. The oxidation was therefore carried out by incubating overnight at 37° C, while constantly shaking. The oxidation was stopped by adding EDTA to a final concentration of 1 mM. The reaction mixture was dialyzed overnight against oxidation buffer containing 1 mM EDTA at pH 7.4 (Feng and Arriaga 2008) (Requena, et al. 2001) (Stadtman and Levine, Free radical-mediated oxidation of free amino acids and amino acid residues in proteins 2003).

4.2.3.2   Preparation of DNP-Labeled Protein Samples

Protein solution (carbonylated cytochrome C or carbonylated BSA) after the oxidation assay was chemically labeled with DNPH, as described by Levine (R. L. Levine 2002). Briefly, 100 µL of 1 mg/ml oxidized protein was added into 500 µL solution of 10 mM DNPH in 2 M HCl. The mixture was allowed to stand at room temperature for one hour before adding 60 mg TCA to the mixture to a final concentration of 10% w/v. The mixture was incubated on ice for 30 minutes. The mixture was then centrifuged at 11000 g for three minutes, the supernatant would be discarded. The pellet was washed with an ethanol-ethyl acetate (1:1) mixture three times. For each

time washing, the mixture is centrifuged at 11000 g for 90 seconds. The pellet was

further dissolved in 100 μl PBS buffer to reach a final concentration of 1 mg/ml.

4.2.4   Antibody Immobilization

The antibody functionalized device inner surface was accomplished by chemical

modification methods. Figure 4-2 depicts the immunosensor fabrication steps, which

includes the covalent immobilization of the anti-DNP onto PDMS μ-chip and the

purification strategy of carbonylated proteins. Sandison's group demonstrated the use of

glutaraldehyde activated PDMS for consecutive attachment of the antibody (Sandison, et

al. 2010). Specifically, oxygen plasma was used to generate hydroxyl groups on the

surface of PDMS. Stalinization solution (5% aminopropyltriethoxysilane (APTES) v/v in

95% ethanol and 5% dH_2O as solvent) was flowed through the device for 10 minutes

followed by ten minutes of incubation time. Then the device was further cleaned with

ethanol, air dried and treated on the hot plate at 80° C for 20 minutes. Crosslinker

solution (glutaraldehyde 1% v/v in H_2O, pH 9.2) was subsequently injected for ten

minutes, followed by ten minutes of incubation time. This crosslinker can further react

with amine group of antibody and result in antibody immobilization on chemically

modified PDMS surface. Anti-DNP solution of concentration 0.2 mg/ml (in pH 9.2

solution) was flowed through the device for ten minutes, followed by 20 minutes of

incubation. The device was washed by pH 9.2 sodium carbonate buffer, containing 0.05%

Tween-20 and 1% sodium cyanoborohydride for ten minutes both prior and after the

antibody injection/incubation to stabilize the Schiff bond. A 1% bovine serum albumin

(BSA) solution (in PBS buffer, pH 7.4, contains 0.05% Tween-20) was flown through the

microchannel for ten minutes to block non-specific protein adsorption sites. Then PBS

buffer was used to wash the device. It is ready for capturing DNP derivatized

carbonylated cytochrome C. All the chemical treatment solutions and washing buffers

were driven through the device channel by a syringe pump with a flow rate of 5 μl per

minute.
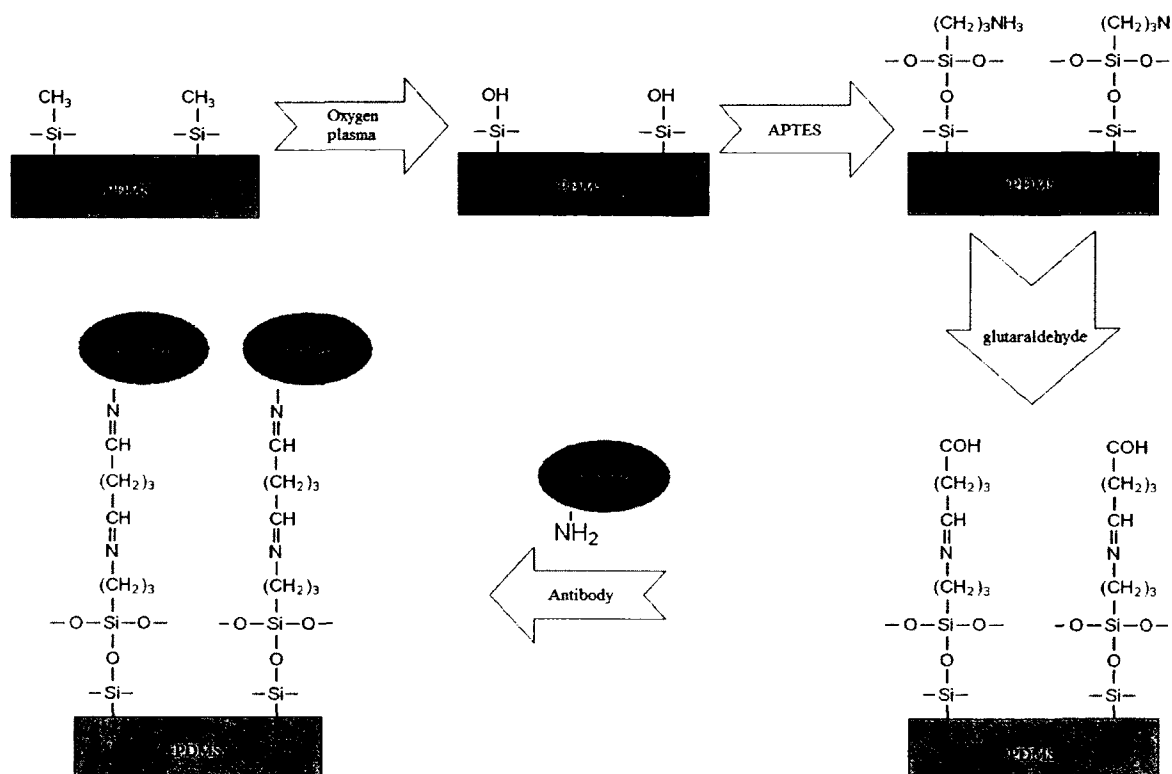
Figure 4-2: Chemical surface modification steps for immobilizing antibody in PDMS μIP device.

4.2.5 Conventional IP for Purification of Carbonylated BSA

A conventional IP for carbonylated proteins was carried out for comparison with

the μ-IP method. Silver stained gel came from conventional IP experiments.

4.2.5.1 Chemicals and Facilities

MagnaBind carboxyl derivatized beads were purchased from Thermo (Rockford,

IL), while chemicals used beads surface modification assays including 1-ethyl-3-[3-

dimethylaminopropyl] carbodiimide hydrochloride (EDC), N-hydroxysuccinimide (NHS) and N-morpholinoethane sulfonic acid (MES) buffer were purchased from Fluka (Steinheim, Germany), Thermo (Rockford, IL) and Alfa Aesar (Ward Hill, MA), respectively. The syringe pump used as the motion supplier of the mobile phase in the μIP device was purchased from Next Advance (Averill Park, NY, USA). XDS 5 Dry vacuum pump used to remove bubbles from PDMS mixture was purchased from EDWARDS (Sanborn, NY).

4.2.5.2   Methodology

After the oxidized proteins (BSA and cytochrome C) were tagged with DNP to form a covalent bond with carbonyl groups, the DNP-tagged proteins were immunoprecipitated using anti-DNP antibodies by using both the conventional method and the μ-IP chip. For conventional IP, MagnaBind carboxyl derivatized beads were covalently coated with anti-DNP antibodies as described by the manufacturer. Briefly, 5 mM EDC and NHS were used to activate and crosslink the carboxyl to the primary amines of 0.4 mg/ml anti-DNP. This conjugation reaction was performed in 0.1 M MES buffer with 0.9% NaCl at pH 4.7 for two hours.

The anti-DNP coated MagnaBind beads were added to the DNP-labeled protein solutions and then incubated for three hours at room temperature with vortexing. The unbound proteins were removed by washing the beads in PBS for 15 minutes, three times. For elution, the carbonylated proteins were eluted from the MagnaBind beads by washing them three times with IgG elution buffer (pH 2.8). The elutes were then heated in the water bath at 100° C for five minutes for denaturing, followed with SDS-PAGE

separation and silver staining visualization according to manufacturer's procedures

(England and Cotter 2004) (Kristensena, et al. 2004).

4.3   Testing the Microfluidic Device

4.3.1   Surface Topology Characterization Using Atomic Force Microscopy

A commercial instrument Nanosurf easyScan 2 was used to study the surface

topology after each modification including pristine PDMS, oxygen plasma treated,

APTES/glutaraldehyde activated, anti-DNP immobilized and BSA blocked PDMS

substrates. As for technical details of the AFM, please refer to Section 3.3.2.

4.3.2   Fluorescence Validation of Surface Modification

A series of fluorescence experiments were used to evaluate the effect of chemical

modification after each chemical treatment steps. The fluorescence surface modification

experiments were carried out with an Olympus IX51 inverted microscope (Olympus

Corporation, Tokyo, Japan). For details of the fluorescence microscope, please refer to

Section 3.5.4. These images were further analyzed by Image J software.

4.3.2.1   Chemical Mapping of Glutaraldehyde and Antibody

To verify the functionality and uniformity of crosslinker glutaraldehyde layer, and

strong immobilization of antibody onto the substrates, PDMS channel (without micro-

pyramid) prepared after oxygen plasma, APTES and 1% glutaraldehyde treatments were

incubated with Alexa-488 labeled anti-DNP solution (0.2 mg/ml) for 30 minutes at room

temperature. A negative control was performed by omitting the addition of crosslinker-

glutaraldehyde to study the effectiveness of crosslinking and the formation of Schiff

bases (compounds having a C=N function). To evaluate the Schiff based covalent bond

formed between anti-DNP antibody and the PDMS substrate, both sample and control

were washed with 1% glutaraldehyde solution for 30 minutes. The samples were studied with the exposure time of one second under fluorescence microscopy using ex/em filter sets of 488/535 nm.

4.3.2.2   Validation of Carbonylated Proteins Capture on Microchips

The anti-DNP functionalized PDMS channel was used to capture FQ-labeled DNP-derivatized carbonylated protein. To evaluate the binding reaction between DNP-labeled proteins with immobilized anti-DNP on the μIP device, PDMS substrate with anti-DNP immobilized were immersed with 20 μM FQ -labeled DNP-labeled carbonylated BSA solution in PBS. After 20 minutes of incubation at room temperature, the samples were then washed with DI water three times and air-dried prior to fluorescence imaging study. Finally, for the validation of elution process of enriched proteins, the PDMS channel with captured FQ-labeled DNP-labeled carbonylated protein was then washed with 1% SDS solution for 30 minutes. After water rinse and drying, fluorescence image was then taken with an excitation wavelength of 488 nm and one second of exposure time.

For FQ labeling of DNP-labeled carbonylated protein, 200 nmol FQ were dissolved in 10 μl of 10 mM potassium cyanide (KCN) solution. Fluorogenic reagent FQ only fluoresces upon covalent binding to the protein primary amine group (-NH2) (Michels et al., 2007). When binding onto the protein, FQ absorbs blue light at 490 nm and emits red fluorescence at 525 nm.

4.4 Quantitative Examination of the Microfluidic Device

4.4.1 Quantification of Capture Efficiency

We also investigated the purification efficiency of the μIP device by quantitatively measuring the capture efficiency of the smaller amount of DNP labeled carbonylated cytochrome C at the presence of a larger amount of blocking proteins-native BSA. Carbonylation of cytochrome C has been associated with oxidative stress induced disease and considered as a biomarker. For NDA labeling, 100 μl of DNP derivatized carbonylated cytochrome C was mixed with 2.5 μl of sodium cyanide solution (0.2M) and 50 μl of NDA stock solution (1 mM). The labeling reaction proceeded for 15 minutes (Gottschlich et al., 2000). Hence, a mixed solution of NDA labeled DNP derivatized carbonylated cytochrome C (1 μg/ml) and TRITC labeled-BSA (50 μg/ml) was flowed through the anti-DNP-immobilized micro-chip with a flow rate of 5 μL/minute for 90 minutes. For each minute, an outflow droplet of 5 μL was collected and its fluorescence at both emission wavelength of 479 nm (for NDA-carbonylated cytochrome C) and 572 nm (for TRITC-BSA) were measured. With every minute collection of flow through, a total of 130 points of fluorescence measurements for each NDA and TRITC-BSA were recorded to calculate each individual capture efficiency changed with time. The μIP device is considered saturated after both outflow of NDA-carbonylated cytochrome C and TRITC-BSA fluorescence intensities have raised to the same intensities as those in the injected solution. The capture efficiency estimates the amount of captured carbonylated protein by the antibody modified microfluidic channel using indirect fluorescence measurement of flow through by a fluorescence meter (Nanodrop 3300). Similar as Eq. 3-1, the capture efficiency is defined as:

Capture efficiency

$$= 1 - \frac{amount\ of\ eluted\ protein\ inflow\ through}{injected\ protein\ amount}.$$

Eq. 4-1

4.4.2   Quantification of Elution Efficiency

After the channel of the µIP device was saturated, the device was washed with PBS buffer and air dried. The elution and release of enriched carbonylated cytochrome C was demonstrated by injecting the eluting buffer (1% SDS) to break the antigen and antibody bond. With the eluting buffer injected in a flow rate of 5 µL/minute for every minute, the fluorescence intensities of outflow were measured using the same procedure mentioned above (as in Section 4.4.1). Similar as in Eq. 3-2, the eluting efficiency is defined as:

$$Elute\ efficiency = \frac{eluted\ protein\ amount}{captured\ protein\ amount}.$$

Eq. 4-2

4.5   Results and Discussion

4.5.1   Surface Topographic Analysis of Surface-Modified PDMS Substrate

Surface topology plays an important role for antibody immobilization and protein purification, because the increased surface roughness enhances the contact surface area, providing more glutaraldehyde-activated and anti-DNP tethered arrays and further increasing the capture efficiency of carbonylated proteins. AFM study was applied on the PDMS substrates after each chemical modification step, which includes (1) unmodified, (2) after oxygen plasma, (3) APTES treated, (4) glutaraldehyde activated, (5) anti-DNP immobilized, and (6) BSA blocked. For each of the substrate studied, the individual representative AFM images are demonstrated in Figure 4-3A-F and the corresponding surface roughness, denoted as the root mean square (rms), is summarized in Figure 4-4.
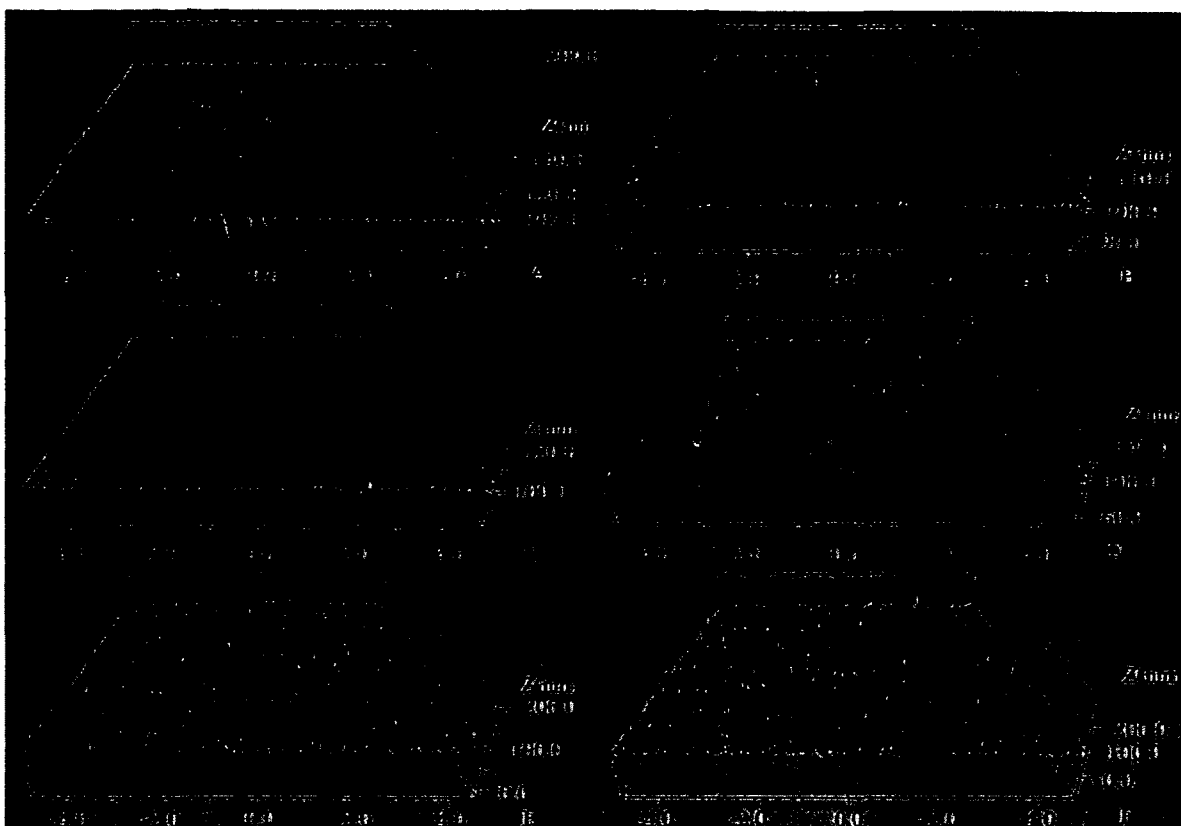
Figure 4-3: A-F. AFM images of unmodified, oxygen plasma treated, APTES treated, glutaraldehyde treated, anti-DNP immobilized and BSA blocked PDMS surface.
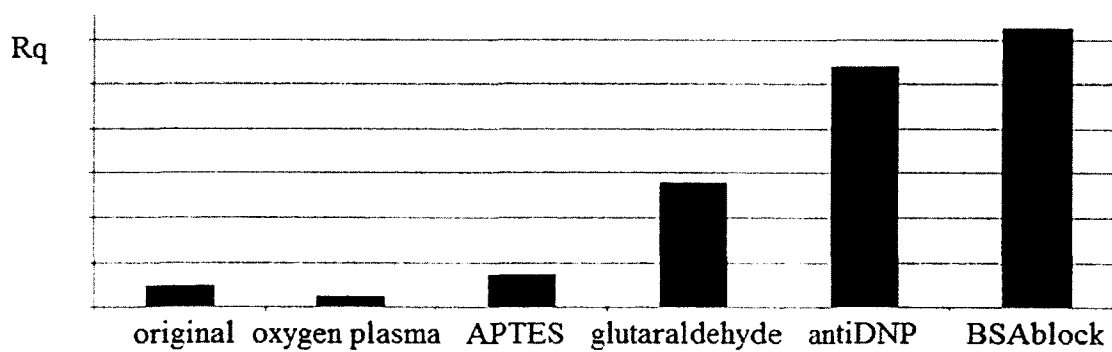
Figure 4-4: Surface roughness root mean square (rms, in the unit of nm) of PDMS surfaces.

Morphology of PDMS surfaces of unmodified and after oxygen plasma treatment are relatively smooth and similar with surface roughness of 2.38 and 1.3 nm, correspondingly. After oxygen plasma treatment, the PDMS surface becomes slightly smoother after oxygen plasma treatment, which is consistent with previous reports (Chang, et al. 2007). The rpm surface roughness for the APTES treated PDMS substrate is around 3.75 nm, while the crosslinker glutaraldehyde treatment increased the surface roughness to 14 nm. A "hilly area" was observed, as shown in Figure 4-3E, which is considered as the precipitation product from the chemical reaction between APTES and glutaraldehyde. Since a monolayer thickness of APTES and glutaraldehyde is theoretically assessed as 0.8 nm and 1.4 nm, those measurements showed that multilayer of APTES and glutaraldehyde were coated, and possible polymerization of glutaraldehyde has occurred (Razumovitch, et al. 2009).

The PDMS surface roughness has a noticeable increase after anti-DNP immobilization and protein blocking with BSA with respective surface roughness of 27 nm and 31.3 nm. Considering the physical size of the proteins with molecular mass of ~60 kDa is around 6 nm, the increase of surface roughness could be attributed by immobilized proteins forming in small groups of conglomeration (~10-15 nm), which is in agreement with the reports from Ling Yu et. al (Yu, Li and Zhou 2005). The increased roughness is desirable for our µIP device, because the rough surface magnifies the wetting and adhesion properties of a solid (Bico, Tordeux and Quéré 2001), which is helpful for the reaction between carbonylated protein targets and the antibody-modified PDMS substrates.

4.5.2   Studies of Surface Modification by Fluorescence Determination

To achieve the objective of capture carbonylated proteins using the immuno-

affinity based purification approach, we used a chemical modification comprised of

salinization of PDMS substrate with APTES followed by coupling with amine-terminated

antibody through glutaraldehyde. To assess the effectiveness of modification, quantitative

fluorescence measurements of each modification were investigated with a fluorescence

microscope equipped with a CCD camera, and the data was analyzed using Image J

software. Software ImageJ 1.45s (National Institutes of Health, USA) was used to

analyze the alteration of fluorescence intensity by comparing the mean value of the

colored pixels. The mean value of RGB pixels is a value between 0-255, which increases

while the color intensifies. For fluorescence figures from Alexa488, green values were

compared; and for fluorescence figures using FQ, red values were compared.

Firstly, we evaluated whether anti-DNP was immobilized onto the PDMS

substrate via Schiff reaction. As demonstrated in Figure 4-5, the crosslinker

glutaraldehyde anchored Alexa 488 labeled anti-DNP onto the surface of PDMS substrate

via strong covalent bonds (Figure 4-5A), while the control without crosslinker treatment

resulted little immobilization of the antibody (Figure 4-5B). As demonstrated in Figure 4-

5F, software ImageJ analysis indicates that PDMS substrates treated with crosslinker

glutaraldehyde has fluorescence intensity of ~2.5-fold than the negative control.

71

P(T<=t)
* 0.05
** 0.01
*** 0.001

F 150

Green 100
value
50

0

***

 Glutaraldehyde treated

 Glutaraldehyde untreated

Red 60
value

40

20

0

***

**

 Capturing
DNP-labeled BSA

 Capturing
regular BSA

 Elute captured DNP-labeled
carbonylated BSA 10 minutes

 Elute captured DNP-labeled
carbonylated BSA 30 minutes
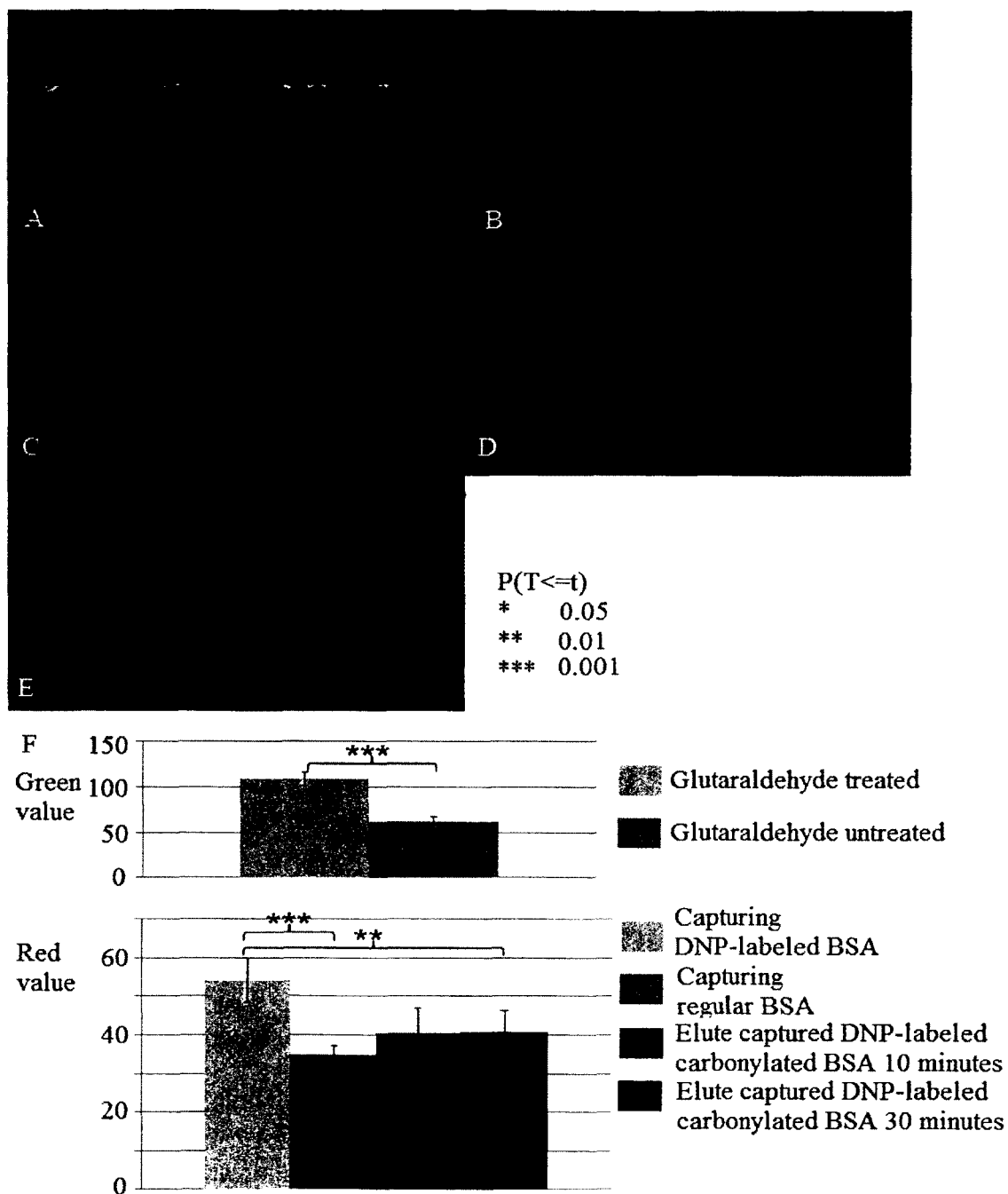
Figure 4-5: A-B. Washing PDMS surface treated with (A) or without (B) crosslinker glutaraldehyde with 1% glutaraldehyde solution for 30 minutes; C. Anti-DNP functionalized channel capturing FQ labeled DNP labeled carbonylated BSA; D. Anti-DNP functionalized channel capturing FQ labeled regular BSA; E. Elute the channel in (C) by 1% SDS solution for 30 minutes; F. Average red value of (A)-(B), and average green value of (C)-(E).

Secondly, we also examined whether the anti-DNP terminated microchannel will specifically capture DNP-labeled carbonylated protein, which represents of the tag labeled PTMs. In order to chemically map the functionality of anti-DNP, FQ-labeled DNP labeled carbonylated BSA were used. Fluorogenic reagent FQ fluoresces only upon covalent binding to the protein primary amide group (-NH_2) in the presence of nucleophile (CN-) group (Michels, et al. 2007). As shown by Figure 4-5C, high intensity fluorescence was observed at an emission wavelength of 560 nm, which represents that the anti-DNP functionalized μ-IP device could interact with and capture DNP-labeled carbonylated proteins. Conversely, no significant reaction was observed for native BSA compared with the specific interaction of anti-DNP against carbonylated BSA (Figure 4-5D).

Lastly, the elution of enriched carbonylated BSA was observed by applying 1% SDS solution (Figure 4-5E). Image J analysis indicates that within 30 minutes, 34.5% of fluorescence intensity was reduced inside the microfluidic channel, which is shown in Figure 4-5F.

The fluorescence imaging helped us to answer three questions: (1) whether anti-DNP could be successfully immobilized on the PDMS channel; (2) if those immobilized anti-DNP are still active and able to capture target proteins; and (3) whether those captured proteins could be eluted out of the device. The fluorescent images give us affirmative answers, which are consistent with those AFM studies, validating the desired functional groups present on the PDMS surface.

4.5.3   Capture Efficiency Quantification

AFM and fluorescence imaging are both semi-quantitative studies, and they are limited as they could only validate the presence of the functional groups without providing quantitative information in regards to how much carbonylated proteins are captured and eluted. Therefore, to quantitatively determine how the µIP device enriches DNP labeled carbonylated BSA by the process of capturing and eluting, quantitative fluorescence measurements are necessary.

To evaluate the specific anti-DNP and DNP derivatized carbonylated protein interaction, we performed the off-chip fluorometric protocol with a mixture of low abundant carbonylated cytochrome C (NDA labeled) and large amount of native BSA (TRITC labeled). We achieve the captured protein estimation by studying the fluorescence intensity difference between the injected protein sample and the outflow. To measure the capture efficiency of DNP labeled carbonylated proteins, aqueous solution of 2 µg/ml NDA labeled DNP labeled carbonylated cytochrome C and 100 µg/ml TRITC-BSA were mixed together to reach a final concentration of 1 µg/ml and 50 µg/ml, respectively. Here, TRITC-BSA is used as protein background.

Before assessing the capture and elution efficiency, the crosstalking between the two fluorescence dyes (NDA vs. TRITC) was investigated. The crosstalk effect is calculated by Eq. 4-3 and Eq. 4-4.

$$Crosstalk\ effect\ of\ NDA$$
$$= \frac{NDA\ fluorescence\ intensity\ at\ 572\ nm}{NDA\ fluorescence\ intensity\ at\ 479\ nm}.$$

<div align="right">Eq. 4-3</div>

Crosstalk effect of NDA

$$= \frac{NDA\ fluorescence\ intensity\ at\ 479\ nm}{NDA\ fluorescence\ intensity\ at\ 572\ nm}\ . \qquad \text{Eq. 4-4}$$

It was found that the NDA to TRITC crosstalking is around 12.37%, while TRITC to NDA is estimated at 4.77%. After factoring the crosstalking effects, we then determined the capture efficiency in every minute segment using Eq. 4-4 in Section 4.4.1 and depicted the values in Figure 4-6.
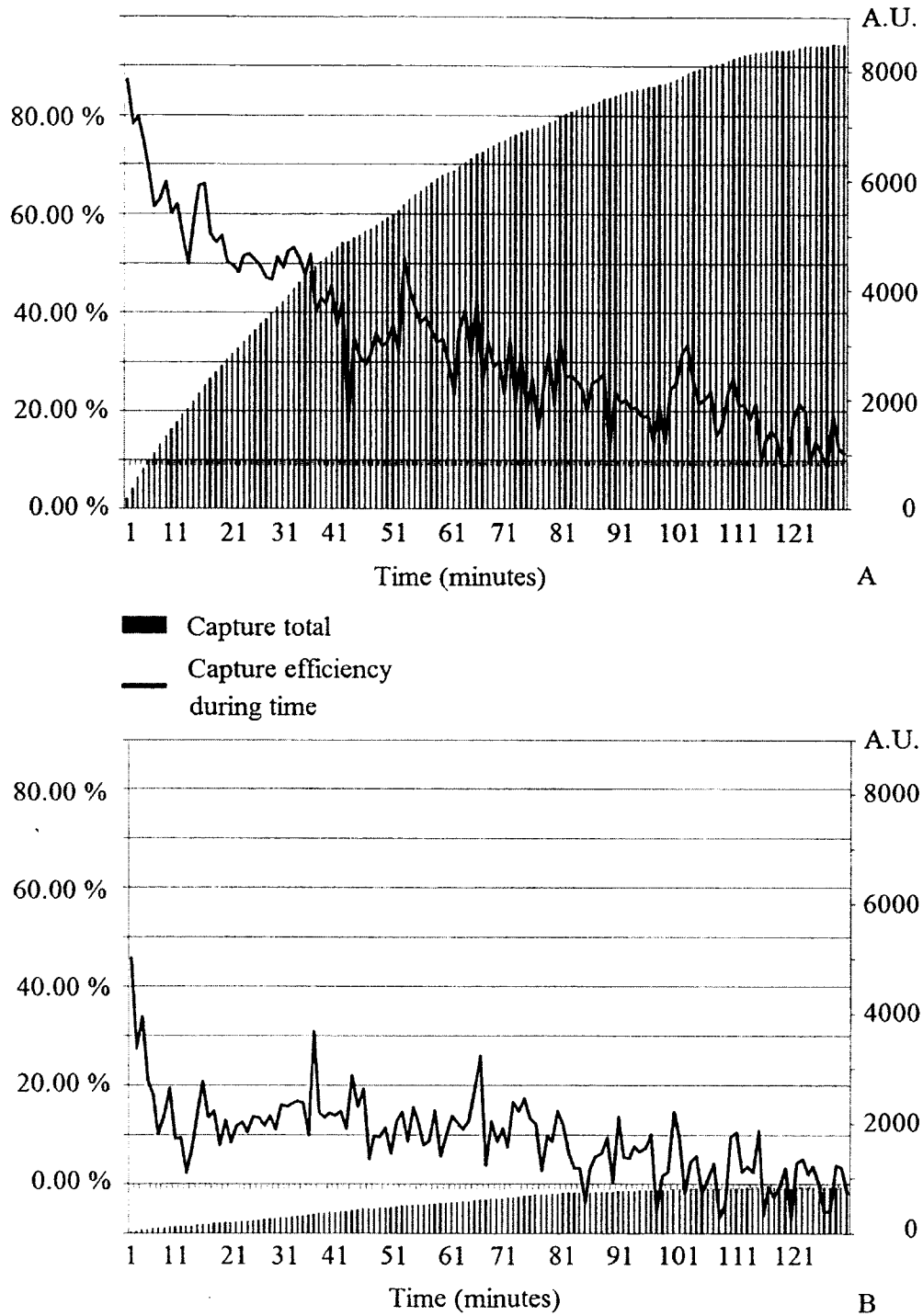
Figure 4-6: Capture efficiency curve and capture total pillars of A. NDA-labeled DNP-labeled carbonylated cytochrome C and B. BSA as control, with anti-DNP functionalized micro-immunoprecipitation device.

By comparing the captured efficiency of carbonylated cytochrome C and background protein BSA as a function of time, we notice that the µIP device has an apparent specificity on enriching carbonylated protein. Here, capture efficiency is defined as the amount of the protein captured in each minute with respect to the amount of the protein injected initially for each minute. As demonstrated in Figure 4-6, the capture efficiency for carbonylated cytochrome C started at a high level of ~80%, and then the curve decreased to ~40% smoothly in 40 minutes. On the other hand, the capture efficiency for background BSA started at ~45%, and then dropped dramatically to ~10% in the first ten minutes. It is theoretical intuitive that the capture efficiency for carbonylated proteins starts high and drop smooth. The capturing process in the immuno-affinity based enrichment microchip is time-dependent, because there are more accessible antibody binding cites at the initial stage of capture, while gradually more active functional sites are occupied by carbonylated proteins with time. It is also observed that the lower capture percentage and easier saturation of BSA by the chip shows an insignificant amount of BSA absorptions via unspecific binding. The initial 45% BSA capture efficiency could be the result of some proteins displacing BSA, which was used to block the chip. As depicted Figure 4-7, BSA capturing reaches its plateau in terms of captured total (A.U.) around the 85th minute, while the µIP device could capture carbonylated cytochrome C until the 110th minute, at which the µ-chip is saturated, indicating no more anti-DNP binding sites available. Correspondingly, the zero capture efficiency indicates that even with continuous injection after saturation, the flow through of the samples can no longer be captured in the µIP and will just elute through. To achieve more captured amount of carbonylated protein, increasing the geometric surface

within the device or increasing the antibody density inside the chip will be a prospective

in further device improvements.
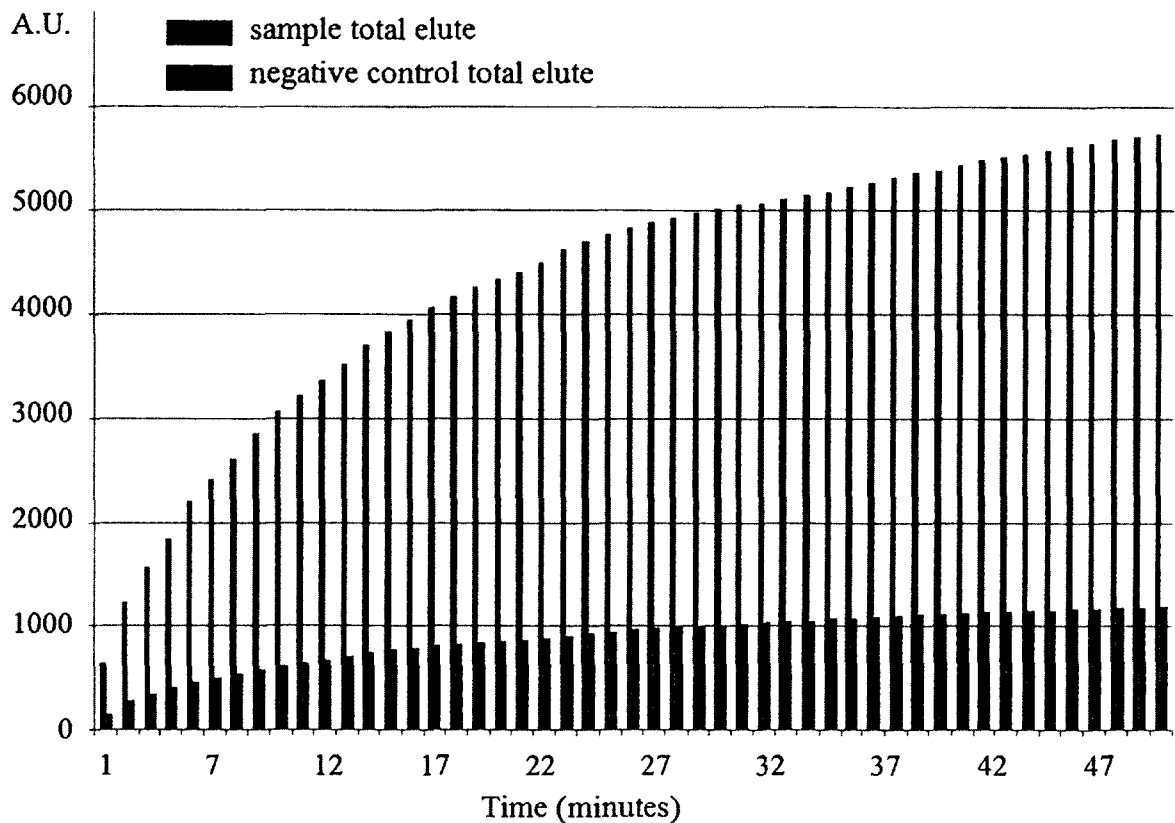
Figure 4-7: Capture total pillars of NDA-labeled DNP-labeled carbonylated cytochrome C and BSA as control, with anti-DNP functionalized micro-immunoprecipitation device.

NDA-labeled DNP-labeled carbonylated cytochrome C (1 µg/ml) was injected

into the device at a rate of 5 µL/minute prior to the capture saturation plateau, for a total

of 110 minutes, 550 ng of carbonylated cytochrome C (or 11 picomole of protein

carbonyl) was injected into the immunoaffinity based microchip and the flow through

was collected every minute. The collected volume was then transferred to fluorescence

spectrometer for fluorescence measurement. All the fluorescence intensity of the captured

NDA labeled carbonylated cytochrome C was summed up with a total of 8249 A.U.

Considering 1 µg/ml NDA-carbonylated cytochrome C solution has an intensity of

268.28 A.U. at 479 nm, a total amount of 159 ng carbonylated cytochrome C were

enriched by the microdevice. Hence, the chip was able to capture 28.0% of the oxidized

proteins over the 110 minutes injection period, whereas only 10.9% of the unoxidized

protein was captured. The interference block protein BSA existed in 50 fold higher than

the test protein, carbonylated cytochrome C. These results show that, even in extremely

low abundance, the chip is highly specific to oxidized proteins.

4.5.4   Elute Efficiency Quantification

After the µIP device was saturated by DNP labeled carbonylated proteins, the

capture proteins were eluted by injecting the elution solution (1% SDS in water solution)

at a flow rate of 5 µL/minute. By accumulating fluorescence values of each minute-

fraction, the total eluted amounts for both eluted carbonylated cytochrome C and

background BSA were shown in Figure 4-7. The fast-increase curve of eluted proteins

indicates that carbonylated proteins could be denatured and eluted in a relatively short

time-span. The fluorescence intensity of eluted NDA labeled carbonylated cytochrome C

was summed up with a total of 5742 A.U., which indicates that elute efficiency of 69.6%

for carbonylated cytochrome C by the microdevice. The eluted carbonylated protein

sample could be further utilized in a proteomic study for discovery of biomarkers. For the

elution of BSA, the total fluorescence intensity of 1194.7 A.U. as shown in the elution

experiment, only a total of 847 A.U. was shown in the TRITC-BSA capturing graph at

572 nm. The redundant fluorescence intensity at 572 nm peak could be resulted by

underestimating the crosstalking effect from the dye NDA. Also, the blocking BSA used

in the device fabrication could also be labeled by excessive TRITC and potentially affect the fluorescence intensity of the TRITC-BSA elute.

As a result of the denaturing effect brought by the elution solution (1% SDS solution), the immobilized anti-DNP are denatured after elution. The PDMS μIP device hereby could not be reusable after an affinity-based enrichment experiment. Nevertheless, the low cost of PDMS substrate and low antibody amount required could make the reusability less of a concern.

4.5.5   Conventional IP for Purification of Carbonylated BSA

A conventional IP for carbonylated proteins was carried out for comparison with the μ-IP method. Silver stained gel from conventional IP experiments, demonstrating three washes (W1-W3) and three elutions (E1-E3) was shown in Figure 4-8. After comparison, μ-IP proved to be more effective because it used significantly less samples (550 ng total protein vs. 5 mg), and required less time (less than three hours vs. six hours).
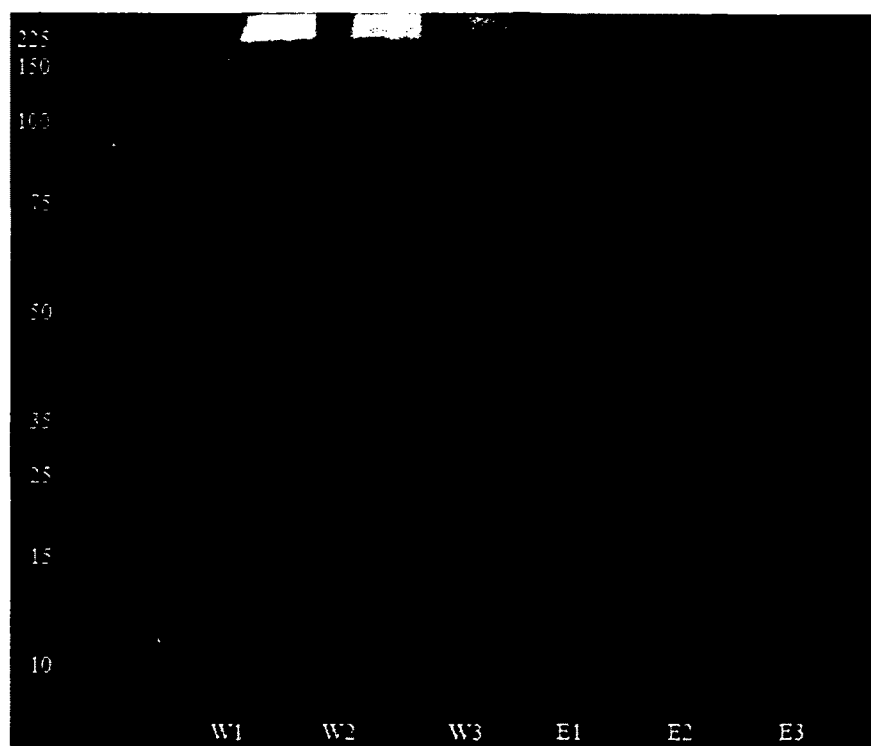
Figure 4-8: Conventional immunoprecipitation of DNP labeled oxidized BSA, shown by silver stained gel electrophoresis result.

Our micrometer-sized immunosensor (~3.1 μL) compared to ~1 mL tube based conventional IP assays accelerates the IP process significantly because of increased concentrations of antibody-coated post arrays and targeted proteins in the μ-chip platform. The close proximity also greatly enhances the encounter rate between the carbonylated proteins with anti-DNP antibody attributed from a short diffusion length.

4.6   Summary

Work described in this chapter shows a specific method for the detection of carbonylated protein using an immunosensor fabricated by the covalent coupling of the antibody onto a PDMMS substrate. This method can be widely extrapolated to other types of post-translational modified proteins. For example, nitrated proteins can be

targeted using anti-nitrotyrosine-body. The specificity of the sensor was illustrated by showing little captured protein when the sensor was exposed to negative control-native BSA using both fluorescence imaging and capture quantification. The specific interaction was further demonstrated in quantitative capture efficiency using off-chip fluorometric assessment. This immunosensor can be readily translated to monitor the other PTM proteins using different monoclonal and polyclonal antibodies.

CHAPTER 5

SIMULATION BASED OPTIMIZATION OF MICROFLUIDIC DEVICES USED FOR MOLECULAR ENRICHMENT

5.1 Introduction

As described in Chapter 3 and Chapter 4, PMMA and PDMS microfluidic devices have been designed and fabricated to biochemically enrich the desired post-translational-modified protein. Various alternative enrichment methods could be used. For example, DNP-labeled carbonylated proteins could be selectively enriched by chemically immobilized anti-DNP on the wall of the microchannel. This method has the advantages of high surface area to volume ratio, increased mass transfer coefficient, portability, and small analyte requirements. However, there are always requirements for microfluidic enricher to capture more molecular targets from the sample solution. Furthermore, microfluidic devices have the disadvantage of a high pressure drop. To optimize the benefits of the microfluidic devices, it is important to understand the effects of the operating parameters on molecular capture efficiency.

This study aims to optimize the molecular capture within the microfluidic device with respect to the geometric and operating parameters. The geometric parameters studied include the shapes and hydraulic diameters of the microposts. The operating parameters studied are Reynolds number, Peclet number and Damköhler number. These parameters are related to the flow velocity, diffusivity, and adsorption/desorption reaction

constants. This work will use finite element analysis software to simulate the fluid mechanics and transport within the microdevice, based on the governing partial differential equations and boundary conditions. Capture efficiency and pressure drop will be obtained for simulations in which the above mentioned operating parameters are varied.

5.2 Nomenclature

The following nomenclature will be used to describe the governing equations.

c_0: concentration of the target molecule in injected solution.

c_{in}: solution concentration on inlet, before reaction (mol/m^3)

c_{out}: outlet solution concentration (mol/m^3)

c_s: concentration of bound reaction sites in reaction on the functionalized surface in the microfluidic device (mol/m^2)

c_{s0}: initial concentration of unbound reaction sites on the functionalized surface in the microfluidic device (mol/m^2)

D: diffusion coefficient (m^2/s)

Da: Damköhler number

D_{hy}: hydraulic diameter (m)

E: capture efficiency

J: diffusion flux (mol/(m^{2}s))

k_{eq}: equivalent reaction constant

k_{off}: desorption reaction constant (s^{-1})

k_{on}: absorption reaction constant (mol/(m^{3}s))

Pe: Peclet number

R: surface molecule generation/consumption rate (mol/(m²s))

Re: Reynolds number, $Re = \rho U_i D_{hy}/\mu$

U: flow velocity (m/s)

5.3   Study Design

Previous studies have compared the performance of the inline and staggered array

arrangements in the microfluidic devices and described their respective advantages and

disadvantages. It is widely agreed that pressure drop is lower in the inline array

arrangement than in the staggered arrangement (John 2010). Those existing works carried

out about evaluating the capture efficiency and pressure drop of microfluidic devices with

microscale posts structures arranged in an inline pattern. The behavior of square shaped

microscale posts is studied in this chapter with respect to the Reynolds number, Peclet

number, Damköhler number, and equilibrium reaction constant. The performance of each

shape is studied with respect to variation in pitch (wall-to-wall spacing between the

posts) in the axial and transverse directions and microscale post aspect ratio. The capture

efficiency and overall pressure drop are used to evaluate the overall performance of the

microfluidic device.

Capture efficiency profile and pressure drop pattern for all the models developed

in this study are obtained by numerically solving the governing equations using the

commercially available computational finite elemental analysis software COMSOL

Multiphysics 4.2.a. A basic microfluidic device 15 mm in length and 1.2 mm in width is

modeled. This basic model included an array of 25 × 3 microscale posts (25-50 in the

axial direction and 2-6 in the transverse direction). For axis and transverse pitch

experiments, the overall length and width of the microchannel is fixed, and the array with

smaller pitch length is placed in the middle of the channel for comparable groups or

results. Figure 5-1 shows the arrangement of arrays of microscale posts for different

transverse pitch.
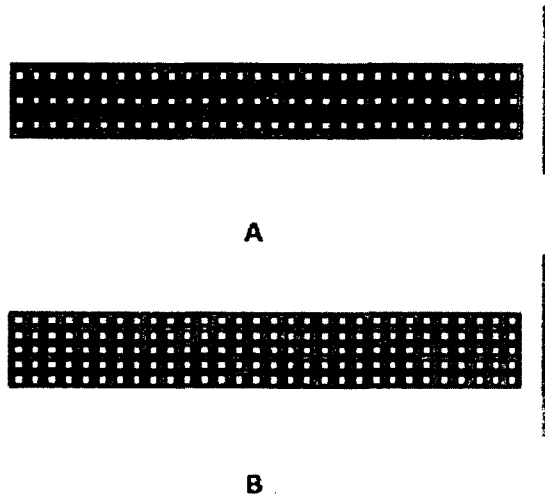
Figure 5-1: Top view of the design of microfluidic device in COMSOL for simulation. A-
B. Arrangement of arrays of microscale posts for 400 μm and 160 μm transverse pitch,
respectively.

Boundary conditions are applied on both sides of the microchannel and the walls

of the microscale posts. The governing equations and the boundary conditions are

discussed in the subsequent sections. The Reynolds number is set between 0.01 and 10;

hence, the flow is considered laminar for all the models. A uniform concentrated solution

is introduced at the inlet of the microfluidic device and the concentration of the target

molecule use the value of 0.004 M.

5.4   Theory

The device was modeled with a microchannel-and-array-of-posts model. A top

view of the microfluidic device is shown in Figure 5-1. The total length of the

microchannel of the device along the x-axis is L, the width of the device is W, the

diameter of the microscale post is d, and the axial and transverse pitches are p_a and p_t,

respectively. To decrease the computational requirements of the simulation, two

assumptions are introduced:

a.   No-slip boundary condition is assigned to the walls of the microchannel

and the microscale posts in contact with the fluid in the model,

b.   The device in considered of a high aspect ratio, so the boundary effects

along the top and bottom layers of the device were neglected.

The concentration profile and the pressure drop mapping of the microfluidic

device are obtained by solving three governing equations numerically. The governing

equations are:

$$\rho(u \cdot \nabla)u = \nabla \cdot [-pI + \mu(\nabla u + (\nabla u)^T)], \qquad \text{Eq. 5-1}$$

$$\nabla \cdot (u) = 0, \qquad \text{Eq. 5-2}$$

$$\nabla \cdot (-D\nabla c) + u \cdot \nabla c = 0. \qquad \text{Eq. 5-3}$$

Eq. 5-1 is the momentum equation of the microchannel while Eq. 5-2 is the

continuity equation. Eq. 5-3 is the concentration equation for the liquid. Certain boundary

conditions are to be defined in order to solve the governing equations of the current

model and these are discussed below.

For the inlet boundary condition, a uniform, unidirectional inlet flow rate was

specified. The inlet flow velocity can be calculated from the Reynolds number and

hydraulic diameter.

$$U_i = \mu Re/(D_{hy}\rho). \qquad \text{Eq. 5-4}$$

The pressure in the device (p) is calculated with respect to the pressure at the outlet, so the outlet pressure boundary condition is given by:

$$p_o = 0. \qquad \text{Eq. 5-5}$$

The non-slip boundary condition is represented by:

$$u_s = 0. \qquad \text{Eq. 5-6}$$

where the subscript s represents all surfaces that are in contact with the flowing fluid.

The transport of the target molecule to the functionalized surface is governed by the diffusion equation:

$$-n \cdot (-\nabla C_s) = R. \qquad \text{Eq. 5-7}$$

Eq. 5-8 and Eq. 5-9 represents the boundary conditions used for solving the advection-diffusion equation. In order to simulate the actual absorption/desorption of species in the device, a uniform concentrated solution flow is applied at the inlet of the model and is represented using Eq. 5-8. In the case of the assumption of the high aspect ratio channel, the width of the channel is neglected in comparison with its height. In this two-dimensional simulation of a microfluidic device, the top and bottom surfaces are not considered:

$$c_{in} = c_0. \qquad \text{Eq. 5-8}$$

On the walls of the microchannel or the microscale posts, the species absorption and desorption, R, is applied as the boundary condition. The "process of capturing" is based on the interaction between molecules, and could be considered as an instant reaction. Thus, at any position that is very close to the wall, the number of molecules captured is the net result of adsorption and desorption. Therefore, for any position very close to the wall in the channel, the surface species generation/consumption rate R is:

$$R = k_{on}c(c_{s0} - c_s) - k_{off}c_s, \qquad \text{Eq. 5-9}$$

where $(c_{s0} - c_s)$ is the concentration of available binding sites on the reactive surface.

The surface species generation/consumption rate R is further described by four nondimensionalized parameters: Reynolds number (Re), Peclet number (Pe), Damköhler number (Da) and equivalent reaction constant k_{eq}. Describing the system with dimensionless parameters could grant this study universal applicability, since the equivalent reaction constant combines the adsorption and desorption constants:

$$k_{eq} = \frac{k_{off}}{k_{on}c_0}. \qquad \text{Eq. 5-10}$$

Damköhler number characterizes the relationship between diffusion transport and reaction, as species in the center of the channel need to approach the channel wall prior to being captured by the reactive sites on the wall:

$$Da = \frac{k_{on}c_{s0}D_{hy}}{D}. \qquad \text{Eq. 5-11}$$

The flow velocity affects the operation of the device by two means. A high flow velocity may result in turbulent flow and hereby result in rapid transport of target species to the channel wall. However, due to the restriction of pressure drop, the flow in the microfluidic enricher remains laminar, where the influence of flow velocity on the molecule diffusion is described by the Peclet number (Pe):

$$Pe = \frac{D_{hy}U}{D}. \qquad \text{Eq. 5-12}$$

Flow velocity differs in the microfluidic device of different scale and structure. To find a more common solution for the micro enricher problem, we use Reynolds number (Re) to replace the flow velocity:

Flow velocity differs in microfluidic device of different scale and structure. To find a more common solution for the micro enricher problem, we use Reynolds number (*Re*) to replace flow velocity, Eq. 5-4, Eq. 5-10, Eq. 5-11, and Eq. 5-12 can be used in Eq. 5-9 to obtain:

$$R = \frac{\left(Da\ Re\frac{v}{\rho}\right)}{C_{s0}\ D_{hy}Pe} c(C_{s0} - c_s) - \frac{\left(Da\ Re\frac{v}{\rho}\right)}{C_{s0}D_{hy}Pe} k_{eq}c_0 c_s.$$ Eq. 5-13

All of the solution that reaches the outlet of the microchannel will leave the device. Thus, an outlet boundary condition can be added to state that the outlet will quench all unabsorbed concentration:

$$-n \cdot (-D\nabla c_{out}) = 0.$$ Eq. 5-14

The diffusion flux of the target molecule toward the wall, and the diffusion flux on wall from a higher concentration region to a lower concentration region, is controlled by a diffusion equation:

$$\Delta c_s = 0.$$ Eq. 5-15

The device capture efficiency is defined by:

$$E = \frac{c_0 - c_{out}}{c_0}.$$ Eq. 5-16

5.5   Mesh Optimization

Finite element analysis requires an appropriate meshing scheme. For the study presented in this paper, a triangular mesh was used. To determine the appropriate mesh size, an initial simulation was run with a relatively coarse mesh, and subsequent simulations were run with progressively smaller mesh elements until the relative maximum difference in capture efficiency between two successive mesh geometries was less than 0.3%. An example of grid dependency for one of the models (square microscale

posts) is shown in Table 5-1. It can be noted from Table 5-1 that the refining of the mesh

for each model is continued until the value of both the output parameters (outlet

concentration and the pressure drop) for two consecutive mesh settings are very close.

Table 5-1: Example of grid dependency for the triangular mesh (for the model size of 10 mm × 1.2 mm).

x-element number	y-element number	number of nodes	capture efficiency difference	pressure drop difference
230	46	217370	-	-
220	44	207621	0.26%	-0.03%
210	42	198049	0.29%	-0.02%
200	40	188806	0.32%	-0.05%

5.6   Results and Discussion

The simulated concentration of the target species is shown in Figure 5-2. The

maximum concentration is at the inlet and the minimum concentration is at the outlet.

This behavior is expected because the wall of the microfluidic device adsorbs the target

species until the surface area becomes saturated. Three cases were considered. In Case 1,

the parameters that govern diffusion and reaction rates were varied. In Case 2, the axial

pitch between the microscale posts is varied. In Case 3, the pitch between transverse

microscale posts is varied.
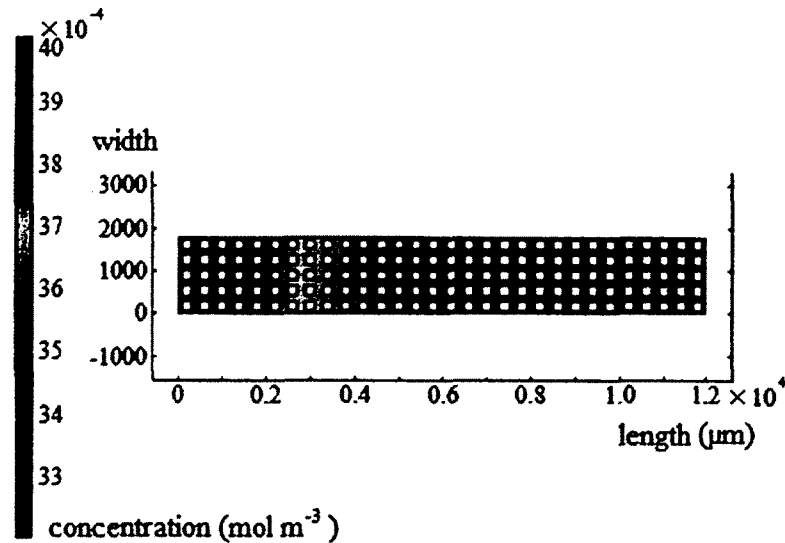
Figure 5-2: Contour plot showing the concentration distribution in the microfluidic device after obtaining the solution of the model.

5.6.1   Case 1: Effect of Transport and Reaction Parameters

The effects of axial and transverse pitch are on both capture efficiency and pressure drop. These effects will also be discussed with respect to the effect of pitch on the microsystem's inner surface area. In these studies, the hydraulic diameter of the microposts was 200 μm. The length and width of the microchannel were fixed as 12 mm and 1.8 mm, respectively. The study is conducted over the range of Re from 0.01 to 10, while not losing the generality of the problem, Pe, Da and k_{eq} use constant value of 0.01.

Figure 5-3 shows capture efficiency as Re ranges from 0.01 to 10. The Pe, Da and k_{eq} values used to generate these data were a constant value of 0.01. Capture efficiency decreased weakly with increased Re, from 13.60% at Re = 0.01 to 13.23% at Re = 10. Since Re represents the flow velocity when the other parameters are left unchanged, the flow velocity does not affect the capture efficiency in this laminar flow microsystem. The effect of Re is greater for smaller Re values. To further examine the

effect of Reynolds number as Pe, Da and k_{eq} change, simulations with Re value from 0.01 to 0.1 will be compared.
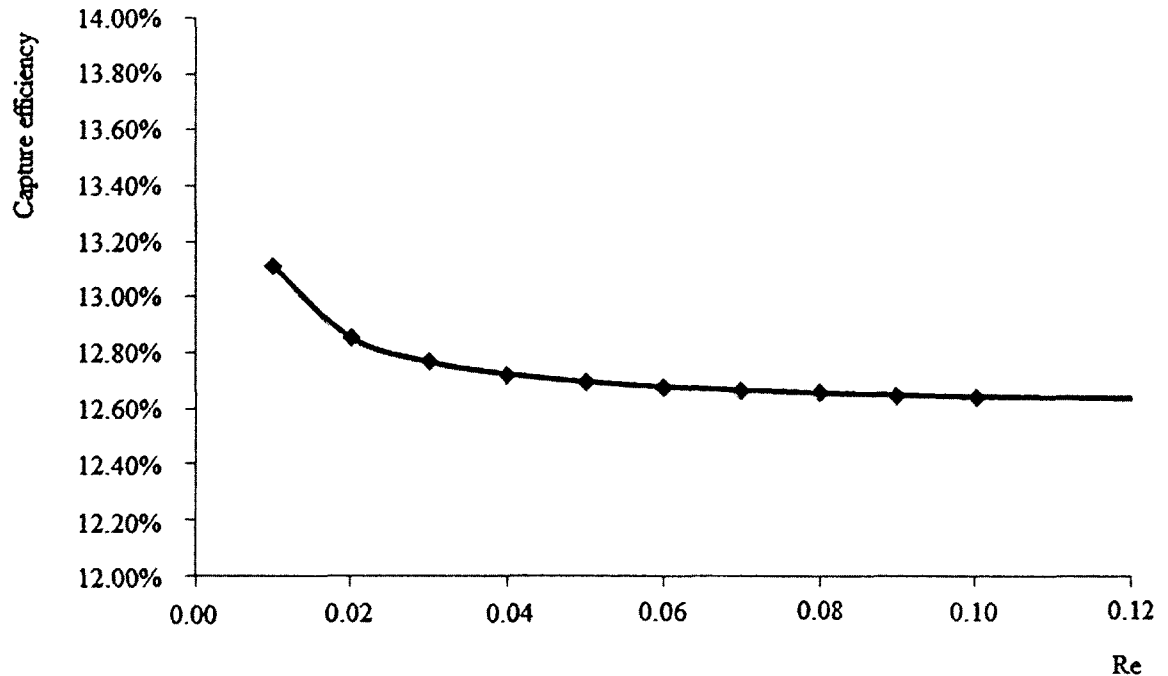
Figure 5-3: Capture efficiency as a function of Reynolds number

Figure 5-4 shows capture efficiency as a function of Re for Pe values of 0.01, 0.1, 1 and 10. The values of Da and k_{eq} were also set at 0.01. As Pe increased, capture efficiency decreased, from 13.60% for $Pe = 0.01$ to 5.29% for $Pe = 0.1$ and further to 0.42% for $Pe = 10$. This result is expected from Eq. 5-12 because an increased Pe indicates a decreased diffusivity, D, and hence diminished transport to the capturing surface. Thus, a target species with a smaller diffusivity will be captured less efficiently in a given microfluidic device than a species with a larger diffusivity. Figure 5-4 also shows that the affection of Re is weaker than the effect of Pe. However, at the highest value of Pe, the percent change in capture efficiency with Re is relatively large.
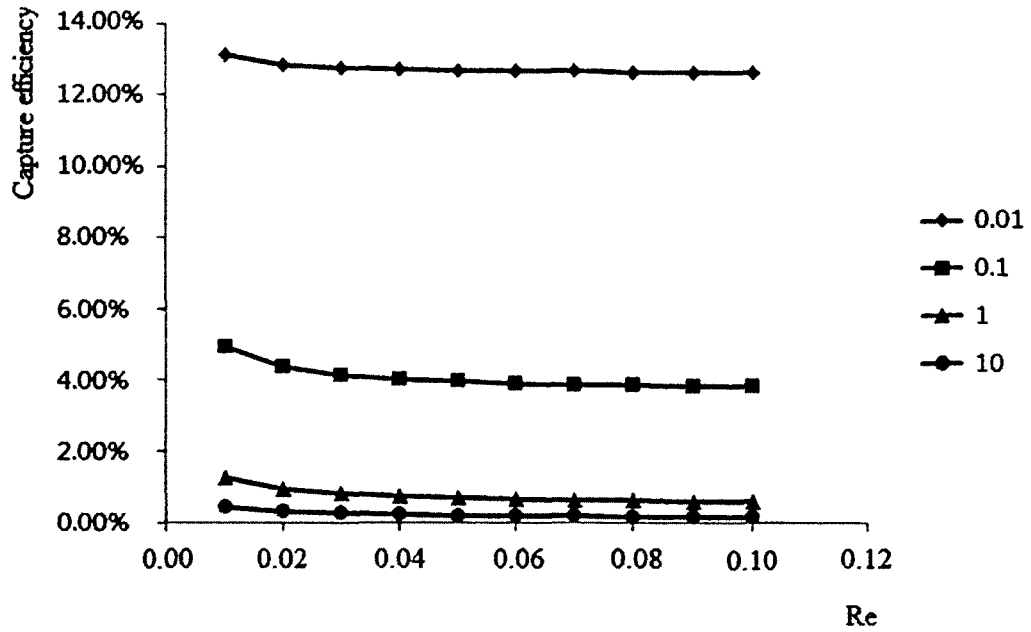
Figure 5-4: Capture efficiency as a function of Reynolds number for different Peclet numbers.

Figure 5-5 shows capture efficiency as a function of *Re* for *Da* values of 0.01, 0.1, 1, and 10. For *Da* values of 1 and 10, the capture efficiency is near 100%, and independent of *Re*. As *Da* decreases, capture efficiency decreases from 66.54% at *Da* = 0.1 to 13.60% at *Da* = 0.01. This decrease is expected from Eq. 5-11 because *Da* is proportional to the adsorption constant, k_{on}, so the rate of reaction with the wall is increased as *Da* increases. Figure 5-5 also shows that the effect of *Da* is much stronger than the effect of *Re*. However, in the design of the microfluidic device the ability to greatly alter k_{on}, and hence *Da*, is likely to be limited. Nonetheless, any increase of *Da* will greatly improve the capture efficiency of the device.
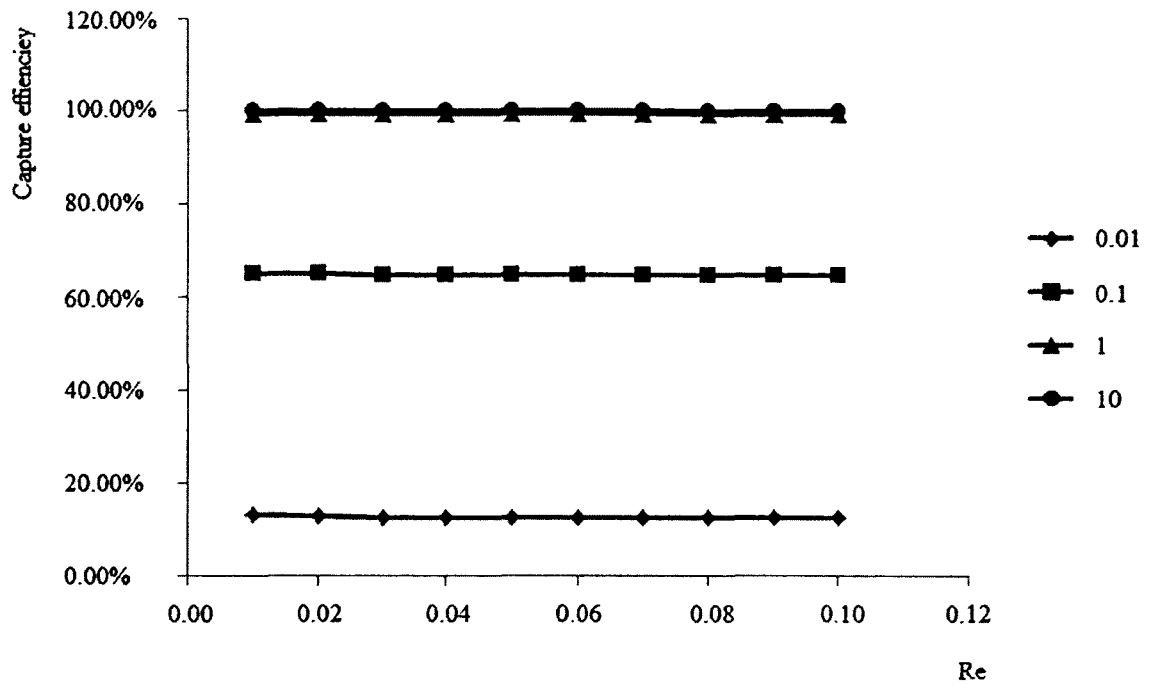
Figure 5-5: Capture efficiency variation with Damköhler number.

Figure 5-6 shows capture efficiency as a function of Re for k_{eq} values of 0.01, 0.1, 1 and 10. As k_{eq} decreases, the capture efficiency decreases. This result is expected from Eq. 5-10, which indicates that k_{eq} is proportional to the releasing reaction constant k_{off}. In this discussion, it is assumed that the Damköhler number, and hence k_{on}, is constant. The effect of reaction constant on the capture efficiency is limited. Even at low Re, where the effect of k_{eq} is strongest, capture efficiency changes by less than 1% for a three order of magnitude change in k_{eq}.
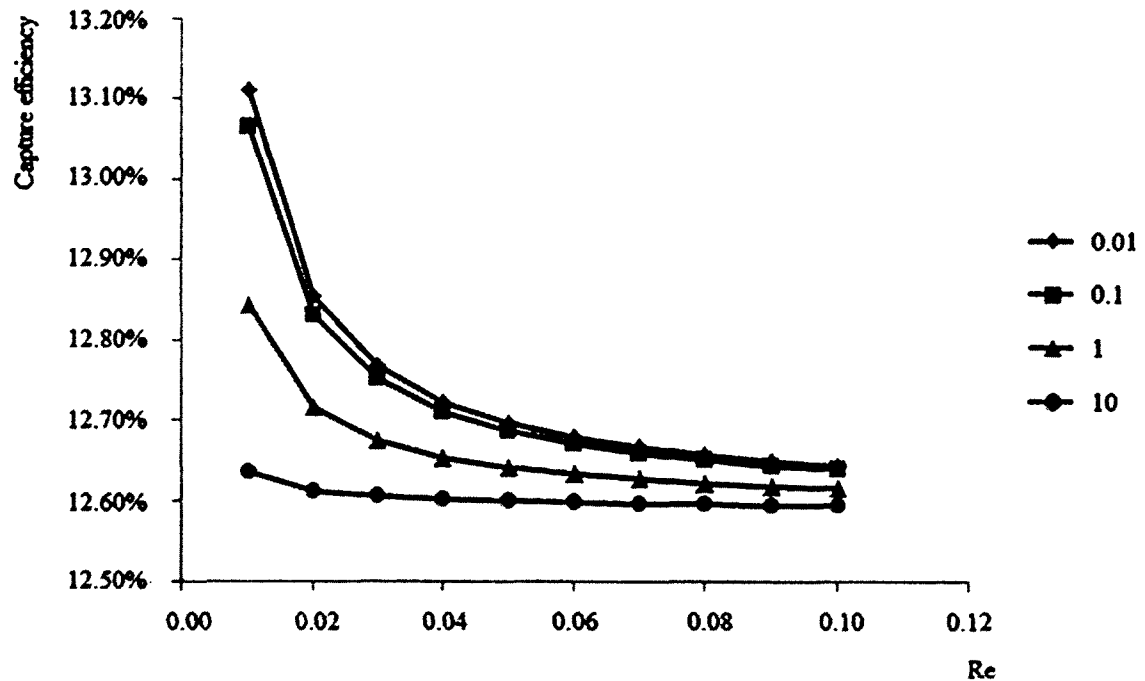
Figure 5-6: Capture efficiency variation with equivalent reaction constant.

5.6.2   Case 2: Effect of Pitch

Simulations were performed to determine the effects of axial and transverse pitch on both capture efficiency and pressure drop. These effects will also be discussed with respect to the effect of pitch on the microsystem's inner surface area. In these studies, the hydraulic diameter of the microposts was 200 μm, The length and width of the microchannel were fixed as 12 mm and 1.8 mm, respectively. The values of Pe, Da and k_{eq} were all 0.01, and simulations were performed for Reynolds numbers from 0.01 to 10.

Figure 5-7 shows the capture efficiency and pressure drop within the microfluidic device as a function of the axial pitch. The transverse pitch was fixed at 200 μm. The efficiency dropped by nearly a factor of 2.7 as the pitch increased from 40 μm to 400 μm, and the pressure drop was reduced by two orders of magnitude.
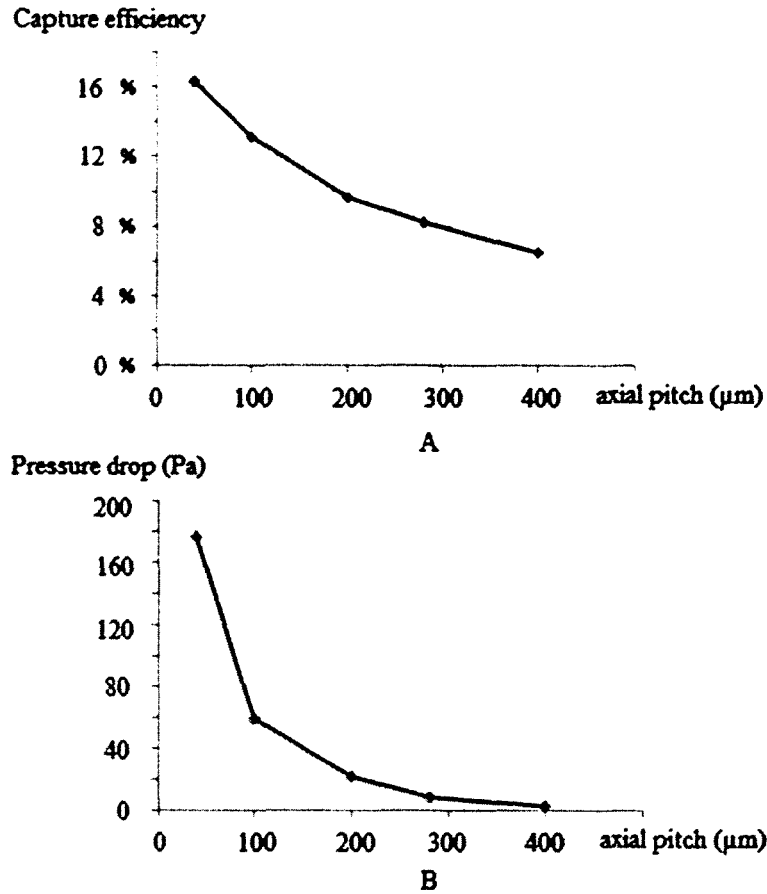
Figure 5-7: A. Capture efficiency variation for different widths of axial pitch distance with a fixed y-axis pitch width of 250 μm; B. Pressure drop variation for different widths of axial pitch with a fixed transverse pitch of 250 μm.

Similar trends were observed when the axial pitch was fixed at 200 μm and the transverse pitch was varied, as shown in Figure 5-8. The decrease in efficiency as the transverse pitch increased from 100 μm to 400 μm was approximately a factor of 2.5, as opposed to the factor of approximately two for the same change in the axial pitch. The decrease in pressure drop for the same range was a factor of approximately 18, and was similar to the decrease for the same change in the axial pitch. The pressure drop across the microfluidic device is almost proportional with Reynolds number applied on the flow for all pitch cases (data not shown). The pressure drop for an axial pitch of 200 μm and a

transverse pitch of 100 μm is similar to the pressure drop for an axial pitch of 40 μm and

a transverse pitch of 200 μm. Thus, narrow transverse spacing between posts more

strongly affects pressure drop than narrow axial spacing. This result is expected. In the

limit of zero transverse spacing and finite axial spacing, the flow would be completely

blocked, so the required driving pressure for finite flow would be infinite, but zero space

between posts in the axial direction would still allow flow to be driven with a finite

pressure.

Capture efficiency

30 %

20 %

10 %

0 %

0   200   400   600   transverse pitch (μm)

A

Pressure drop (Pa)

200

160

120

80

40

0

0   200   400   600   transverse pitch (μm)

B
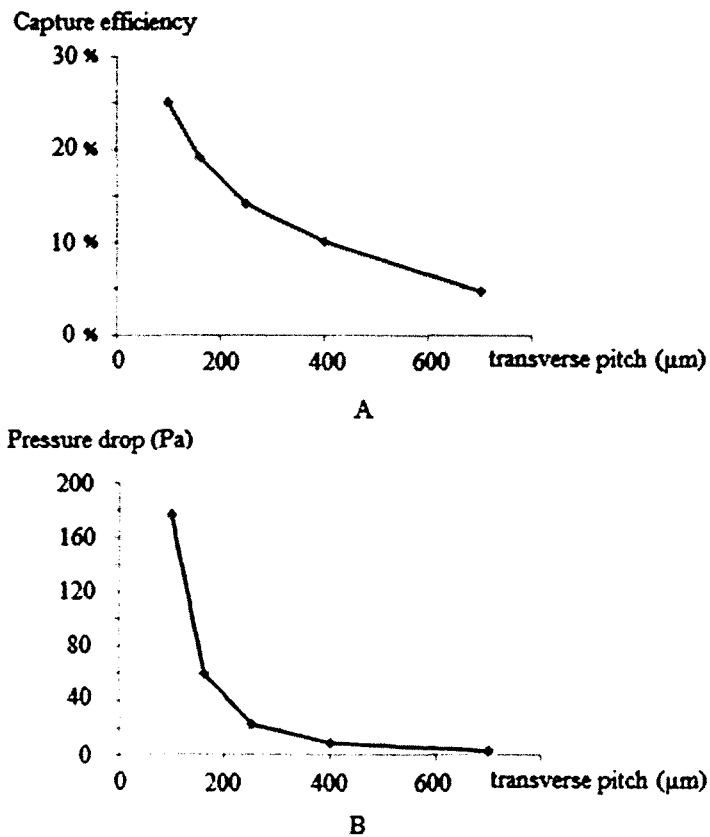
Figure 5-8: A. Capture efficiency variation for different widths of transverse pitch distance with a fixed axial pitch width of 200 μm; B. Pressure drop variation for different widths of transverse pitch with a fixed axial pitch of 200 μm.

The decrease in capture efficiency with an increased pitch may be strongly caused by the corresponding large decrease in the reactive functionalized inner surface area within the microchannel. This effect is examined in Figure 5-9 which shows the capture efficiency as a function of the inner functionalized surface area for the simulation results that were obtained from the axial and transverse pitch studies. The efficiency increased linearly with functionalized area for both studies. The slope for axial pitch variation is greater than that for transverse pitch variation, so efficiency increases more rapidly with increased surface area when transverse spacing is decreased than when axial spacing is decreased.

Capture efficiency
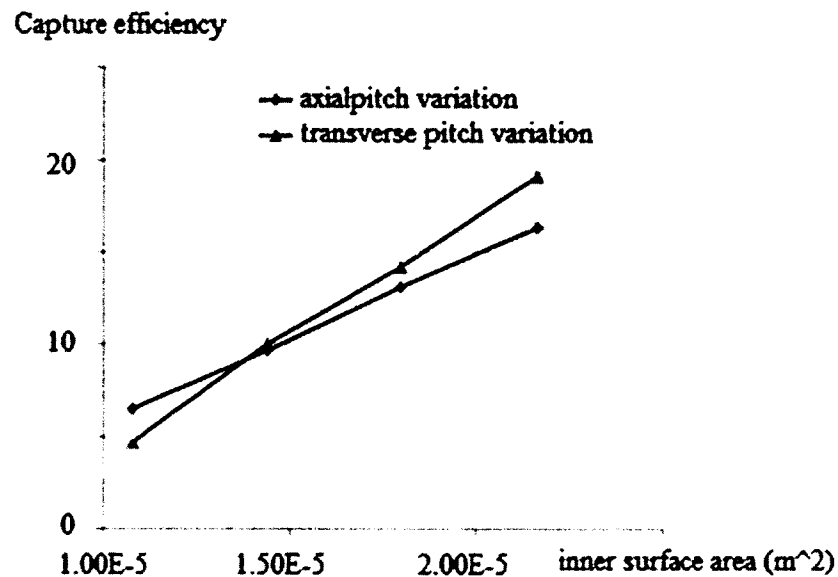
Figure 5-9: Relationship between capture efficiency of the microfluidic device and its inner functionalized surface area.

5.6.3   Case 3: Effect of Aspect Ratio of the Microscale Posts

Figure 5-10 shows the effect of the aspect ratio, length to width (L/W), of the rectangular shaped microscale posts on the capture efficiency and pressure drop of the microfluidic device. In all cases, the post structures had the same hydraulic diameter, 200

μm, and the aspect ratio was varied from 1/3 to 3. For each aspect ratio, the total length

and width of the microchannel was adjusted to keep the axial and transverse pitch

constant. Thus, length ranged from 8.33 to 15 mm and width ranged from 1 to 1.8 mm.

Re, Pe, Da and k_{eq} were all set to 0.01.
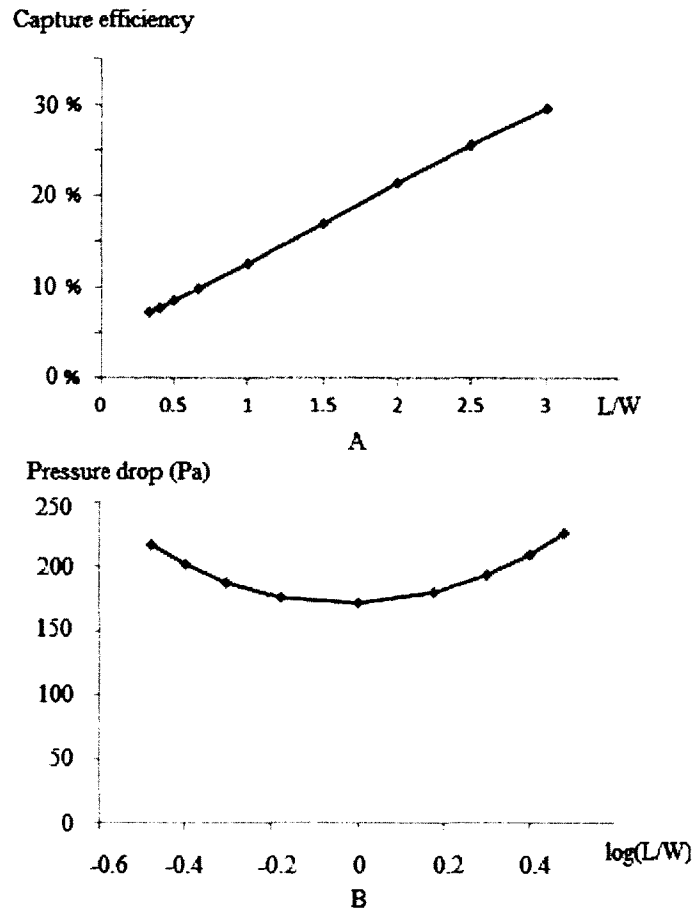
Figure 5-10: A. Capture efficiency variation for arrays of different length to width ratio of rectangular shape microscale posts; B. Pressure drop variation for arrays of different length to width ratio of rectangular shape microscale.

As the aspect ratio increased, the capture efficiency for the microfluidic device

also increases. This effect is expected because microscale posts with longer axial edges

will overlap the flow line more and hence provide more chances for the target species in the solution to diffuse toward and react with the functionalized wall.

The change in pressure drop with the logarithm of the post aspect ratio follows a symmetric curve. Thus, microfluidic devices with arrays of the same dimension (e.g. rectangular shapes with aspect ratios of 3:1 and 1:3) will have similar pressure drops when the axial and transverse pitches are maintained.

5.7   Summary

The overall performance simulation of the microfluidic device designed for the separation and purification of target molecule are studied in this paper. The microfluidic device is evaluated in terms of its capture efficiency and pressure drop. The adsorption reaction constant strongly affects the device's capture efficiency. The diffusion and desorption constants are also important. As a result, a high affinity between the functionalized surface and target molecule enhances the efficiency of the device when the flow velocity is low and the diffusion rate high. The effects of the device geometry on the capture efficiency and pressure drop of the device were also studied. The results demonstrate that a microchannel with a high density packed array of microscale posts with high aspect ratio along the flow direction is beneficial for high capture efficiency. However, high density packed posts will lead to a large pressure drop. Practical devices will need to balance the need for large capture efficiency with the need for a low pressure drop.

CHAPTER 6

CONCLUSION AND FUTURE WORK

In this dissertation, the design, fabrication, application and simulation of

microfluidic chips interfaced to post-translational modified proteins for proteomic

applications is described. Two sets of pressure driven microfluidic device allows target

protein to be enriched, detected by fluorescence spectrometry eluted for MS analysis. A

simulation model of molecular enrichment microfluidic device based on geometric and

operation parameters have been built. Overall, the significance of this work lies in the

ability of the microfluidic devices to serve as a fast and effective analytical tool for

proteomic research works.

In Chapters 3 and 4, this work illustrated the direct use of affinity and antibody-

antigen based microdevice to enrich carbonylated BSA. An obvious extension of the

study is to apply this biomedical micro device in the selectively enrichment of

carbonylated proteins from protein mixtures. We used carbonylated protein as a

representative post translational modification (PTM) to highlight this novel strategy

employed to enrich PTM in modification-specific proteomics. However, this microdevice

is suitable for any protein that can be derivatized and labeled with biotin tags. For

example, nitrosylated proteins (Pr-SNO) can be specifically reduced to free thiol groups

on cysteine amino acid site, and then further labeled by thiol-specific biotin maleimide

tags (Jaffrey and Snyder 2001). Likewise, another type of PTM, glutathionylated proteins (Pr-SSG) can be enzymatically converted to thiol groups and consecutively tagged with biotin (Reynaert, et al. 2006).

The further proteomic study on carbonylated proteins will provide a better understanding of major proteins and pathways/functions that may be responsible for aging and Alzheimer's disease. Ultimately, the device described above will help on developing therapeutic approaches to prolong useful life and to treat or prevent diseases. Future work based on the design of the microfluidic device in this work, which can detect, capture and elute biotinylated carbonylated BSA, are likely to be suitable for affinity enrichment for complex proteomics screening.

Another great potential of the microdevice in this work is to enrich PTM peptides. In order to accomplish this, protein lysate of interest will undergo digestion prior to injecting the proteolytically digested peptides into this affinity based enrichment microdevice. This potential application will help identify the modification sites of PTM and further disclose the possible pathways involved. Lastly, this subproteome enrichment micro-device can be assembled with other lab-on-a-chip components for follow-up protein analysis.

In the area of heat transfer, optimizing geometric features in designing heat fins has a long history (Cobble 1971). Also, great amount of work have been done in simulation enhanced optimization of find in heat-exchanger (Tsai, Sheu and Lee 1999) and heat-sink (Grannisa and Sparrowb 1991).

There is a long history to designing and optimizing geometric features based on specific requirements and cases in the area of heat transfer devices (Kaye 1956), which

are originally widely applied in the electronic industry. In the work of heat sink design, until now, the inner geometric design is still on very importance about the heat sink performance (Bhatti, Joshi and Johnson 2002) (Cannell, Cooley and Garman 2004). In the work of protein enriching device design, there is requirement of decrease experiment time, and increase capture efficiency per surface area: shorter time means higher performance, while smaller inner surface area with high capture efficiency means decrease of non-specific protein enriching. Future work should focus on the optimization of the geometric design of the microfluidic device depending on operation parameters such as target molecular diffusion rate, absorb/desorb rate. Also, optimization work of the microfluidic device that reduces sample loss, for example, reduces dead volume of the device is also necessary. Mathematic tools, including simulation software will play an important role in this work.

BIBLIOGRAPHY

Adams, A.A., et al. (2008). "Highly Efficient Circulating Tumor Cell Isolation from Whole Blood and Label-Free Enumeration Using Polymer-Based Microfluidics with an Integrated Conductivity Sensor." *J Am Chem Soc*, 130(27), 8633-8641.

Afanassiev, V., V. Hanemann, and S. Wölfla. (2000). "Preparation of DNA and protein micro arrays on glass slides coated with an agarose film." *Nucleic Acids Res*, 28(12), e66.

Andrade, J. D., and V. Hlady. (1986). "Protein adsorption and materials biocompatibility: A tutorial review and suggested hypotheses." *Adv Polym Sci*, 79, 1-63.

Becker, H., and L. E. Locascio. (2002). "Polymer microfluidic devices." *Talanta*, 56(2), 267-287.

Bhatti, M. S., S. M. Joshi, and R. S. Johnson. (2002). High performance heat sink for electronics cooling. U.S. Patent 6024531.

Bico, J., C. Tordeux, and D. Quéré. (2001). "Rough wetting." *Europhys Lett*, 55(214), 214-220.

Boveris, A., and E. Cadenas. (2000). "Mitochondrial production of hydrogen peroxide regulation by nitric oxide and the role of ubisemiquinone." *IUBMB life*, 50, 245-250.

Boyd-Kimball, D., et al. (2005). "Proteomic identification of proteins oxidized by $A\beta(1-42)$ in synaptosomes: Implications for Alzheimer's disease." *Brain Res*, 1044, 206-215.

Buranda, T., G. M. Jones, J. P. Nolan, J. Keij, G. P. Lopez, and L. A. Sklar. (1999). "Ligand Receptor Dynamics at Streptavidin-Coated Particle Surfaces: A Flow Cytometric and Spectrofluorimetric Study." *J Phys Chem*, 107(17), 3399-3410.

Cannell, M. J., R. Cooley, and R. W. Garman. (2004). Fluid-cooled heat sink with turbulence-enhancing support pins. U.S. Patent 6729383.

Chang, T. Y., et al. (2007). "Cell and Protein Compatibility of Parylene-C Surfaces." *Langmuir*, 23, 11718-11725.

Chen, X., H. Wu, and C. Whitesides, G. M. Mao. (2002). "A Prototype Two-Dimensional Capillary Electrophoresis System Fabricated in Poly(dimethylsiloxane)." *Anal Chem*, 74(8), 1772-1778.

Choi, J., C. A. Malakowsky, J. M. Talent, and C. C. Conrad. (2002). "Identification of oxidized plasma proteins in Alzheimer's disease." *Biochem Biophys Res Commun*, 293, 1566-1570.

Cobble, M. H. (1971). "Optimum finshape." *J Franklin I*, 291, 4, 283-292.

Cui, H., Y. Kong, and H. Zhang. (2012). "Oxidative Stress, Mitochondrial Dysfunction, and Aging." *J Signal Transduct 2012*, 1-13.

Dalle-Donne, I., R. Rossib, D. Giustarinib, A. Milzania, and R. Colombo. (1999). "Protein carbonyl groups as biomarkers of oxidative stress." *Clin Chim Acta* (Oxford Univ. Press), 329, 23-38.

Dodge, A., K. Fluri, E. Verpoorte, and N. F. de Rooij. (2001). "Electrokinetically Driven Microfluidic Chips with Surface-Modified Chambers for Heterogeneous Immunoassays." *Anal Chem*, 73, 3400-3409.

Drouge, W. (2002). "Free radicals in the physiological control of cell function." *Physiological reviews*, 82, 47-95.

Drummond, J. E., and M. I. Tahit. (1984). "Laminar viscous flow through regular arrays of parallel solid cylinders." *Int J Multiphase Flow*, 10(5), 515-540.

Duffy, D. C., J. C. McDonald, O. J. A. Schueller, and G. M. Whitesides. (1998). "Rapid Prototyping of Microfluidic Systems in Poly (dimethylsiloxane)." *Anal Chem*, 70(23), 4974-4984.

Dulm, P. V., and W. Norde. (1983). "The adsorption of human plasma albumin on solid surfaces, with special attention to the kinetic aspects." *J Colloid Interf Sci*, 91(1), 248-255.

Edwards, D.A.(2007). "Steric hindrance effects in thin reaction zones: applications to BIAcore." *Ima J Appl Math*, 72(6), 865-893.

England, K., and T. Cotter. (2004). "Identification of carbonylated proteins by MALDI-TOF mass spectroscopy reveals susceptibility of ER." *Biochem Biophys Res Commun*, 320(1), 123-130.

Ethier, M., W. Hou, H. S. Duewel, and D. Figeys. (2006). "The Proteomic Reactor: A Microfluidic Device for Processing Minute Amounts of Protein Prior to Mass Spectrometry Analysis." *J Proteome Res*, 5(10), 2754-2759.

Faure, K. (2010). "Liquid Chromatography on chip." *Electrophoresis*, 31(15), 2499-2511.

Feng, J., and E. A. Arriaga. (2008). "Quantification of carbonylated proteins in rat skeletal muscle mitochondria using capillary sieving electrophoresis with laser-induced fluorescence detection." *Electrophoresis*, 209(2), 475-482.

Figeys, D., and D. Pinto. (2001). "Proteomics on a chip: Promising developments." *Electrophoresis*, 22(2), 208-216.

Freire, S. L. S., and A. R. Wheeler. (2006). "Proteome-on-a-chip: Mirage, or on the horizon?" *Lab Chip*, 6, 1415-1423.

Genova, M.L., et al. (2001). "The site of production of superoxide radical in mitochondrial complex I is not a bound ubisemiquinone but presumably iron–sulphur cluster N2." *FEBS Lett*, 364-368.

Grannisa, V. B., and E. M. Sparrowb. (1991). "Numerical simulation of fluid flow through an array of diamond-shaped pin fins." *Number Heat Tr A-Appl*, 19(4), 381-403.

Griffiths, J. (2008). "A microfluidic chip measures embryo metabolism." *Anal Chem*, 80(17), 6461-6461.

Harman, D. (1972). "A biologic clock: the mitochondria." *J Am Geriatr Soc*, 20(4), 145-147.

Harman, D. (1956). "Aging: a theory based on free radical and radiation chemistry." *J Gerontol*, 11, 298-300.

Haynes, C. A., and W. Norde. (1994). "Globular proteins at solid/liquid interfaces." *Colloid Surface B*, 2(6), 517-566.

Henry, A. C., et al. (2000). "Surface Modification of Poly (methyl methacrylate) Used in the Fabrication of Microanalytical Devices." *Anal Chem*, 72(21), 5331-5337.

Herr, A. E., et al. (2007). "Microfluidic immunoassays as rapid saliva-based clinical diagnostics." *National Acad Sciences*, 104(13), 5268-5273.

Holmberg, A., A. Blomstergren, O. Nord, M. Lukacs, J. Lundeberg, and M. Uhlén. (2005). "The biotin-streptavidin interaction can be reversibly broken using water at elevated temperatures." *Electrophoresis*, 26(3), 501-510.

Honda, K., G. Casadesus, R. B. Petersen, G. Perry, and M. A. Smith. (2004). "Oxidative Stress and Redox-Active Iron in Alzheimer's Disease." *Ann NY Acad Sci*, 1012, 179-182.

Houseman, B. T., J. H. Huh, S. J. Kron, and M. Mrksich. (2002). "Peptide chips for the quantitative evaluation of protein kinase activity." *Nat Biotechnol*, 20, 270-274.

Jacobson, S. C., A. W. Moore, and J. M. Ramsey. (1995). "Fused Quartz Substrates for Microchip Electrophoresis." *Anal Chem*, 67(13), 2059-2063.

Jacobson, S. C., L. B. Koutny, R. Hergenroeder, A. W. Jr. Moore, and J. M. Ramsey. (1994), "On-chip Capillary Electrophoresis with an Integrated Postcolumn Reactor." *Anal Chem*, 66(20), 3472-3476.

Jaffrey, S. R., and S. H. Snyder. (2001). "The Biotin Switch Method for the Detection of S-Nitrosylated Proteins." *Sci STKE*, 86, 11-11.

James, P. (1997). "Protein identification in the post-genome era: the rapid rise of proteomics." *Q Rev Biophys*, 30, 279-331.

Jenner, P. (2003) "Oxidative stress in Parkinson's disease." *Ann Neurol*, 53, supp 13, S26-S38.

Jensen, O. N. (2004). "Modification-specific proteomics: characterization of post-translational modifications by mass spectrometry." *Curr Opin Chem Biol,* 8(1).

John, T., Mathew, B., Hegab, H. (2010). "Parametric study on the combined thermal and hydraulic performance of single phase micro pin-finheat sinks part I: Square and circle geometries." *Int J Therm Sci*, 49(11), 2177-2190.

Katsuhiko, A., N. Takashi, and M. Tsuyoshi. (2006). "Immobilization of Biomaterials to Nano-Assembled Films (Self-Assembled Monolayers, Langmuir-Blodgett Films, and Layer-by-Layer Assemblies) and Their Related Functions." *J Nanosci Nanotechnol*, 6(8), 2278-2301.

Kaye, J. (1956). "Review of Industrial Applications of Heat Transfer to Electronics." *Proceedings of the IRE*, 44(8), 977-991.

Kazakevich, Y., and R. LoBrutto. (2007). *HPLC for Pharmaceutical Scientists.* Hoboken: John Wiley & Sons, Inc.

Kelleher, N. L., H. Y. Lin, G. A. Valaskovic, D. J. Aaserud, E. K. Fridriksson, and F. W McLafferty. (1999). "Top Down versus Bottom Up Protein Characterization by Tandem High-Resolution Mass Spectrometry." *J Am Chem Soc*, 121(4), 806-812.

Kristensena, B. K., P. Askerlund, N. V. Bykova, H. Egsgaard, and I. M. Moller. (2004). "Identification of oxidised proteins in the matrix of rice leaf mitochondria by immunoprecipitation and two-dimensional liquid chromatography-tandem mass spectrometry." *Phytochemistry*, 65(12), 1839-1851.

Lee, J, S. A. Soper, and K. K. Murray. (2009). "Development of an efficient on-chip digestion system for protein analysis using MALDI-TOF MS." *Analyst*, 134, 2426-2433.

Levine, R. L. (2002). "Carbonyl modified proteins in cellular regulation, aging, and disease." *Free Radic Biol Med*, 32(9), 790-796.

Levine, R.L., J. Williams, E. R. Stadtman, and E. Shacter. (1994). "Carbonyl assays for determination of oxidatively modified proteins." *Methods Enzymol*, 233, 346-357.

Lion, N., J. Gellon, H. Jensen, and H. H. Girault. (2003). "On-chip protein sample desalting and preparation for direct coupling with electrospray ionization mass spectrometry." *J Chromatogr A*, 1003(1-2), 11-19.

Lionello, A., J. Josserand, H. Jensen, and H. H. Girault. (2005). "Protein adsorption in static microsystems: effect of the surface to volume." *Lab Chip*, 254-260.

Lundström, I. (1985). "Models of protein adsorption on solid surfaces." *Prog Coll Pol Sci S*, 70, 76-82.

Mann, M., and O. N. Jensen. (2003). "Proteomic analysis of post-translational modifications." *Nat Biotechnol*, 21, 255-261.

Mark, D., S. Haeberle, G. Roth, F. V. Stetten, and R. Zengerle. (2010). "Rofluidic lab-on-a-chip platforms: requirements, characteristics and applications." *Chem Soc Rev*, 39, 1153-1182.

Martinoia, S., M. Bove, M. Tedesco, and M. Grattarolaa. (1999). "A simple microfluidic system for patterning populations of neurons on silicon micromachined substrates." *J Neurosci Methods*, 87(1), 35-44.

McCarley, R. L., et al. (2005). "Resist-Free Patterning of Surface Architectures in Polymer-Based Microanalytical Devices." *J Am Chem Soc*, 842-843.

Michels, D. A., L. J. Brady, A. Guo, and A. Balland. (2007). "Fluorescent Derivatization Method of Proteins for Characterization by Capillary Electrophoresis- Sodium Dodecyl Sulfate with Laser-Induced Fluorescence Detection." *Anal Chem*, 79(15), 5963-5971.

Mirzaei, H., and F. Regnier. (2005). "Affinity Chromatographic Selection of Carbonylated Proteins Followed by Identification of Oxidation Sites Using Tandem Mass Spectrometry." *Anal Chem*, 77(8), 2386-2392.

Murakami, Y., T. Takeuchi, K. Yokoyama, E. Tamiya, I. Karube, and M. Suda. (1993). "Integration of enzyme-immobilized column with electrochemical flow cell using micromachining techniques for a glucose detection system." *Anal Chem*, 65(20), 2731-2735.

Nägele, E., M. Vollmer, and P. Hörth. (2003). "Two-dimensional nano-liquid chromatography–mass spectrometry system for applications in proteomics." *J Chromatogr A*, 1009(1-2), 197-205.

Norde, W. (1986). "Adsorption of proteins from solution at the solid-liquidinterface." *Adv Colloid Interface Sci*, 25, 267-340.

Orr, W.C., and R.C. Sohal. (1994). "Extension of life-span by over-expression of superoxide dismutase and catalase in Drosophila melanogaster." *Science*, 263(1), 128-130.

Orth, R. N., T.G. Clark, and H.G Craighead. (2003). "Avidin-Biotin Micropatterning Methods for Biosensor Applications." *Biomed Microdevices*, 5(1), 29-34.

Osiri, J. K., H. Shadpour, S. Park, B. C. Snowden, Z. Chen, and S. A. Soper. (2008). "Generating high peak capacity 2-D maps of complex proteomes using PMMA microchip electrophoresis." *Electrophoresis*, 29(24), 4984-4992.

Peterson, D. S., T. Rohr, F. Svec, and J. M. J. Fréchet. (2002). "Enzymatic Microreactor-on-a-Chip: Protein Mapping Using Trypsin Immobilized on Porous Polymer Monoliths Molded in Channels of Microfluidic Devices." *Anal Chem*, 74(16), 4081-4088.

Piran, U., W. J. Riordan, and D. R. Silbert. "Effect of hapten heterology on thyroid hormone immunoassays." *J Immunol Methods*, 133(2), 207-214.

Poon, H. F., V. Calabrese, G. Scapagnini, and D. A. Butterfield. (2004). "Free Radicals: Key to Brain Aging and Heme Oxygenase as a Cellular Response to Oxidative Stress." *Journal of Gerontology: Medical Sciences*, 59A(5), 478-493.

Rao, S. V., K. W. Anderson, and L. G. Bachas. (1999). "Controlled layer-by-layer immobilization of horseradish peroxidase." *Biotechnol Bioeng*, 65(4), 389-396.

Razumovitch, J., K. França, F. Kehl, M. Wiki, W. Meier, and C. Vebert. (2009). "Optimal Hybridization Efficiency Upon Immobilization of Oligonucleotide Double Helices." *J Phys Chem B*, 113(24), 8383-8390.

Requena, J. R., CHao C., R. L. Levine, and E.R. Stadtman. (2001). "Glutamic and aminoadipic semialdehydes are the main carbonyl products of metal-catalyzed oxidation of proteins." *Proc Natl Acad Sci,* 69-74.

Reynaert, N. L., A. Vliet, A. S. Guala, T. McGovern, and Y. M. W. "Janssen-Heininger. (2006). Dynamic redox control of NF-κB through glutaredoxin-regulated S-glutathionylation of inhibitory κB kinase β." *Biochim Biophys Act*, 103(35), 13086-13091.

Ricci, J. E., N. Waterhouse, and D. R. Green. (2003). "Mitochondrial functions during cell death, a complex (I-V) dilemma." *Cell death differ*, 10, 488-492.

Rogers, K. R. (2000). "Principles of affinity-based biosensors." *Mol Biotechnol* 14(2), 109-129.

Ross, D., J. G. Shackman, J. G. Kralj, and J. Atencia. (2010). "2D separations on a 1D chip: gradient elution moving boundary electrophoresis—chiral capillary zone electrophoresis." *Lab Chip*, 10, 3139-3148.

Rossi, R., D. Giustarini, A. Milzani, and I. Dalle-Donne. (2008). "Cysteinylation and homocysteinylation of plasma protein thiols during ageing of healthy human beings." *J Cell Mol Med*, 13(9b), 3131-3140.

Sandison, M. E., S. A. Cumming, W. Kolch, and A. R. Pitt. (2010). "On-chip immunoprecipitation for protein purification." *Lab Chip,* 10, 2805-2813.

Shacter, E., J. A. Williame, and R. L. Levine. (1994). "Differential susceptibility of plasma proteins to oxidative modification: Examination by western blot immunoassay." *Free Radic Biol Med*, 17(5), 429-437.

Shadpour, H, H. Musyimi, J. Chen, and S. A. Soper. (2006). "Physiochemical properties of various polymer substrates and their effects on microchip electrophoresis performance." *J Chromatogr A*, 1111(2), 238-251.

Silberzan, P., L. Leger, D. Ausserre, and J. J. Benattar. (1991). "Silanation of silica surfaces. A new method of constructing pure or mixed monolayers." *Langmuir*, 7(8), 1647-1651.

Silberzan, P., S. Perutz, E. J. Kramer, and M. K. Chaudhury. (1994). "Study of the Self-Adhesion Hysteresis of a Siloxane Elastomer Using the JKR Method." *Langmuir*, 10(7), 2466-2470.

Skidmore, G. L., B. J. Hortsmann, and H. A. Chase. (1990). "Modelling single-component protein adsorption to the cation exchanger S Sepharose® FF." *J Chromatogr A*, 198, 113-128.

Soper, S. A., S. M. Ford, S. Qi, R. L. McCarley, K. Kelly, and M. C. Murphy. (2000). "Peer Reviewed: Polymeric Microelectromechanical Systems." *Anal Chem*, 72(9), 642A-651A.

Srinivasan, R., and S. Lazare. (1985). "Modification of polymer surfaces by far-ultraviolet radiation of low and high (laser) intensities." *Polymer*, 26(9), 1297-1300.

Srisa-Art, M., E. C. Dyson, A. J. deMello, and J. B. Edel. (2008). "Monitoring of Real-Time Streptavidin–Biotin Binding Kinetics Using Droplet Microfluidics." *Anal Chem*, 80(18), 7063-7067.

Stachowiak, T. B., et al. (2003). "Fabrication of porous polymer monoliths covalently attached to the walls of channels in plastic microdevices." *Electrophoresis*, 24(21), 3689-3693.

Stadtman, E. R. (2006). "Protein oxidation and aging." *Free Radical Res*, 40(12), 1250-1258.

Stadtman, E. R., and R. L. Levine. (2003). "Free radical-mediated oxidation of free amino acids and amino acid residues in proteins." *Amino acids*, 25(3-4), 221-226.

Steen, H., and M. Mann. (2004). "The abc's (and xyz's) of peptide sequencing." *Nat Rev Mol Cell Bio*, 5, 699-711.

Sun, X, B. A. Peeni, W. Yang, H. A. Becerril, and A. T. Wooley. (2007). "Rapid prototyping of poly(methyl methacrylate) microfluidic systems using solvent imprinting and bonding." *J Chromatogr A*, 1162(2), 162-166.

Terry, S.C., J.H Jerman, and J.B. Angell. (1979). "A gas chromatographic air analyzer fabricated on a silicon wafer." *IEEE Trans Electron Devices*, 26(12), 1880-1886.

Tsai, S. F., T. M. H. Sheu, and S. M. Lee. (1999). "Heat transfer in a conjugate heat exchanger with a wavy fin surface." *Int J Heat Mass Tran*, 42(10), 1735-1745.

Van Raamsdonk, J.M., and S Hekim. (2009). "Deletion of the mitochondrial superoxide dismutase sod-2 extends lifespan in Caenorhabditis elegans." *PLoS Genet*, 5(2).

Volkmuth, W. D., and R. H. Austion. (1992). "DNA electrophoresis in microlithographic arrays." *Nature*, 358, 600-602.

Wallace, D.C., and S. Melov. (1998). "Radicals r'aging." *Nature Genet*, 105-106.

Wang, C., R. Oleschuk, F. Ouchen, J. Li, P. Thibault, and D. J. Harrison. (2000). "Integration of immobilized trypsin bead beds for protein digestion within a microfluidic chip incorporating capillary electrophoresis separations and an electrospray mass spectrometry interface." *Rapid Commun Mass Spectrom*, 14(15), 1377-1383.

Washburn, M. P., D. Wolters, and J.R. Yates. (2001). "Large-scale analysis of the yeast proteome by multidimensional protein identification technology." *Nat Biotechnol*, 19(3), 242-247.

Wei, S., B Vaidya, A. B. Patel, S. A. Soper, and R. L. McCarley. (2005). "Photochemically Patterned Poly(methyl methacrylate) Surfaces Used in the Fabrication of Microanalytical Devices." *J Phys Chem B*, 109,(35), 16988–16996.

Whitesides, G. M., E. Ostuni, S. Takayama, X. Jiang, and D. E. Ingber. (2001). "Soft Lithography in Biology and Biochemistry." *Annu Rev Biomed Eng*, 3, 335-373.

Wilchek, M., and E. A. Bayer. (1990). "Introduction to avidin-biotin technology." *Method Enzymol*, 184, 5-13.

Winterbourn, C. C., and I. H. Buss. (1999). "Proteincarbonylmeasurement by enzyme-linked immunosorbent assay." *Method Enzymol*, 300, 106-111.

Xu, B., X. Feng, Y. Xu, W. Du, Q. Luo, and B. Liu. (2009). "Two-dimensional electrophoresis on a microfluidic chip for quantitative amino acid analysis." *Anal Bioanal Chem*, 394(9), 1911-1917.

Yang, S., J. Liu, C. S. Lee, and D. L. DeVoe. (2009). "Microfluidic 2-D PAGE using multifunctional in situ polyacrylamide gels and discontinuous buffers." *Lab Chip*, 9, 592-599.

Yin, H., and K. Killeen. (2007). "e fundamental aspects and applications of Agilent HPLC-Chip." *J Sep Sci*, 30(10), 1427-1437.

Yoo, B. S., and F. E. Reginer. (2004). "Proteomic analysis of carbonylated proteins in two-dimensional gel electrophoresis using avidin-fluorescein affinity staining." *Electrophoresis*, 25(9), 1334-1341.

Yu, L., C. M. Li, and Q. Zhou. (2005). "Efficient probe immobilization on poly(dimethylsiloxane) for sensitive detection of proteins." *Frontiers in Bioscience*, 10, 2848-2855.

Zhao, X., Y. Xia, and G. M. Whitesides. (1997). "Soft lithographic methods for nano-fabrication." *J Mater Chem*, 7,1069-1074.

Zhao, Y., and O. N. Jensen. (2009). "Modification-specific proteomics: Strategies for characterization of post-translational modifications using enrichment techniques." *Proteomics*, 9(20), 4632-4641.

Zhou, X., et al. (2004). "Determination of SARS-coronavirus by a microfluidic chip system." *Electrophoresis*, 25(17), 3032-3039.

Zhu, H., et al. (2001). "Global Analysis of Protein Activities Using Proteome Chips." *Science*, 293, 2101-2105.

Ziober, B. L., M. G. Mauk, E. M. Falls, Z. Chen, Ziober, A. F., and H. H. Bau. (2008). "Lab-on-a-chip for oral cancer screening and diagnosis." *Head & Neck*, 30(1), 111-121.